USING BIREFRINGENCE AS A TOOL TO INVESTIGATE BIOMECHANICAL PROPERTIES OF AN ELASTIC BIOPOLYMER PROTEIN

by

David Wesley Didier

B.Sc. University of British Columbia, 1992
B.Ed. University of British Columbia, 1994

A THESIS SUBMITTED IN PARTIAL FULFILLMENT OF
THE REQUIREMENTS FOR THE DEGREE OF
MASTER OF SCIENCE

in

THE FACULTY OF GRADUATE STUDIES
(Zoology)

THE UNIVERSITY OF BRITISH COLUMBIA
(Vancouver)
July 2009

Abstract:

Egg capsules from *Busycon canaliculatum* were examined to determine the microscopic mechanical properties. Previous macroscopic studies of this whelk's egg capsules had determined that the protein polymer of these egg capsule cases have an interesting two-phase stress/strain curve and that this material fully recovered from yield strains. The previous study also demonstrated that stress/strain curves had a large hysteresis, and that these properties could be reversibility suppressed using heat or acid.

It was hypothesized that these properties were intrinsic to the macromolecules and not related to the crisscross laminar structure of the capsule walls. A careful study of fiber samples teased out of the capsule walls confirmed that these traits were indeed properties of the macromolecular structure. The microscopic stress/strain tests produced results that were very similar to the macroscopic studies results. The microscopic study revealed two new areas (toe region and tertiary modulus) on the stress/strain graphs. The initial toe region represents the taking up of slack in the fibrous protein matrix as the fibers are loaded. The tertiary modulus showed up at strains that would have caused failure in the laminar structure of the capsule walls in the macroscopic study.

This study also incorporated birefringence measurements as an instantaneous measure of order in the sample during stress/strain tests. This data was used to hypothesize about what was happening to the protein molecules are they were strained. Using this data and x-ray diffraction data from an unpublished related study a model was developed to explain the properties of this organic polymer. It is believed that the two-phase stress/strain curves are produced by stress-induced changes to the α-helical components of whelk egg capsule protein. Straining α-helixes produces the initial stiff region. At the yield point the H-bonds in the α-helixes are over-strained and begin to pop-open, resulting in a loss of overall order (measured using birefringence) in the sample as α-helical structures are lost. Pulling on the primary molecular chains that form the α-helixes produces the tertiary modulus. The α-helixes spontaneously reform on recoil, allowing the protein to fully recover from the strain. β-sheet x-ray signals have been detected in this material under strain (unpublished results) but the fact that it totally recovers on recoil indicates that no stable β-sheets were formed during these tests.

Table of Contents

List of Tables

List of Figures

List of Equations

List of Abbreviations and Symbols

Γ	Retardation
θ	Angle of retardation
I	Average intensity of light from birefringence
I_r	Relative intensity of birefringent light
K	Retardation constant of polarizer, slope of the plot I_r vs. $\sin^2 \theta$
MPa	Mega Pascal
MN	Mega Newton
n_e	Refraction of the extraordinary ray
n_o	Refraction of the ordinary ray
nm	Nanometer
t	Thickness of the sample (nm)
μm	Micron
WECP	Whelk egg capsule protein

Acknowledgments

This thesis was made possible through the support of a number of people.

I thank my supervisor Dr. R. Shadwick who gave me the chance to work in his lab on this great project. Bob was willing to look past a shaky start as an under grad and gave me the chance to prove my self through some volunteer work that kicked off the study. Bob was always available to talk over any question I had and gave me my introduction into biomechanics for which I will always be grateful.

This study would not have been possible with out the assistance of Dr. John Gosline. It was John who introduced me to Bob and started me down this great adventure. The majority of my work has taken place in John's lab and I thank him for letting me use his equipment and space. Like Bob, John was always available to discuss my findings and guide me on my way.

I thank Dr. Carl Michael for being on my committee and helping with my thesis. I am sorry that we did not have more time to look at this material together.

Thank you to Dean Grant Ingram and Barbara Crocker both of whom helped me find funding for my research.

Finally, I give a special thanks to my wife and children. Antonieta, Victor and Erick have persevered with me through this time in my academic endeavors. They have put up with some lean times economically so I could achieve this goal and their support is gratefully acknowledged and appreciated.

1 Introduction

The advent of modern chemistry and physics has led man to the discovery of numerous physical properties of a multitude of elements and compounds. Using that knowledge we have been able to create and manufacture a variety of useful materials. Materials Engineering has become a large field of study. In recent years people have gained a respect for biomaterials. The once common belief that we could come up with designs that were better than nature's has given way to a realization that evolution has tried, tested and possibly even perfected many useful materials. Biologists have led the investigation into nature's solutions.

These investigations have turned up many interesting materials. Resilin for example is a pure material that is an almost perfect spring. First described in 1960 by Torkel Weis-Fogh, this resilient material is now produced synthetically by Dr David Merritt, UQ, Brisbane, Australia (Bennet-Clark, 2007). Bone and keratin, on the other hand, have taught us a lot about composite materials (Meyers, 1995). We have learned that mixing hard materials and flexible materials can produce tough resilient materials that have the strength of the hard components tempered by the flexibility of the bendable components. The trick then is to find interesting biological materials and study them to see what we can learn.

Whelks are marine snails that lay their eggs in capsules. The capsules provide a safe environment for the young until they emerge as miniature adults. These capsules are made up of a protein secretion that is laid down in successive layers. This laminate structure is similar to plywood in that successive layers have distinct fiber orientations that are laid out in a crisscrossing pattern (Rappaport and Shadwick, 2002). The protein undergoes a not yet fully understood processing that transforms the initial soft secretion, which has almost no mechanical integrity, into a resilient protective case. These capsules survive for months tethered on the ocean bottom. Our observations confirm that they do not foul or change much in appearance during this time period. The young whelks

themselves do not break through the capsule, but rather they emerge though a mucus plug. Figure 1.1 shows a *bussycon canaculatum* secreting a string of capsules.

Now that we have identified an interesting candidate for study, the testing begins to see what can be learned. When investigating physical properties there are a variety of things that can be done to the samples. The purpose of these tests is not to emulate "real-life' conditions but rather to illicit responses that tell us something about the material. Strain is a measure of how much a material has been stretched in relation to its original length. Stress is a normalized measure of the amount of force applied. Together they can tell us a materials toughness (energy required to break it), its response to stress (what happens when a force is applied to it), its stiffness/modulus (a ratio of stress vs. strain), its yield point (the start of a normally non-recoverable deformation), its maximum extensibility, if parts creep apart under stress, how resilient it is, etc. The results, when taken together then allow us to propose models about how that material works. If we follow the principles laid out in the text "Viscoelastic Properties of Polymers", by J.D. Ferry, an elastic material like resilin, for example, could be modeled as a spring, while molasses could be modeled as a dashpot that represents the flow of a Newtonian fluid. Combined, the models can describe simple viscoelastic materials, which act both like a spring and a viscous fluid. If extended quickly they spring back. If extended slowly or held while extended parts of the sample flow past each other.

Whelk egg capsules have an interesting stress strain behavior, see figure 1.2. The first thing that catches your attention is that the material is extremely durable. If you consider the behavior of a material such as the plastic that holds a six-pack of beverages together, you would note that it is elastic if you stretch it a little and that if pull too far it yields and permanently deforms. This what we think of as the "norm" i.e. yields indicate a permanent deformation of the material. With whelk egg capsule protein (WECP) this expectation is dashed. Rappaport and Shadwick (2002) found that WECP fully recovers from yield deformations so well that successive extensions produce plots that lie on top of each other. They documented that the whole capsule sections they tested had a Hookean region where the material followed Hooke's Law (a linear-elastic model of how

springs work) and that the modulus decreased by an order of magnitude following the yield point. So it is a stiff material that becomes soft if strained more than 5%. Another interesting result from that study was that the unloading curve was significantly lower than the loading curve, this is referred to as a hysteresis loop, and it indicates that the yield process dissipated a large amount of energy (i.e. it has low elastic resilience). Figure 1.3 from Rappaport and Shadwick 2006 shows the effect of temperature on whole capsule strain tests. The initial stiff region is lost when WECP is heated and it recovers when it is cooled. They also reported that the same effect could be produced using 88% formic acid.

Another powerful way to learn about things is to look at them closely. Scientists have come up with a variety of ways to do this. We can use magnification, stains, and a variety of different light filters to learn about how materials are arranged. According to Born and Wolf 's, *Principles of Optics*, 7th Ed. 1999, refraction is the bending of light as it passes from one medium to another medium with different refraction index. Differences in refraction indices are what produce the illusions that things are larger under water, that sticks bend at the surface of the water and mirage effects. Birefringence is an optical effect generated by ordered structures in objects and by differences in refraction indexes between media. Since birefringence is generated by order on a molecular level, birefringence can in turn be used to measure how much order there is within an object, how that order changes with strain and in which direction subunits are lined up on. Birefringence scans of the capsules revealed that the material was highly birefringent (i.e. very ordered) and that the layers that make up the capsule were crisscrossed like plywood (Rappaport and Shadwick 2007), see figure 1.4.

The macroscopic structure of one species of whelk's egg capsules was previously investigated. Rappaport and Shadwick (2007) laid out how *Kelletia kelletii* forms its capsules and the development of mechanical properties associated with this three-step process, see figure 1.5. The protein WECP initially has no mechanical integrity, then it is elastically cross-linked, and finally it develops the initial stiff modulus. The development of these properties is thought to be a chemical maturation process involving the

development of covalent bonds. The end result is the production of a highly ordered protein polymer, as indicated by the birefringent properties seen in figure 1.4.

Since all of the work prior to this study was performed on sections of whole capsules, I decided to take a closer look at the layers that form the capsule. The first question addressed here is what are the properties of the fibrous matrix within the capsule wall. My hypothesis was that the interesting yield and recovery properties of the capsule were biomechanical properties of the protein, rather than properties that arise from the reorientation of the protein micro-fibrils in the various layers of the capsule. I predicted that the stress strain curves of microscopic fiber samples would be similar in shape to those of the intact capsule. The goal of this part of the study was to document and compare the micro-properties of the capsule fibers with the macro-properties of the whole capsule.

The second focus of this thesis is the interesting optical properties of the capsule protein. As previously mentioned, the capsules are birefringent. This means that the capsules appear bright when viewed with polarized light. In other words, the protein has sufficient order to produce different indices of refraction and it changes the polarization of the light passing through it. Previous work by Rappaport and Shadwick (2002) proposed that the capsule protein was a highly ordered structure made up of α-helixes (unpublished x-ray data from Miserez et al. detected α-helixes) that are disrupted when the protein is strained beyond the Hookean region, see figure 1.2. The α-helixes are part of the basic building block molecules of this polymer. Rappaport and Shadwick (2002, 2007) have previously suggested that this material is a keratin analog. In this paper the polymer is modeled as having six levels of organization.

α-helixes are structures formed by proteins, which are the basic building block molecules that connect together to form chains that are in turn connected to form micro-fibrils, which interlink to form a fibrous -matrix and finally layers of fibrous -matrix make up the egg capsule walls, see figures 1.6 and 1.7. If this material is a keratin analog, as suggested, then the building block molecules are likely to be similar to known

keratin molecules. These molecules would then form dimers that chain together, which in turn form intermediate filaments (micro-fibrils).

I used birefringence as an index of order within the material. This order can be generated in two ways. Form birefringence is produced by the fact that the speed of light within the sample is different in two directions because the refractive index of the material you are viewing is different than the refractive index of the medium the material is in. Intrinsic birefringence is caused by light refracting in two directions as it tries to pass between parallel object that are closer together than the wave length of the light. This type of birefringence in seen in crystalline structures and highly ordered structures such as the α-helixes, which we know are present in the WECP. Straining bonds can produce or increase the intrinsic birefringence.

I based my study on the commonly known property that many materials become birefringent under strain. Glass for instance will become birefringent when strained (Lau et al 2003). The generally accepted hypothesis when dealing with rubbery materials is that as you stretch a rubbery material you impose more order on that material. See Figure 1.8 for an explanation of this phenomenon. Given that this protein is proposed to have highly ordered α-helixes, there are two possible predictions: 1: the material will increases its order when stretched, or 2: it will lose order as the α-helixes are pulled apart. The results showed that with WECP, both things happen.

2 Methods

We received two supplies of whelk egg capsules. The initial supply was a string of capsule collected on a Masseuses beach by a commercial collection company. A second sample was collected by a SCUBA diver, and judging by the size of the whelks in the capsule it was much fresher. They were frozen and stored in a –80 C freezer until needed. Individual capsules were thawed when needed and stored in distilled water in the lab refrigerator. Samples were obtained by teasing out pieces of the capsules with tweezers. The middle layer was selected for testing because it yielded fibrous samples of relatively uniform width. The inner and outer layers came apart in ragged and unpredictable ways, making them unsuitable for this experiment, see figure 2.1. The inner and outer layers of the capsule appear to be made out of the same protein, but these layers are much denser and look more like a gel. Preliminary testing of all layers produced similar stress/strain curves, with an expectedly higher yield stress due to its denser nature. The teasing process produced a random assortment of fragment from which specimens were selected and mounted for testing.

The first thing that was done with the samples was to measure the width on a side view apparatus. Samples were held taut on upright insect pins to measure the width, see figures 2.2 & 2.3. The width of samples was obtained using a Leitz orthoplan polarizing microscope and a Diagnostics Instruments RT-SE-900 monochrome digital camera (Sterling Heights, MI, USA). Images were analyzed with the digital analysis program, SPOT, provided by the manufacture and with Image-J. The sample was then cut off the apparatus and the mid section was mounted on the testing apparatus.

All stress strain tests were performed on an apparatus I designed and built. The apparatus consists of an ASI model 6228H muscle lever arm (Aurora Scientific Interments, Aurora, Ontario, Canada) controlled by an ASI model 600A digital controller and a model 604C digital interface. Force was recorded using a Kronex Technologies KX801 micro-force

sensor (Oakland, CA, USA) and a Measurements Group model 2310 strain gauge conditioning amplifier (Raleigh, N Carolina, USA). Temperature was controlled using a Phystemp TS-4ER Thermal Microscope Stage (Clifton New Jersey). The temperature of the sample was measured using a Physitemp MT-26/4 hypodermic needle microprobe. Figures 2.4 & 2.5 show the mechanism used and the lab setup.

Test samples were mounted onto to insect pins from the bottom of the apparatus. They were fixed onto the test apparatus using cyanoacrylate glue while the sample was still wet. The bottom of the test chamber was then sealed using an inner ring of silicone-rubber and an outer ring of rubber cement. The silicone-rubber provided a watertight barrier, and the rubber cement provided instant adhesion. The seal on the transducer side was completed by the hydrophobic forces of the Teflon dam (piece of Teflon cut from a one inch piece of hosing) around the insertion point of the insect pin.

Because the lever arm moves in an arc, there was a potential for the motion to become non linear. This could affect the focus when photographing the sample and would distort strain data if the arc motions were large. A glass capillary tube was used to guide the control arm pin so that the extension motion would be linear. Keeping the initial sample length short so that the motion reported by the computer was as linear as possible further controlled distortions (Typical length: 1 mm +/- 0.2mm).

The distance between attachment points was measured using a Leitz orthoplan polarizing microscope and the digital analyzing program SPOT to find the initial length. The sample was then subjected to a series of stress tests that varied the speed, duration, length, and other variables such as the addition of pauses and varying the amount of recoil (see test protocols below). The ASI digital controller recorded force and distance measurements. Digital images of the tests were recorded for analysis as well. Images were taken with a Leitz L 10x polarized light objective (na=0.22). Exposure time was set at 10 ms and photos were taken every 0.5 sec (this rate was chosen base on the processing speed of the computer taking the pictures).

2.1 Test Protocols

Investigation of biomechanical properties requires the development of test procedures that allow you to see how the material reacts under different conditions. Heat is a useful variable because it affects the free motion of molecules. In terms of viscosity this means that as things heat up they flow more easily. For H-bonds it means that as the temperature rises there is more energy available to break these bonds, so secondary structures are less stable. Previous investigations of the WECP described it as viscoelastic, and H-bonds had a role in the properties (Rappaport and Shadwick 2002 & 2007). I tested my samples at 5C, 20C and 70C. The cover slips fogged over at 5c, so no photos were available for analysis at this temperature. Room temperature, 20C, was chosen for convenience. The 70C high temperature limit represented the highest temperature my unit could achieve; bubble formation and evaporation contributed to this limit.

As previously noted, any change in stress/strain relationship can potentially expose unknown properties of the sample and may support or refute models that seek to explain its material properties. With this in mind I designed the following series of tests. All samples were tested at 20C first and then at high temperature and finally at low temperature. The rationale behind this was that the sample could fail at any time during testing. (i.e. the glue could fail or the sample could tear.) Starting at a constant temperature allowed me to build a database of "typical" samples. Moving to 70C next gave me a wide temperature range for comparison. Samples were retested at 20C to see if they recovered and then at 5C if they were still intact.

Description of tests:

1. Ramp extensions at varying rates: a constant rate extension of the sample to a set strain and then a constant rate controlled recoil of the sample to observe changes in stress and birefringence.

2. Stress relaxation pause at end of ramp extension: The recoil motion is delayed to observe if there is any stress relaxation and to see how birefringence changes.
3. Stress relaxation pause during ramp extension: The extension motion is paused to see how stress and birefringence curves are changed when the extension is resumed following a period of relaxation.
4. Stress relaxation pause during recoil: The recoil motion is paused to see how the stress and birefringence curves are changed.
5. Incomplete recoil: The recoil motion is stopped before complete recovery and a new extension is preformed to see how the stress and birefringence curves are changed.

The stress, strain and birefringence data from all tests were recorded on computers. Stress and lever arm position were recorded on the Aurora Scientific Instruments control computer, provided by ASI with the muscle lever arm. Data was recorded as a text file containing instantaneous readouts of force and lever arm position at 10Hz.

Digital photos of the sample were recorded on a separate computer in gray scale in 1360x1024 pixel images. Resolution in the photos was 1.699 pixels/μm.

2.2 Stress/Strain

Stress/strain curves were generated from test data using Excel and Sigma Plot.

Force was recorded in mN, and the cross sectional area of the sample was calculated. These measurements were then used to normalize the data by converting it into engineering stress (MPa = mega Pascal=10^6 N/m^2) for comparison.

Strain was calculated by finding L_0 and then calculating the amount the sample was stretched beyond L_0. L_0 was found using a two-step process. Initially L_0 was estimated

by manually adjusting the lever arm to find the point where force first registered on the force transducer. All force tests were then started a distance 10% shorter than the estimated L_0. During analysis of the data L_0 was recalculated once again by looking for the lever arm position where the force transducer first registered force. Strain was then calculated using the following formula.

$$\text{Strain} = \frac{(L - L_0)}{L_0} \qquad (1)$$

The stress/strain plots and the digital images of the tests were reviewed, and samples that displayed uniform deformation were analyzed. Plots that appeared to be affected by mechanical glitches or heterogeneous stretching patterns were discarded. Mechanical failures sometimes occurred when the controller program moved the arm in an unexpected way, when glue bonds became loose, when the arm hooked on debris or if the guide was out of alignment. Heterogeneous stretching patterns were identified when viewing the photos of the test. Some samples had weaker sections that strained at different rates. I.e. if points A, B and C were all in a line on the strain axis of the sample point A would be moving away from point B faster than Point B was moving away from point C. Because samples were teased from egg capsules that are composed of a protein secretion formed into successive layers of the capsules wall within the whelk's reproductive tract, a high degree of variability in macro-structure was expected. It is not surprising therefore that some samples were not uniform.

2.3 Birefringence

Birefringence was measured using a Wild Senarmont 546 compensator with a 546 nm interference filter. The sample was rotated to its darkest view between two crossed polarizers (in parallel to the first polarizer) and then rotated to 45 degrees (point of

maximum brightness). Light intensity (I) is measured using the mean gray value (an averaged reading of how much light the CCD array of the camera detected). The birefringence is calculated using the relative intensity (I_r) of the light associated with the birefringent material (total light measured less the bias of the camera and background noise). Setting up for this calculation requires a calibration of the polarization field used. There are several relevant equations that were use for this part of the study.

Relative intensity of light retarded by sample as measured by the camera.

$$\text{RelativeIntensity}(I_r) = \frac{\text{AverageIntensity}(I) - \text{Bias} - (\text{EmptyFieldIntensity} - \text{Bias})}{(\text{EmptyFieldIntensity} - \text{Bias})} \quad (2)$$

I: average intensity of light from birefringent light
I_r: relative intensity of birefringent light
Bias frame: the average light value recorded when the shutter closed
Empty Field Intensity: background noise, average light value in the dark area of the photo

The relative intensity of the sample as it relates to retardation is described by the following equation in which the rotation angle of the polarizer was linearized using $\sin^2$ so that k could be easily calculated.

$$I_r = k \sin^2 \theta \quad (3)$$

k = retardation constant of polarizer, slope of the plot I_r vs. $\sin^2 \theta$
θ = angle of retardation

Calculating birefringence requires that you know how much the sample has retarded (rotated) the light. To do this a blank field calibration was preformed as follows. A series of 20 empty field photos starting with the polarizer plates cross-polarized and followed

by rotating one polarizer by one deg after each photo was taken. This produced a series of increasingly bright photos ranging from $\theta = 0$ to $\theta = 19$ degrees. A plot of the relative intensity of the blank field against $\sin^2 \theta$ was created and the slope of this line, k, was determined. Knowing k and I_r allowed the calculation of the angle of retardation produced by the sample.

Solving for θ we get

$$\theta = \arcsin \text{sqrt}(I_r / k) \quad (4)$$

Retardation was then calculated as follows.

$$\Gamma = \theta \times 3.03 \text{ nm/deg} \quad (5)$$

Γ = Retardation

Wood (1964) defined birefringence as the numerical difference between the two indices of light refraction of an anisotropic material, where n_o is the refraction of the ordinary ray and n_e is the refraction of the extraordinary ray. The comparison is therefore the difference between the undisturbed light passing to one side of the sample and extraordinary ray produced by the birefringent sample.

$$B = n_e - n_o \quad (6)$$

The retardation angle is then used to calculate the birefringence of the sample. In accordance with Kliger et al. (1990) birefringence was calculated as Γ/t, where Γ is the optical retardation measured using a Senarmont $\lambda/4$ compensator plate and t is the thickness of the sample. (Sénarmont compensation is an elegant technique that utilizes monochromatic light, together with a rotatable, graduated analyzer, for accurately determining small retardation values with the accuracy of the unit of the monochromatic

light (nanometers) Delly (2004). This procedure was used to calculate k for use in equation 4, which in turn provided the angle of retardation Γ).

$$B = \Gamma / t \text{ (nm)} \qquad (7)$$

Γ: angle of retardation as calculated in equation 5
t: thickness of the sample (nm)

Birefringence was calculated using images taken during the tests using the following procedure.

1. The start and end photos for the tests were identified.
2. An easily identifiable area of the sample was selected for measurement.
3. The mean gray value (light intensity) for each photo was measured and recorded.
4. The background noise and camera bias was subtracted from the gray values to get an I_r value for the sample.
5. These sample values were converted into birefringence measurements as described above.

Birefringence results were then analyzed by plotting them versus time, strain and stress to look for trends.

2.4 Estimation of Error

The force transducer was calibrated by hanging nine known masses on the arm and graphing a regression line to find the volts per gram readout. A typical regression had an R^2 value of 0.999. This process was repeated for each transducer used.

The ASI high-speed length controller model 322c muscle lever arm has a reported resolution of 0.5 μm. Typical lengths for the samples were in the 0.6-1.3 mm range. Accuracy of movement is therefore estimated to be 0.0000 mm $^{+}/_{-}$ 0.0005mm.

Measurements of thickness were made with digital photos and analyzed using ImageJ (National Institute of Health, USA). The accuracy of measurement is estimated at one pixel or $^{+}/_{-}$ 1.7 μm. The original length of the sample (L_0) was measured same way. L_0 was then recalculated based on force and length readouts as described above. Accuracy of measurements used to calculate strain are therefore estimated to be $^{+}/_{-}$ 4.298 μm (1.699 pixel error + 0.5 mm arm position error, doubled for the two lengths used to calculate strain).

The average gray values were measured using Image J and viewing the images at 100% of actual size. Error for these measurements is estimated at $^{+}/_{-}$ 0.2% based on comparisons of the same sample area on multiple images of the same sample taken seconds apart.

3 Results

There are two basic forms of analysis used in this thesis. The first type is stress/strain analyses of physical properties. The second analysis uses birefringence to probe for information about molecular order.

3.1 Mechanical Testing Results

The whelk egg capsules have multiple levels of organization. For this investigation a micro-fiber sample is as teased out section of one of these layers. The fibrous-matrix samples tested produced very similar stress/strain cures, when compared to the whole capsule. Figure 3.1 shows various views of whelk egg capsule fibers. Rappaport and Shadwick (2002, 2007) described the macroscopic capsules as being made up of laminated layers of crisscrossing protein. These layers are in turn made up of a fibrous-matrix. This fibrous-matrix is visible in figure 3.2. When viewed in cross-section the whelk capsule reveals three distinct layers. The inner and outer layers have a similar appearance and seem to be made up of more transparent compact arrangement of WECP, with a more variable orientation of the fibers The exterior layers held together better indicating a stronger cross-linking of the successive layers. The middle layer is more fibrous in nature and proved much easier to tease into uniform fiber samples for testing. This layer was estimated to be about 2/3 fluid space and 1/3 WECP, initial testing found that the modulus of the mid layer was 1/3 of the inner and outer layers, a difference that was attributed to its sponge like layout of WECP. Directionality of the birefringence is clearly visible under polarized light. Figure 3.2 shows a sample imaged using second harmonic imaging (an imaging method that uses this proteins natural florescent properties to view the material). In this figure it is clear that the layer is composed of an interlinking mesh of filaments, which in turn must be made up of individual interlinked

protein molecules. A hierarchical model to explain the overall structure is proposed in the discussion.

Figures 3.3 and 3.4 show typical stress/strain data for a capsule fiber sample. The graph is divided up into several identifiable regions. The toe region where there is very little stress associated with the strain applied. The initial modulus (Hookean) region where the sample acted like a linear spring and highest stress/strain ratio was recorded. The yield regions, areas where the stress/strain ratios changed dramatically. The post yield plateau region where the stress/strain ratio was the lowest and the Tertiary Modulus where the stress/strain ratio increased again just before the sample broke under strain.

The graphs reflect all of the interesting traits found in the whole capsule studies. There is a distinct initial modulus (Hookean region) at the start of the extension where the capsule fibrous -matrix displays a very stiff initial modulus of 23-40 MPa. The yield stress was 1.8-3.9 MPa and the yield strain 0.069-0.13. A post-yield region with a modulus of 1.3-3.6 MPa follows this stiff section. There is a large hysteresis of 40-60 % as the sample is allowed to return to its initial length.

The lower portion of the loop appears to mirror the upper region. The modulus for the yield region was 1.1-3.7 MPa and the initial modulus (Hookean region) had a modulus of 10.1 to 20.4 MPa. The yield regions had almost the same modulus and the initial modulus only differed by a factor of 2.

The recovery appears to be almost complete between each successive loop and the plots lie almost on top of each other.

A summary of these tests is shown in table 3.1

	Rate /Sec	Initial Modulus (MPa)	Post-Yield Plateau Modulus (MPa)	Unload Post-Yield Plateau (MPa)	Unload Initial modulus (MPa)	Yield Strain	Yield Stress (MPa)	Percent Hysteresis
5c	12% n=5	33.3+/-4.0	2.9+/-1.1	3.4+/-1.5	10.4+/-1.9	0.094+/-0.021	2.4+/-0.9	54.0+/-7.5
	6% n=3	27.6+/-11.6	26+/-1.2	2.3+/-1.0	11.3+/-1.1	0.086+/-0.029	2.6+/-0.4	47.8+/-0.1
	3% n=3	26.0+/-8.3	2.6+/-1.2	2.1+/-1.0	11.9+/-2.7	0.091+/-0.024	2.1+/-0.8	47.4+/-0.7
20c	12% n=10	33.6+/-5.5	3.2+/-1.9	2.7+/-0.9	11.4+/-4.0	0.094+/-0.019	2.3+/-0.7	48.6+/-8.0
	6% n=5	29.4+/-11.7	3.7+/-2.0	2.5+/-0.98	13.5+/-4.8	0.075+/-0.011	1.9+/-0.2	43.1+/-5.0
	3% n=5	30.0+/-10.2	3.2+/-1.5	6.1+/-9.5	14.4+/-6.1	0.078+/-0.014	1.9+/-0.1	43.5+/-4.9
70c	12% n= 5	24.6+/-7.5	1.7+/-0.6	2.3+/-2.2	6.0+/-8.0	0.056+/-0.014	0.9/-0.5	59.1+/-11.3
	6% n=3	20.7+/-9.8	1.4+/-0.6	1.7+/-0.7	2.8+/-3.5	0.060+/-0.002	1.0+/-0.4	50.0+/-5.6
	3% n=3	17.4+/-6.7	1.2+/-0.6	1.2+/-0.5	4.2+/-4.8	0.068+/-0.014	1.0+/-0.3	51.8+/-7.8

Table 3.1: A summary of test data, reported as an average value +/- standard deviation.

The samples were tested at a variety of standardized strain rates. The initial rate was chosen at random because it was easy to program the lever arm at that rate. The other rates were chosen because each was half of the previous rate. This was done to see if the sample was sensitive to the speed it was strained at. The 12% strain rate was used for the 1^{st} and 2^{nd} ramps. There was no consistent pattern between which ramp 1 or 2 produced the highest modulus, so the data were lumped together and reported as a single plot. All three strain rates produced almost identical curves.

3.2 Partial Recoils and Pauses

Other tests looked at how the material responded to partial recoils and holds. Partial recoils were defined as strain tests in which the sample was re-extended before it had recoiled to its original length. Holds were defined as any test that maintained a constant strain on the sample for a period of time. Holds were performed during extensions, at the end of extensions and during recoil.

When allowed to partially recoil, the material shows a recovery of the stiff Hookean attributes if it is allowed to recoil to below the yield strain beyond the yield region, see figure 3.5 A and B. If the loading begins again at strains above the yield strain while in the yield region, the modulus does not recover the initial Hookean stiffness but rather displays an intermediate modulus as the plot rises back up to join the initial load portion of the curve. See figure 3.5.

Pausing during the extension allows the fibrous -matrix sample to partially relax. Figure 3.6 shows the effects of pausing at various strains. In all cases force begins to fall immediately in a pause. When the extension is resumed, the plot quickly rejoins the uninterrupted plot profile. In the Hookean region this seems to have little effect on the modulus, see figure 3.6 A and B. The sample does, however, show some recovery of the Hookean stiffness in the yield region, see figure 3.6 C, D, and E.

3.2.1 Stress Relaxation

Viscosity describes the ability of a material to flow over itself when a force is applied to it. Molasses for example is more viscous than water. Viscous flow can be a basic property of many materials. Stress relaxation experiments test for this property by

holding a sample under stress at a fixed length to see if stress will fall indicating that some internal molecular reorganization has occurred. i.e. the sample has relaxed.

Stress relaxation experiments of WECP all display very similar drops in force. All of the samples were put through a series of relaxations with a gradual increase in the final strain. Figure 3.7 shows the strain/time and force/time plots. Stain is applied to the samples and stress rises with strain. When the strain is kept constant, the force plots all show an immediate sharp drop in force and then a slower tapering off. Figure 3.8 plots a series of holds at increasing strain. The sample was allowed to go slack (strain =–10%) between loadings.

The data shown here are for a relatively short, 10 sec, hold, but experiments with one minute and five minute holds show the same pattern. Figure 3.9 shows raw force data for one sample vs time in minutes. We can see the same initial rapid drop in force during the first few seconds when strain becomes constant. By the 30 sec mark the slope of the force plot is leveling off. Force continues to decline but at a much slower rate.

Normalizing the data in figure 3.9 so that all the relaxations start at time index zero shows that there are some differences in the level of stress but that the slopes are very similar. Plotting the data on a logarithmic scale compress the data but the general shape remains indicating that the original curves are not simple logarithmic decays (exponential decays are easily modeled), see figure 3.10. Extending the hold to five minutes still finds the force fading away, see figure 3.11.

3.2.2 Temperature Effects

Whole capsules stress/strain curves display a slow steady decay of the initial modulus and the yield point (both stress and strain) as the temperature rises. Figure 1.3 from

Rappaport and Shadwick 2006 shows the effect of temperature on whole capsule strain tests.

The apparatus used in this experiment was capable of holding the sample at various temperatures. The samples were tested at three temperatures to see if they followed the same pattern. Figure 3.12 shows the results from one test. As expected the fibrous -matrix samples were stiffest at 5^{o} C and most compliant at 70^{o} C. The current setup did not allow the sample to be heated beyond 70^{o} C. The results fit with the whole capsule findings in that 5^{o}c was slightly stiffer than the 20^{o}C and heating the sample to 70^{o}c resulted in a ~50% drop in yield stress. There is also a noticeable decline in hysteresis. Comparing the height between the load and unload lines in the post yield region the plots go from 2.1 MPa, to 1.6 MPa and finally 1.1 MPa for 5^{o}, 20^{o}, and 70^{o} C respectively.

3.2.3 Micro-Fiber Maturation

All of the fibrous -matrix samples tested had integrity and produced very repeatable Stress/strain curves. There were however variations in the shape of these curves. The vast majority had a well-defined initial modulus (Hookean region) in the loading cycle, but not all showed this region in the unload cycle and some samples lacked these regions altogether. Figure 3.13 shows the variations in the hysteresis curves. These curves showed some similarity to the stress/strain curves associated with the capsule maturation time line in Rappaport and Shadwick (2006).

When the immature looking sample pictures were analyzed for changes in birefringence they had very different birefringence curves. Birefringence varied directly with strain.

Some possible implications of these similarities are examined in the discussion.

3.3 Polarized Light Results

The polarized light studies yielded many interesting results. As previously described the expected result of stretching a random-coil network is that the more you stretch the material the more the random-coils align in the direction of the stretch. This means that order with in the system is increasing and the material can become birefringent. This was confirmed using latex rubber from a dental dam, which became birefringent under strain, see figure 3.14. The results from the latex strain experiment were graphed to test the supposition that polarized light was effective in measuring order within samples held in my apparatus. Figures 3.15 & 3.16 show a positive correlation between strain and birefringence.

The latex rubber sample produced the expected increase in birefringence when stretched. The whelk egg capsules, however, produce a far different pattern. Initially the birefringence rises as the sample is strained in the Hookean region. When the strain reaches the yield point however the pattern reverses. The molecules within the capsule are being stretched in the direction of the strain but retardation measurements are falling. The measure of retardation shows that order within the system is falling during the ramp extension, see figure 3.17.

In Figure 3.17 birefringence clearly shows an increase paralleling the initial rise on the force trace. This trend however ends as the sample enters the post-yield region, and the birefringence falls rapidly with further extension (note: no calculation was used to adjust for strain induced thinning). The recoil portion of the trace (as indicated by the strain) is a mirror image of the extension, showing that the process is reversing its self as the sample recoils. The second peak on the birefringence curves is usually lower than the first peak and was never higher.

The traces take on an interesting shape when pauses are added to the strain tests, see figure 3.18. Moving the pause to the end of the extension in figure 3.19 produce an entirely different pattern in the stress/strain curve. We no longer see the pause as a dip in the stress/strain curve. Now the force relaxation is almost entirely hidden; if the data points were not plotted and the plot was shown as a simple line, the pause graph would be undistinguishable from the simple ramp extensions. The birefringence/time plots on the right in figure 3.19, however, clearly show a steady state during the force relaxation just as in the previous graphs of pauses.

Figure 3.20 shows results from a similar experiment in which the specimen underwent incomplete recoil and a pause test, reveals another interesting phenomenon. In this case the sample was allowed to begin to recoil from a 50% strain, and then it was held in a fixed position at about 40% strain for a few seconds before being re-extended. Force and birefringence actually rise during the pause. The stiffness following the pause is high and birefringence drops again to the same low value upon full extension. Folding the graph to eliminate the pause and re-extension would clearly give us the same pattern as a simple extension. This is true of all the modified extension patterns. The notable difference in this series is that the three birefringence peaks clearly show a downward trend indicating that not all of the order that was disrupted on the extension has been restored yet.

Figure 3.21 is a series of incomplete recoils and re-extensions. All the previously noted trends are present. Birefringence rises in the toe/initial modulus regions and falls in the post yield plateau during extension. The trend is mirrored during recoil. The first and the final birefringence peaks show a downward trend through out the series.

I was not able to collect images of the 5C test sample because fogging of the cover slips obscured the view. The heated samples however were viewable. Figure 3.22 shows a comparison between a sample at 20C and three runs of the same sample at 66C. The changes caused by the heat were completely reversible. The primary effect seems to be

that the initial rise in birefringence diminishes with the reduction in the yield stress caused by heating the sample, rising from 5.7 x 10^{-4} to 6.8 x10^{-4} for the same sample.

What is not apparent in these samples is even more puzzling. While the change in normalized birefringence showed only a diminishing of peaks in the birefringence it hid a second change. The absolute value of the birefringence rose by about 19% as a simple function of temperature. The starting birefringence for the 20C sample was 0.00057, while the 66C starting birefringence was 0.00068, indicating that the rise in temperature by itself was responsible for 0.00011 rise in birefringence, see figure 3.23.

Approximately 15% of the samples examined were immature, unfortunately the insight of identifying these samples as immature came during the writing phase of this thesis and as such most of these samples had been rejected after the initial stress/strain test. The data sets for immature fibers consists therefore of only a few samples that appear to be in various stages of maturation. Examination of one of these samples proved interesting. In this case the birefringence showed a positive correlation with strain throughout the extension. During the recoil birefringence briefly dipped below the initial birefringence value. This sample also showed a fall in birefringence during the force relaxation in contrast to the mature samples that showed no change in birefringence during the force relaxation, see figure 3.24 (also 3.13 B for stress/strain curve). The loss of the initial modulus region therefore associated with the WECP acting like more like a rubber. The stress/strain loops were repeatable indicating that the protein molecules are liked in a stable matrix but the component responsible for the stiff initial modulus has not been established. It should also be noted that actual birefringence values for the immature sample were much smaller. The mature samples had initial birefringent values of 0.6-1.3 x 10^{-3} while the immature sample started at 7.0 x 10^{-5}, an order of magnitude in difference. The implications of this result are explored in the discussion.

The birefringence results were looked at as functions of both stress and strain. Figures 3.25 and 3.26 both show a hysteresis loops associated with the birefringence. In both

cases birefringence returns to the original level but the recovery of the birefringence lags behind stress and strain.

4 Discussion

The discussion is broken into three sections. Two for each of the two lines of inquiry described in the results and a general discussion of conclusions drawn from both studies.

4.1 Stress/Strain

As predicted the WECP fiber samples displayed the same general properties reported for the whole capsule. There are several interesting features that show up in the ramp tests. The consistent repeatable results of the stress/strains curves and the hysteresis are good examples. This material displays a remarkable ability to recover when stretched at a variety of rates. There is no apparent mechanical breakdown in the material. Each ramp test produces almost identical hysteresis loops in both whole capsule and fiber sample tests. The transition that occurs between the initial modulus or Hookean region and the yield states absorbs a lot of energy. The numbers are variable but 45.6% $^{+}$/- 6.8% hysteresis was consistently observed in a variety of tests, see figure 4.1. This means that on average about 45% of the energy used to extend the sample was lost in the process.

The fact that the slopes on the initial extension and the relaxation closely resemble each other indicates that the material is undergoing a strain dependant reversible change in modulus. The proposed model for this behavior is two fold. In the initial stiff region it is believed that the stress is carried predominantly by H-bonds that stabilize the α-helixes, see figure 4.2. It has been proposed (Rappaport and Shadwick 2007) that the model for this protein is a coiled coil similar to that proposed by L. Kreplak et al. (2002). In this region the material is very stiff and resistant to strain. At the yield point however it appears that the α-helixes begin to pop open and the material becomes very compliant. At this point increases in strain produce markedly smaller increases in stress. The modulus at this point drops by an order of magnitude at all the recorded temperature (table 3.1).

This theory is further supported by the behavior of the material during incomplete relaxation loops. If the material is allowed to pass back into the Hookean region, it redevelops the Hookean stiffness. This is significant because it indicates that the α-helixes and coiled-coils attributed with producing this property must be reforming while the material is still under strain. The loops that start the reloading in the yield region (figure 3.5) show an increased stiffness, but it is intermediate between the initial modulus and the yield modulus. Assuming that the post-yield modulus represents pulling open α-helixes in the coiled-coils, the stiffening would seem to indicate that some α-helixes are starting to reform and carry load, but that the original cross-linking matrix (bundles of α-helixes covalently linked together in a way that facilitates load transfer between adjacent α-helixes, Rappaport and Shadwick 2007) has not fully reformed and the stress is being born between a mix of α-helixes and the strained yield format (presumably a jumble of α-helixes in various stages of unwinding).

The pattern produced by pausing the loading during extension suggests the same phenomena. Two things happen during this experiment: First, the force drops during the hold and second when the extension resumes the modulus is noticeably increased. This mirrors the effect seen in incomplete recoils. Once again it appears that the α-helixes may have been partially restored to produce the increase in stiffness. Or, alternatively, the viscoelastic flow is catching up to the strain rate and thus we see a fall in force as this stress is alleviated. This explanation recognizes that the force needed to strain the material is a measure of composite resistance. Some of the force represents the cost of breaking H-bond in the α-helixes. Another part of this force is the frictional resistance of the molecules as they are rearranged by the extension imposed on the WECP. This is the force that decays when the strain is held constant in the force relaxation experiments. When the material is stretched further, the cost of breaking H-bonds is the same and the viscous force component rises as the extension once again forces the molecules to move relative to each other. As the extension continues the viscous force component rises back up to the level it would have been without the pause, and the stress/strain curve is restored to it expected shape.

Force relaxation experiments show that the relaxation has two distinct phases. The first is a rapid drop in force that lasts for about 2 sec. The second is a much slower but steady drop in force; the slope has changed from the initial nearly vertical decline to an almost flat trace. This decline cannot be fitted to a single exponential decay, indicating that the recovery of Hookean properties cannot be explained by a simple exponential equation. This in turn means that a simple spring and dashpot model cannot explain the material properties of WECP, see figure 4.3.

One of the interesting findings of this investigation is that the capsules do not appear to be uniformly mature. Figure 3.13 shows a proposed sequence of maturation. This process of maturation is at present unknown, but there is some speculation that this process may involve covalent cross-links forming that stabilize the material (Rappaport & Shadwick 2007). With time more cross-links may form, increasing this stability. When compared with the maturation process laid out in Rappaport and Shadwick (2007), it seems reasonable to say that the capsules do not mature evenly. Some areas appear to be less mature, i.e. the chemical cross-linking process was incomplete. We still do not know what this process is so we cannot definitively say what is happening during the massaging stage (described in Rappaport and Shadwick (2007)) when the full mechanical integrity is developed. What we can say is that something is increasing the stability of the protein matrix. It may be enzymatic, it may be proximity stimulated, it may be the addition of metal ions or other stabilizing elements, but there is definitely some chemical process at work. The concept of finding regions that did not get a full helping of the hardener is not that surprising and would certainly fit the data.

Kushner et al (2007) looked at the use of unfoldable cross-linkers that increase strength and extensibility, see figure 4.4. What we may be seeing in whelk capsule protein could be an analogous phenomenon, affecting the H-bonds that hold a-helixes together. The H-bonds would be affected by heat and pH stresses. This agrees with the data collected to date for this material. The stability of the protein and ability to recover after the tests would then be a result of covalent bonds that help the H-bond domains find each other again. The regeneration of stiff Hookean properties while under strain would be

explained by some of the H-bonding domains being able to reconnect by some reorientation process involving some parts of the molecule contracting by the taking up of slack in the overall molecule created by multiple H-domains splitting apart. Kushner et al. (2007) described a polymer with H-bond stabilization that can be reversibly broken. Their model molecule is much simpler than WECP but it has two key qualities that make it a useful comparative model. First there are H-bonds that are broken by strain. Second these H-bond domains are held in the overall structural framework of the polymer in a way that allows these regions to line up again and reform H-bond when the strain is removed. If we use the model in figure 4.4A a partial recovery during a hold might look like the diagram in figure 4.4B. For whelk capsules the model is likely to be more complicated, involving the opening and reforming of α-helixes in coiled coils (see figure 4.2 & 4.5). It this case the covalent bonds, shown linking the α-helixes in 4.5 & 4.6, probably joins the protein backbones of the α-helixes and connects the coils. Such an arrangement would encourage H-bond formation by holding H domains in proximity to each other. Schwaiger et al (2002) proposed the same explanation for single myosin coiled-coil, figure 4.5. The stress/strain data for the myosin coiled-coil is very similar in shape to the WECP data, exept that it has a smaller hysteresis loop. This may be due to uncoiled a-helixes tangling with adjacent molecules and/or b-sheets trying to form.

In any case the proposed explanation for the hysteresis loops is as follows. The toe region represents the tensioning of the protein network. The initial modulus is the straining of the α-helixes. The yield region is where the α-helixes are reaching maximum extension and beginning to pop open. The post yield plateau represents a region of disrupted α-helical coiled coil structures that can no longer hold their form because the α-helical coils that form them are being pulled apart. A model based on intermediate filament proteins and polarized light data is provided in the general conclusions section.

4.2 Polarized Light Discussion

The light experiments with the latex rubber (a random-coil network) dental dam clearly demonstrated that birefringence could be used to measure order. The random-coil network, which was initially non-birefringent, began to show birefringence as it was stretched and lost the birefringence as it recoiled. See figures 3.14 and 3.15. Figure 3.16 showed that there was a direct relationship between strain and birefringence.

The data for the whelk egg capsule protein experiments are therefore taken at face value and interpreted as changes in the order of the system. It is clear from the data that there are interesting things happening within the protein matrix. The first is that there is a high degree of order in the micro-fiber samples (Birefringences of 5×10^{-4} or greater) when they are at rest, as evidenced by the way the samples appear to glow under polarized light. Pure intermediate filaments have a resting birefringence of 4×10^{-3} (Fudge 2003) while the dental dam (not pure rubber) started at 5×10^{-5}) There is a clear pattern in all of the experiments to date. When the WECP is strained in the toe and initial stiff region the stress/strain curve the α-helixes are being pulled into alignment with the axis of the strain and the α-helix's H-bond are being strained. Recall that figure 3.2 showed that the micro-fiber samples are made up of a web like fibrous-matrix. The imposed strain would pull on these filaments, causing them to become more oriented with the axis of strain, is somewhat similar to the birefringence generated in latex rubber in that the birefringence rises as the material is strained and falls as the material recoils because of strain induced ordering of its molecules. Strained crystalline structures (i.e. α-helixes in WECP) also produce increases in birefringence (Crawford, 1953). The interesting results come when the material reaches the yield point (5-20%). Here we see the birefringence peak and then it declines as the material is strained in the post-yield region. This indicates that the yield is associated with a drop in order within the system.

Models for this protein have proposed that it is made up of intermediate filaments which form α-helical coiled coils (Rappaport and Shadwick 2007). Unpublished results from

A. Miserez UCSB, have confirmed the presence of α-helixes using x-ray diffraction. It has also been suggested that the yield region represents a breakdown of these helixes. β-sheet formation (figure 4.7) was detected by x-ray diffraction at high strains in excesses of 100%. I have no data showing β-sheet formation in my tests. I can assert however that no stable β-sheets were formed because the samples tested all produced repeatable hysteresis loops indicating that the WECP repeatably returned to its initial state. The formation of stable β-sheets would have changed its stress/strain properties in subsequent cycles. It is possible that I did not strain any of the components sufficiently to produce β-sheets; it is also possible that this material is not able to form stable β-sheets due to some as yet undisrupted constraint, such as interference from side groups or other molecules.

If the above-mentioned model is accurate, the sample should lose order, as the helixes break open. My data support this hypothesis because there is a clear drop in birefringence and therefore order in the system when the samples are strained in the yield region. At this point there are two opposing forces affecting birefringence measurements. Opening α-helixes is reducing order and stretching the random loops create when the α-helixes open is increasing the order. Accurately measuring this change in order is complicated by the fact that path length used to calculate the birefringence is decreasing as the sample thins due to stretching. Having taken that limitation into consideration, however, it is still reasonable to assert that the loss of a-helical structure is dominating the overall birefringence and that on average order is declining in the post-yield plateau.

Consider that birefringence (double refraction of light) can be generated in two ways. Form birefringence is created by light bending at the edges of objects. This is a property of refraction and it can be compensated for by surrounding the object in a medium that has the same refraction index as the sample under examination.

Intrinsic birefringence is also a result of the double refraction of light but it is caused by order at the molecular level. When the latex rubber became birefringent it was a result of intrinsic birefringence that gained strength as more and more of the random coiled rubber molecules (isotropic condition) were lined up in the same orientation (anisotropic

condition), and the refraction increased as the molecules became more ordered, see figure 4.8. Intrinsic birefringence is also seen in crystalline structures such as topaz and quartz where the molecules are arranged in highly ordered structures.

Total Birefringence = Form Birefringence + Intrinsic Birefringence

The birefringence measured by my experiment is a combination of these two sources of birefringence. Initially straining the sample (strain<5%) does not affect α-helices structures. The strain merely loads the α-helixes and aligns them in the direction of the strain. This has the effect of introducing more intrinsic birefringence, while leaving form birefringence unaffected. When the extetion exceeds the maximum length of the H-bonds in the α-helixes they have to unravel and this affects the intrinsic birefringence produced by the structural order of the protein molecules. This effect becomes apparent when the strain passes the yield point and birefringence begins to fall. At this point the contribution from the intrinsic birefringence is declining, as the structures that produced it are pulled apart. Keep in mind that the loss of α-helixes creates disordered random loops (loss of birefringence) that are then pulled into alignment with the strain (increasing birefringence), see figure 4.6c. The key point is that the net effect of all these interactions is an overall loss of order in the system.

Figure 3.17 shows a typical stress/strain experiment in which the birefringence was tracked. The forces progress through the toe region, initial stiff modulus, yield and post yield plateau regions. Qualitatively there is little visible change in the sample to the eye (some shadows change but over all they appear similar). The birefringence measurement however record a 14% overall change in birefringence in this experiment. Clearly things are changing as the experiment progresses. The interpretation of these results is that the strain is imposing changes to the material on a molecular level. The toe region most likely represents the taking up slack in the system (at the fibrous network level); loading has barey begun, but strain-induced ordering is clearly visible in the birefringence plot. As previously mentioned the initial stiff modulus is where the strain is born by the α-

helixes. These are stable, stiff structures that do not easily yield. At the yield point however something gives. The fact that the birefringence goes down at this point strongly supports the hypotheses that the α-helixes are popping open as illustrated in figure 4.6. The reasoning behind this is that α-helixes of hagfish slime intermediate filaments are highly birefringent (birefringence 4 $x10^{-3}$) Fudge (2003). Fudge et al. (2003) demonstrated the formation of β-sheets in hagfish intermediate filaments under strain; a condition that could only occur if the α-helixes popped open and reformed into β-sheets (see figure 4.7). The post yield plateau therefore represents the cost of opening these α-helixes. At this point everything that has happened is completely reversible. A variety of hold experiments, some as long as five minutes, produced no significant change in subsequent hysteresis loops, indicating that a stable set of cross-links must be anchoring the intermediate fibers in a fixed matrix. Stress is deforming the protein temporarily, but it is not destroying the original network.

Looking at the birefringence results from various experimental protocols gives us more interesting results. Experiments that extended the fibers beyond the yield point typically had a lower birefringence in the final peak than the initial peak. This clearly showed although recovery of ordered structures is occurring during the recoil, the sample has not yet fully recovered at the final peak. This is most clearly seen in figure 3.21. This could be for two reasons; first of all there must be sufficient slackening of the strain to allow reformation of the α-helixes and second there may be a time lag in the restoration of the α-helixes. The hysteresis in the birefringence/strain curve (figure 3.26) clearly supports this explanation.

Figure 3.18 shows that a hold during the extension produced a flat section in the birefringence. This demonstrated that whatever process is taking place in the stress relaxation is neutral in terms of birefringence. In the initial stiff modulus region this is probably because there is very little happening. Stress relaxation here is very small but it increases as the sample is extended into and beyond the yield region. In the post yield plateau the stress relaxation is much more noticeable and there is clearly a rearrangement taking place because stress curves show a regeneration of some of the initial stiffness.

The simplest explanation of this is that popping open of α-helixes during extension is a random event that occurs at various locations. When this happens it would create slack in the WECP. The stress relaxation is then a redistribution of this slack; the drop in force is due to viscoelastic flow catching up to the strain. We had speculated based on the increase in modulus following a pause that there was some reformation of some of the α-helixes that have opened during the extension. The graphs, however, do not show an increase in birefringence, in fact if anything they show a slight drop in birefringence. Examining pauses at the end of the extension, figure 3.19, we can see that the pause produces the aforementioned flat region in the birefringence curves, while force on the other hand is clearly relaxing. Any proposed reorganization would have to be birefringentce neutral because any order restored by the reformation of α-helixes is at the expense of other sections that are coming apart. In any case, splicing out the pauses during extension, figure 3.18, gives the same birefringent plot as a simple extension/relaxation. Interestingly figure 3.20 shows that if the sample is paused during recoil it has a stress increase and a corresponding increase in birefringence. This argues that order is reestablishing even under strain. This is supported by the mirroring of the initial stiffness on the unload curve. This phenomena should be looked at further with better time resolution of the optical data to fully explore what is happening during this pause.

When incomplete recoils are examined the birefringence curves once again show remarkable repeatability. The midsections could easily be spliced out to produce curves that look like the simple extension/recoils. Once again, this argues that the WECP molecules must be bound together by stable links and that it responds to stress in very predictable ways. What does change in this case is that the second and third peaks of the birefringence do not reach the same initial level of the first peak. This indicates that incomplete recoils are preventing a full reestablishment of the original order seen at the start of the experiment. An interesting result given that the force curves rejoin the first extensions have similar profiles but the re-extension curves are always jut a little under the original primary extension curves. Given the relatively short distance of 0.16 – 0.20 nm that H-bonds operate over, however it is not surprising that even small strains would

be capable of disrupting bonds. An incomplete-recoil could therefore be interpreted as having an incomplete restoration of H-bonds in the α-helixes. The results from this experiment show that the material needs to recoil into the toe region or further to re-establish all of the α-helixes.

Temperature had the effect of lowering the force of extension. This is significant because heat denatures proteins by weakening H-bonds. Zhuang and Prohofsky (1989) reported values for melting H-bonds in DNA helixes at 67-77C. Kato A. and Takagi T. (1988), found α-helix denature in favor of forming β-sheets over the range of 74-84C. These are very close to the 78-92C region were the initial stiff modulus disappeared in whelk capsule protein stress curve. See figure 1.3 for a summary of whole capsule results and figures 3.12 and 3.23 for capsule fiber results. Heating fiber samples to 70C caused my samples to lose about 50% of the yield stress. This is consistent with the whole capsule data in figure 1.3. The effect seen in the birefringence data is small but noticeable; the sharpness of the birefringence peak in figure 3.23 and 3.24 is lost and the absolute value of the birefringence shifts up. Heat lowers the yield stress and the toe region disappears. Heat also affects the birefringence measurements. With the loss of the toe region the initial rise is much reduced and the minimum is much lower.

The immature fiber data gave us further food for thought. These samples had a stress/strain curve that resembled wet hagfish slime threads (Fudge et al 2003), figure 4.11. These hagfish threads were identified as being made up of intermediate filaments joined together by bond interactions in the soft globular end regions of the filaments. Under this model strain occurred primarily in the globular regions and the associated stress was low. The same model is proposed for WECP. It is believed that the immature sample lacks the cross-linking bonds necessary to carry the stress from α-helix to α-helix. Soft globular regions therefore carry the load and the immature fiber acts like a random coil network.

This supposition is supported by the fact that birefringence is positively correlated with strain and stress in the extension portions of graphs 3.24 A and B. The birefringence

inceases in these graphs is stress-induced birefringence. During the stress relaxation in figure 3.24 B we see the birefringence fall in parallel with stress. The dip in birefringence below initial values during the recoil is attributed to some α-helixes having popped open during the strain needing time to recover. By the end of the strain we see that birefringence has completely recovered and that the protein is in a structurally stable crosslinked matrix. This same trend is clearly seen in figures 3.21 and 3.22. In both plots the recovery of birefringence clearly lags during recoil and the recoil birefringence peak is lower than the extension birefringence peak indicating that the restoration of order lags behind stress and strain during recoil.

Both immature and mature WECP samples are birefringent when at rest. This birefringence is attributed to the crystalline α-helical structures in the WECP. These structures would have to be present in all samples of the WECP because these are self-assembling structures that would spontaneously form during protein synthesis. The variation in initial birefringence values for these samples must therefore indicate a difference in the overall alignment of these helixes. If the α-helixes were randomly arranged their individual birefringences would cancel out. The immature sample must therefore have directional alignment; the difference between the mature and immature samples initial birefringences would therefore indicate that alignment of the helical structures has increased in the mature samples. Once again the data supports the model (see general discussion), as it is reasonable to propose that cross-linking the helixes would increase alignment between adjacent helixes.

4.3 General Conclusions

The whelk egg capsule protein fibers tested showed the same overall properties as the whole capsule samples. Toe region, initial high modulus, yield and post yield plateau are present in both whole capsule and fiber samples. The highly repeatable hysteresis loops have now been demonstrated to be a property of the fibers and not a result of the

macroscopic laminar nature of the whole capsules. The most notable differences between the whole capsule data and the fibers are that failure in the latter comes at a much higher strain and is accompanied by a rise in modulus. This is likely due to failures on different levels. With whole capsules the stress/strain curve reflects fiber properties but failure is more about the delaminating of the crisscrossed layers. In this study the failure measured was the failure of the fibers that make up the layers. The tertiary modulus seen in the failure curve for the fiber sample most likely indicates that there are no more α-helical structures to break open and that we are now straining the backbones of the molecules that form the α-helices. At this point β–sheet structures are expected and unpublished x-ray data detected some β–sheet signal at high strains, but the signal is lost on recoil indicating that stable β–sheets did not form. Keep in mind that hagfish slime threads, which are pure intermediate filaments, do form β–sheets, Fudge at al (2003).

Figure 1.5 shows how the egg capsules develop mechanical properties over time. This was proposed to be a chemical maturation involving the cross linking of the α–helical protein chains. My own investigations found that the fiber samples had a variety stress strain curves that could be arranged in a progressive sequence. This was interpreted to be an artifact of the maturation process. Simply put, whatever enzyme or chemical process was responsible for crossing linking the α–helixes had not occurred homogenously through out the egg capsule. Some samples still exhibited traits associated with the immature capsule. Figure 3.13 showed a progression of stress/strain graphs contrasting how properties may develop as the protein matures. The initial graph is the only case where there was some non-recoverable deformation, but that only showed up on the first extension. Subsequent extensions produced stable loops; indicating the initial extension had caused a rearrangement of the material. What is interesting however is that molecules appear to have only slid past each other so far and then they locked into place. This suggests that there is some sort of self-assembly mechanism that holds the immature protein in the right conformation for cross-linking. In our model this deformation would be represented as the “Q-tip” ends of the α–helical coiled coils sliding along another α–helical coiled coil until a binding site is found and a stable link is made, figure 4.9 show possible alignments for dimer-dimer alignments. Figure 1.6d is a TEM scan of

WECP; it shows a regular banding pattern that could be attributed to the lining up of these globular heads.

Fudge and Gosline (2003) examined hagfish slime threads (intermediate filaments in water) and compared them to hard keratins (composite materials made up of intermediate filaments held together in a matrix), figure 4.10 insert. They proposed a cross-link model for the hagfish slime intermediate filaments and they noted that wool and hagfish slime had substantially different initial modulus. They proposed that the difference was in cross-linking. Figure 4.11 shows similarities between hagfish slime threads and immature whelk protein. Figure 4.11A & B are hagfish slime. Figure 4.11 C & D are whelk protein samples that resemble the hagfish slime thread samples. The hagfish samples are known to be made up of intermediate filaments. If the whelk protein is a keratin analog as previously proposed, then it to should be made up of intermediate filaments. The fact that immature samples seem to resemble the hagfish slime threads supports this assertion. It also points at the maturation process as being the key to the development of the whelk proteins stiff initial modulus. This makes sense if you compare the mature whelk protein capsule data with merino wool (hard keratin). In this case the intermediate filaments are embedded in a hard matrix and the curve is similar in shape to the whelk protein hysteresis loops, see figure 4.10.

My conclusion is therefore that the mechanical properties of this protein arise from the interaction of two factors. One is that components similar to intermediate filaments in the whelk egg capsule fibers are cross-linked in a stable matrix. The second is that the α-helixes of the filaments are functioning both as the stiff elements in the initial modulus and as the yield components in the yield and post yield plateau. Unpublished work from UCSB has detected α-helixes using x-ray diffraction. This signal diminishes as the material in strained indicating that the α-helixes are being disrupted by the strain. This supposition is supported by Rappaport and Shadwick (2007) findings that formic acid and heat cause the initial stiff modulus to melt away. My own tests confirm the same effects on fiber samples. A model for theses attributes is proposed in figures 4.2 and 4.6.

Figure 4.12 is a summary diagram that explains the hierarchy of structure in whelk egg capsules. The primary level is the α-helixes referred to above. The next level of hierarchy requires that the α-helixes must be cross linked in some way that allows the transfer of stress from helix to helix throughout the fiber sample. Figures 4.12 B and C show models of how intermediate filaments join at this level of organization. 4.12 D is a TEM of the capsule. 4.12 E is a 3D second harmonic scan that shows the porous nature of the middle layer of the capsule. 4.12 F is a cross section showing the three layers that make up the capsule.

Future research should seek to sequence the protein(s) that make up the capsule. Identifying if the capsule is composed of intermediate filaments or if it is a new α-helical protein will be very informative. Further attempts should be made to use second harmonic imaging to probe for changes during extensions as this could also provide useful information. This process uses the natural florescent properties of the protein to generate images of the protein. Because the signal come directly from the protein, not a dye tag, it has the potential to visualize changes in the samples microfilaments during extensions. The second harmonic system I had access to proved inadequate for the task because it was not designed **specifically** for second harmonics. A more sensitive system would have a better chance of detecting real time changes in the material as it is stressed. The keratins that this material has been compared to have a matrix surrounding the intermediate filament coiled coil bundles. A careful examination of the capsules with x-rays or NMR may find that there is a soft protein matrix associated with helical elements of this keratin like protein. Given this WECP ability to fully recover on recoil it seems likely that this may be the case.

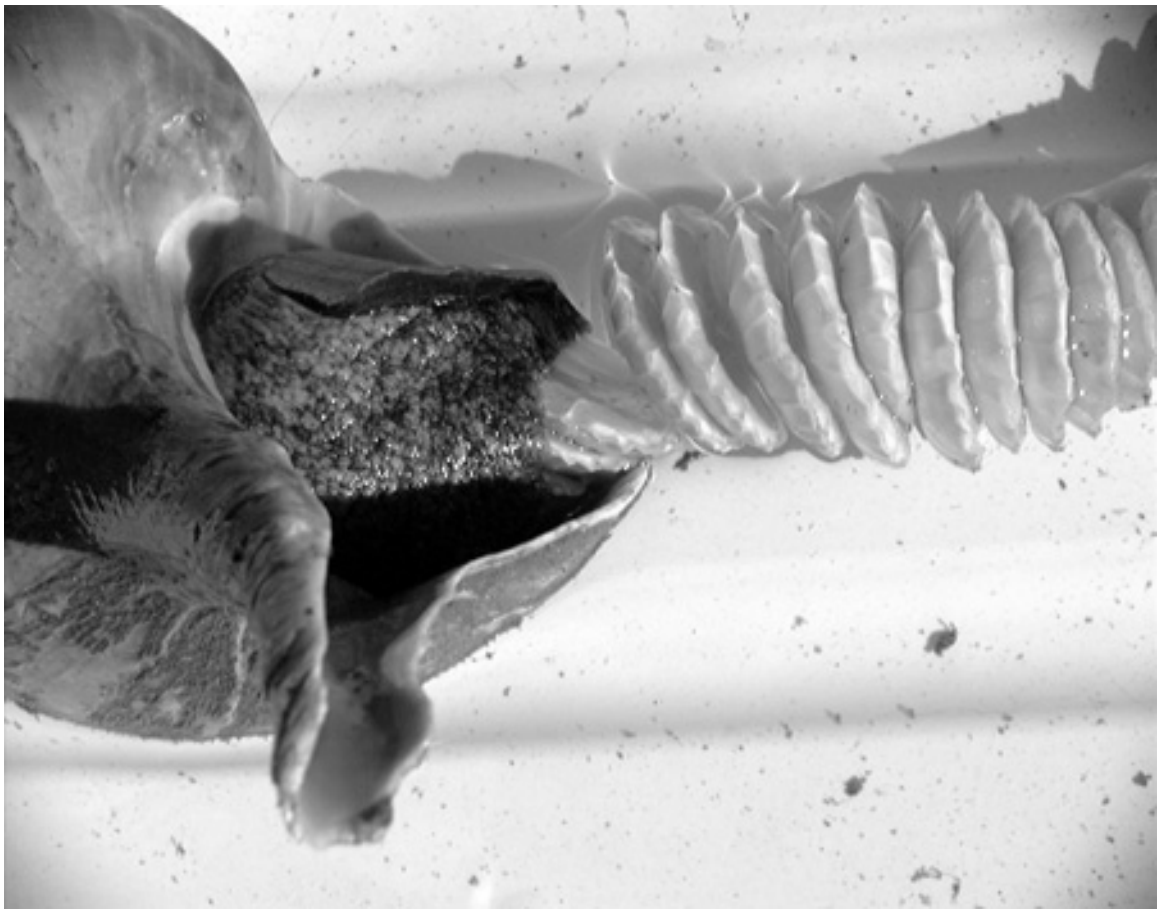

Figure 1.1: Photo of *bussycon canaculatum* secreting a string of capsules.

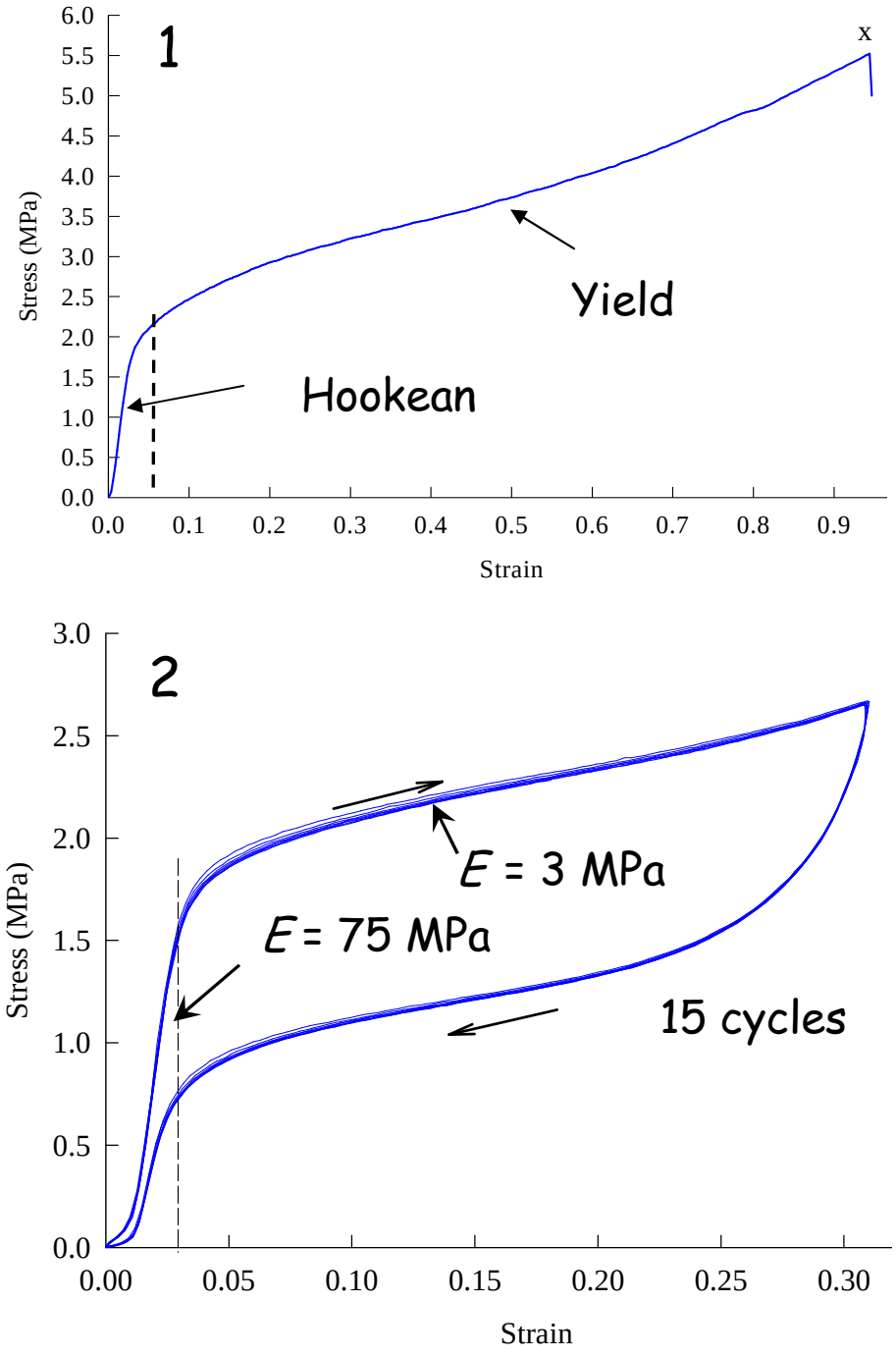

Figure 1.2: Tensile tests show the capsule polymer is an elastomer with two-phase behavior. **1**. The capsule has high stiffness at strains of <5% (Hookean region). With further extension, the material yields to a rubbery stiffness and breaks at about 100% extension. **2**. with load cycling it is apparent that the material is stable to repeated extension, with the yield being transient and reversible. *E* = elastic modulus. Reproduced with permission from Biomacromol Rapoport & Shadwick, 2002 .

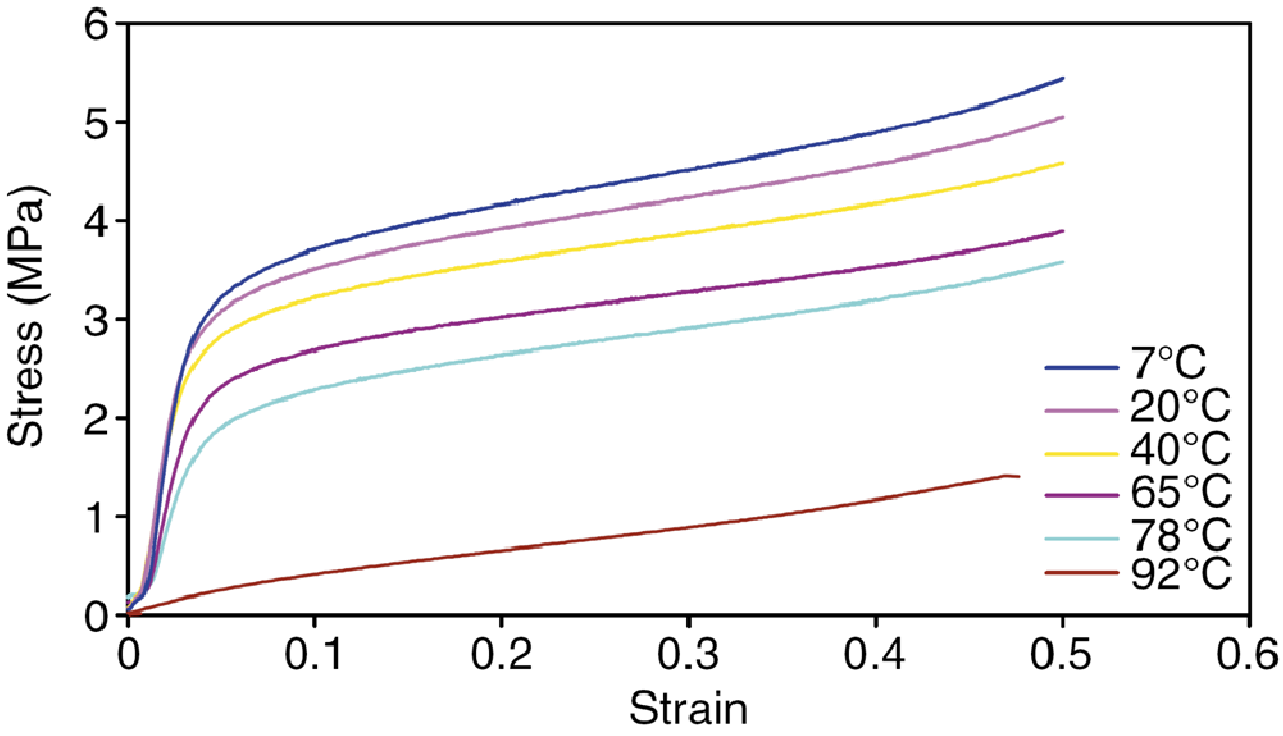

Figure 1.3: Successive tests of whole capsules at increasing temperature. There is a progressive drop in the yield stress with increasing temperature. Reproduced with permission from Journal of Experimental Biology, Rappaport and Shadwick 2007.

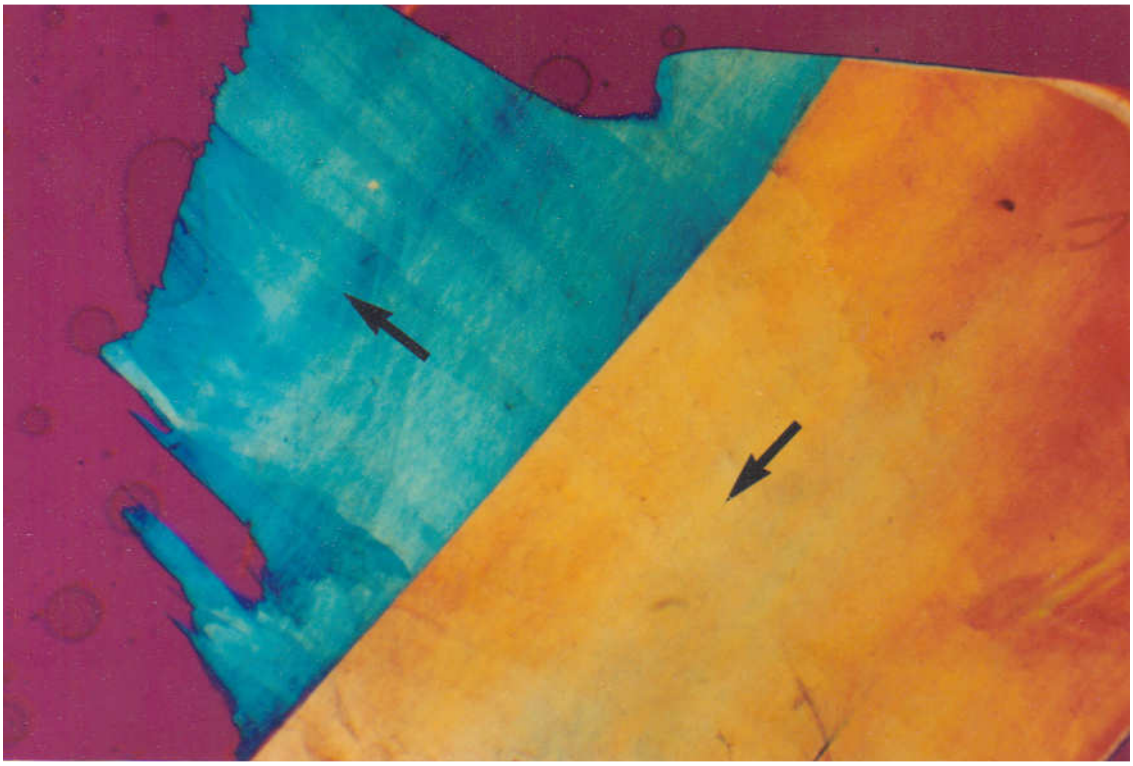

Figure 1.4: Whelk egg capsules are made up of successive laminations of crisscrossing layers. A birefringence microscopy image using false colour indicate the orientation of the fibers in the layers.

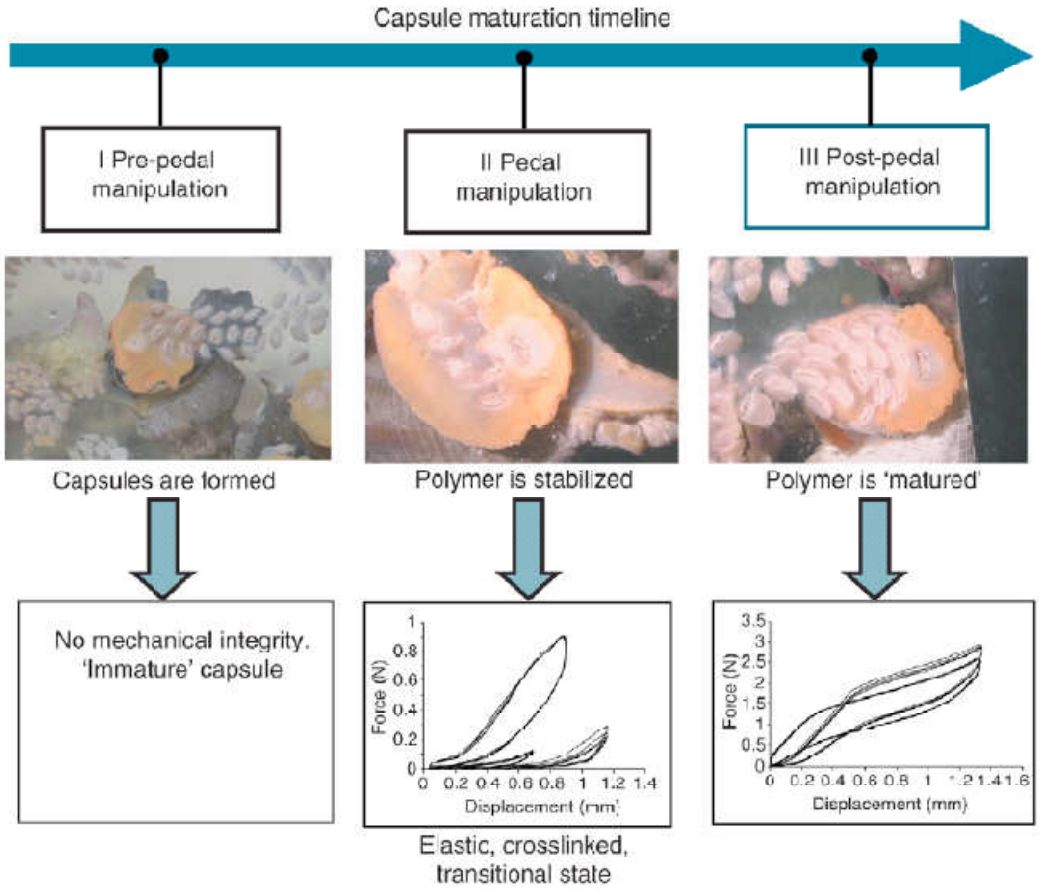

Figure 1.5: A reproduction from Rappaport and Shadwick 2007 outlining the development of mechanical properties in whelk egg capsules. Reproduced with permission from Journal of Experimental Biology, Rappaport and Shadwick 2007.

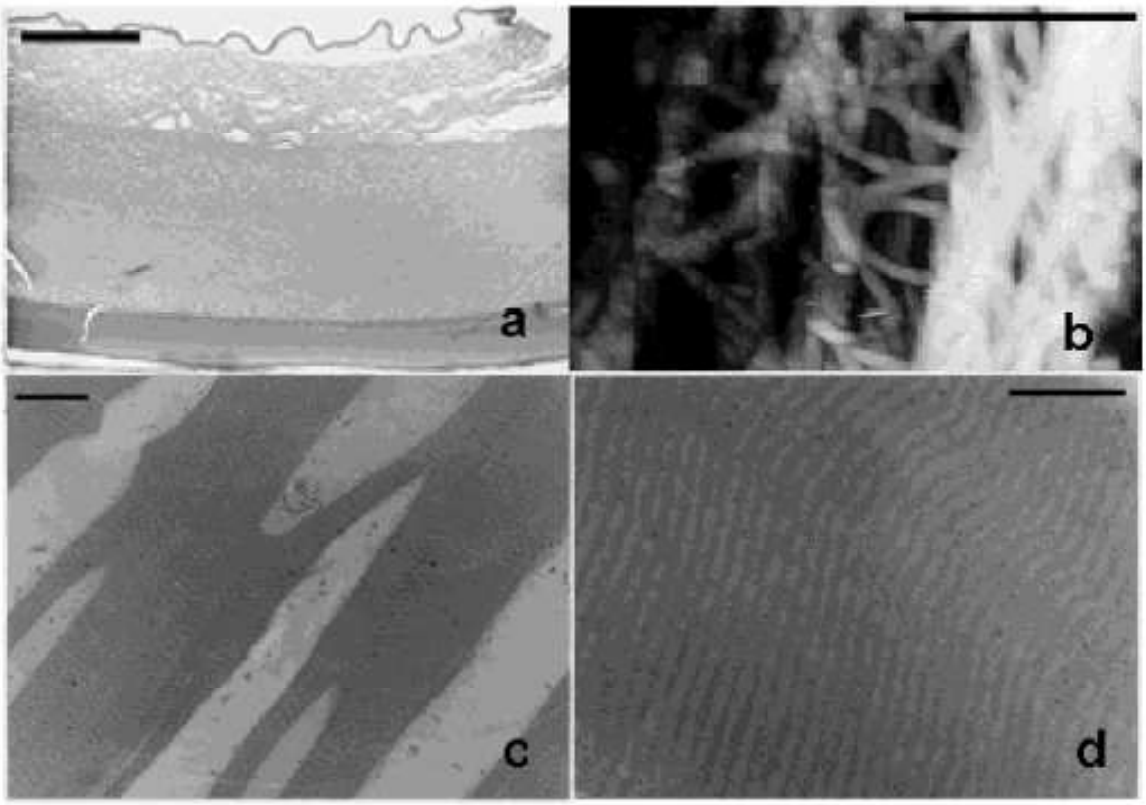

Figure 1.6: Earlier Microscopy of a B. canaliculatum egg capsule. (a) Light micrograph of a section perpendicular to the face of a capsule. Top layer is directly exposed to the marine environment. Bottom layer is the interior of the egg case. Scale bar is 40 ím. (b) AFM of interior surface of egg capsule. Scale bar is 4 ím. (c) TEM, scale bar is 750 nm. (d) TEM, scale bar is 250 nm. Dark bands areapproximately 3.2 nm in width.Periodicity of banding pattern repeat from both B. carica and B. canaliculatum varied from approximately 48 nm to approximately 52 nm. In both capsules there are amorphous-appearing regions where striations are not detected via TEM. Reproduced with permission from Biomacromol, Rapoport & Shadwick, 2002.

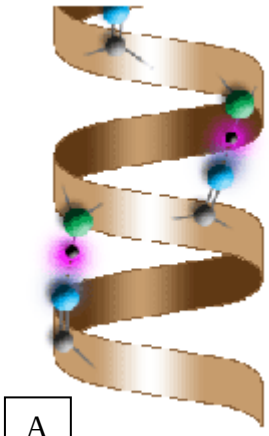

A

5.4 A
(3.6 residues per turn
5.15 A pitch)

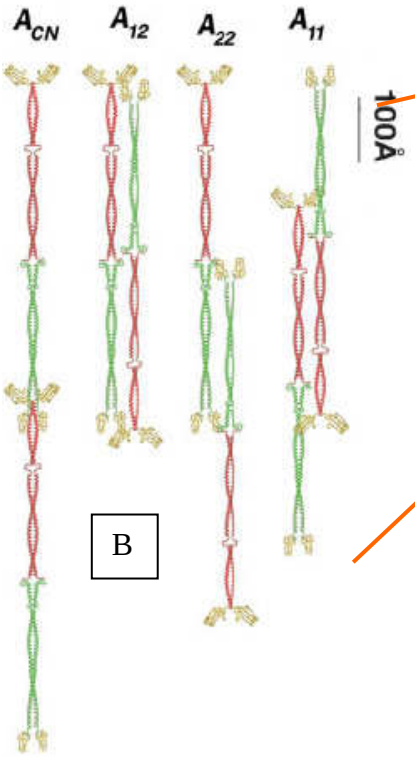

B

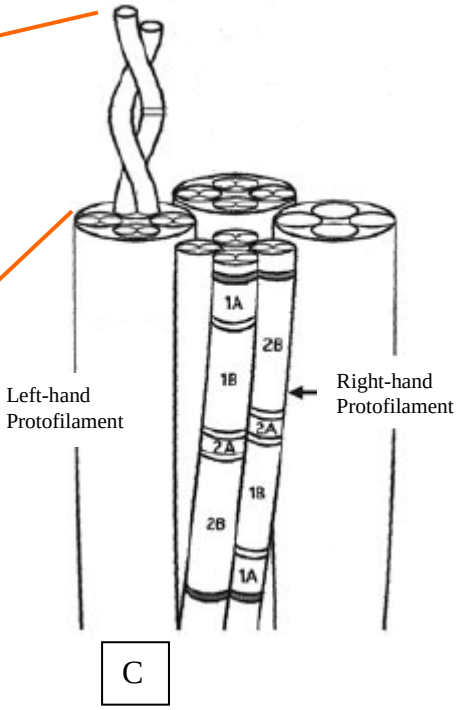

C

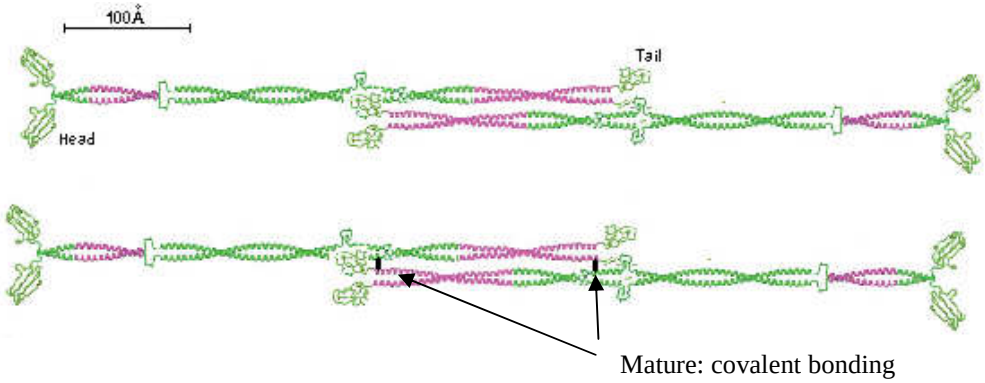

D

Figure 1.7: A hierarchical model showing the arrangement of α-helical components of intermediate filaments fit together A: α-Helix; Known to be a component of WECP. B: Models of how coiled coil components of IF could join. Our model assumes that WECP is made up of similar components, linked by covalent bonds. C: A model of Intermediate filaments; WECP exhibit similar properties. The globular portions of the Dimers my produce the banding pattern in figure 1.4d. D: Proposed covalent linking of a-helixes to transfer load when strained.

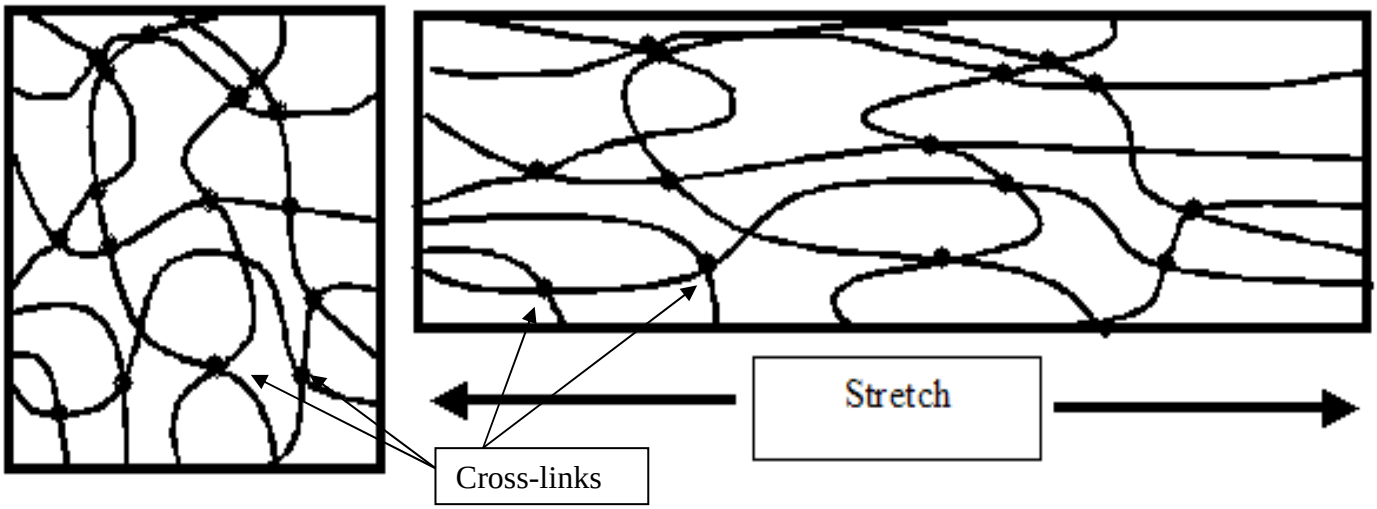

Figure 1.8: Basic theory of order in a rubbery elastic material. The rest state for a rubber is random network of molecules. When a rubber is stretched order is imposed on this random network as molecules begin to line up with the direction of the stretch. Cross-links prevent molecules from flowing, so the molecules must change shape.

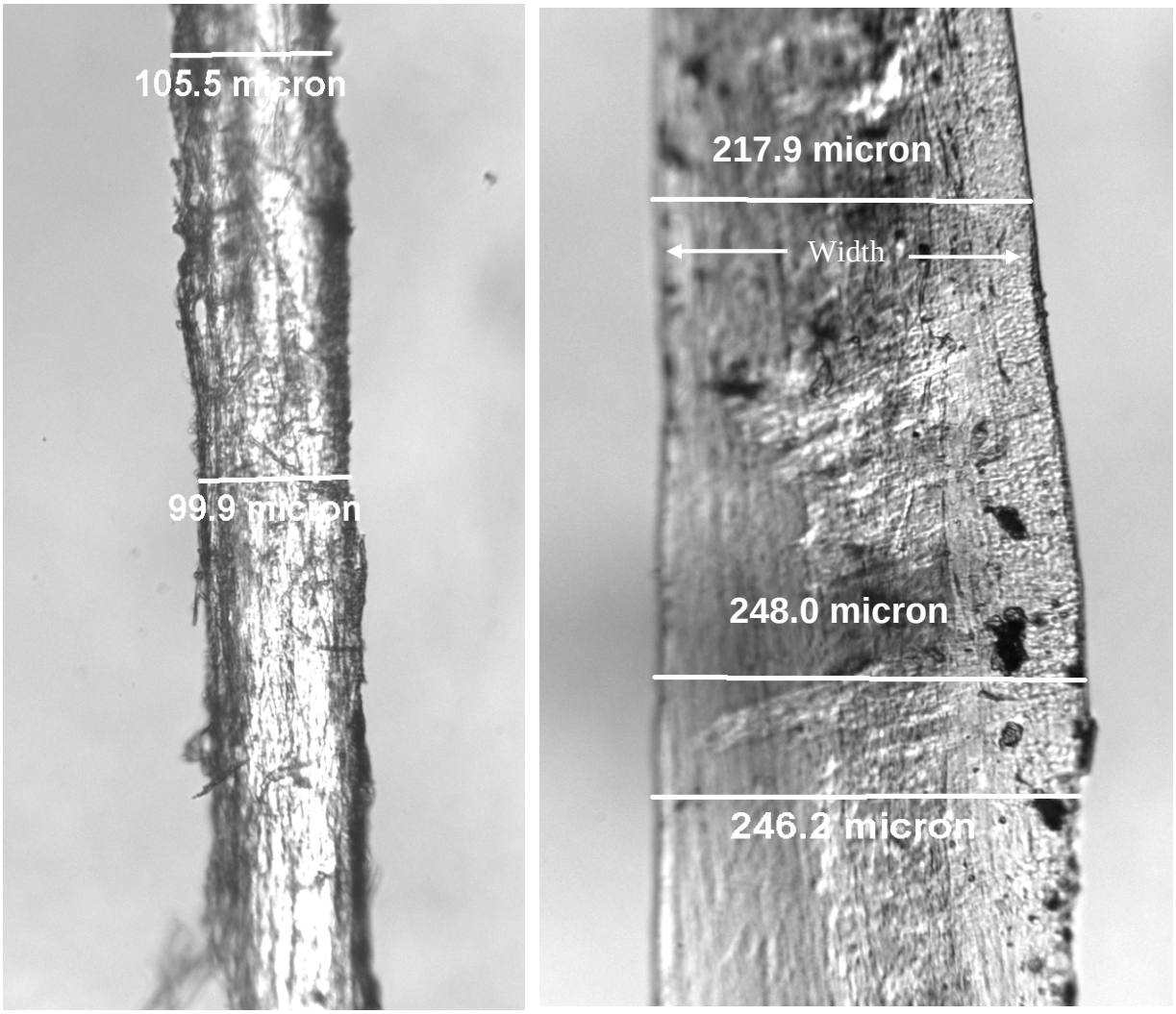

Figure 2.1: Light microscopy of fiber samples from a whelk egg capsule. The sample on the left is from the middle layer, which looks like network of fibers. It teases apart into long fibrous strips of relatively uniform in width. The sample on the right is characteristic of samples from the inner and outer layers. These layers look like a continuous sheet and it is very difficult to tease out samples with uniform widths. The stress/strain curves for both layers where similar in shape, indicating that the only real difference between them was the fibrous vs. sheet layout motifs (i.e. density). The mid layer is estimated to be 1/3 WECP and 2/3 open spaces. Mid-layer samples were used for all experimental analysis. All sample exhibit a strong axis of alignment when viewed under polarized light (top to bottom in these photos).

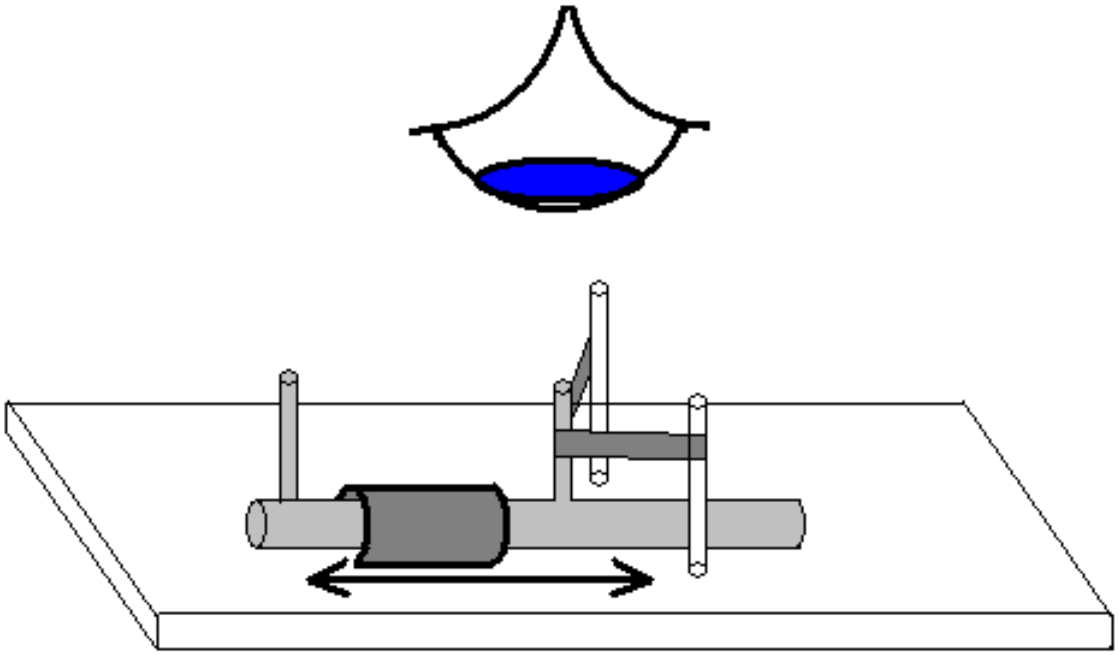

Figure 22: Schematic of thickness measurements. The sample was glued to two fixed posts and then lightly tensioned to hold the fiber for an edge on view.

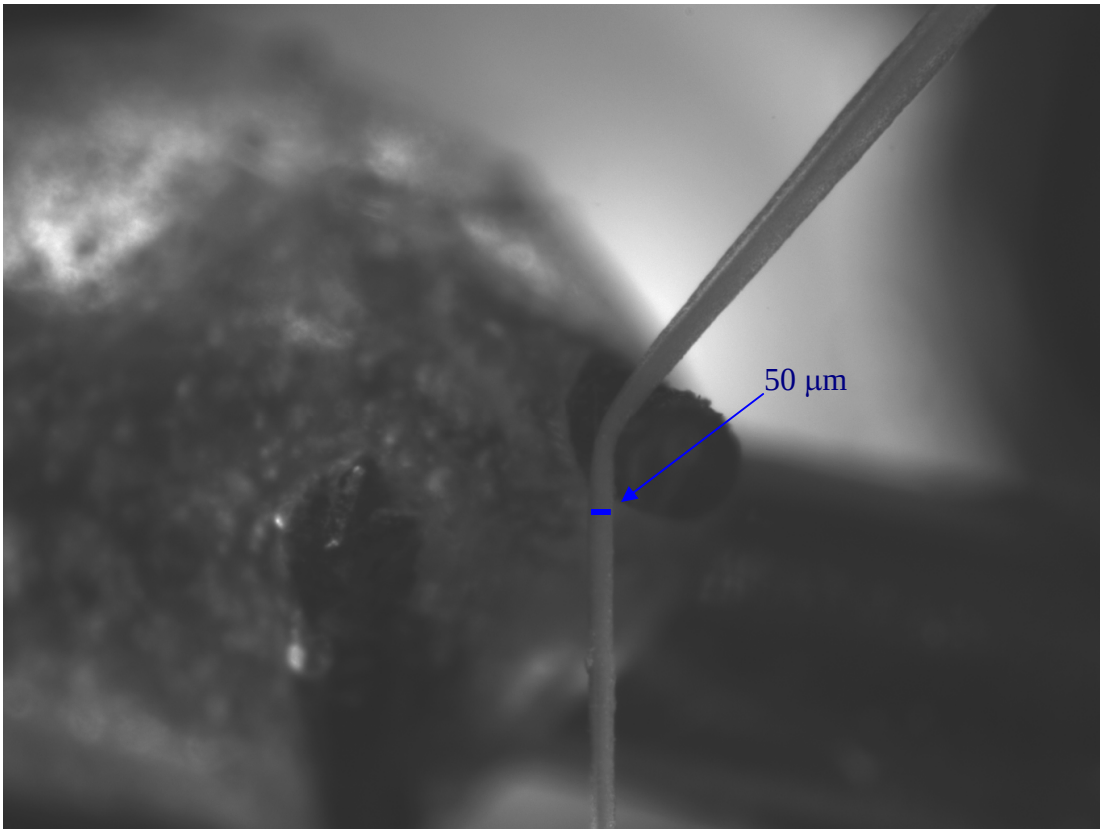

Figure 2.3: Image of a fiber sample being held for thickness measurement.

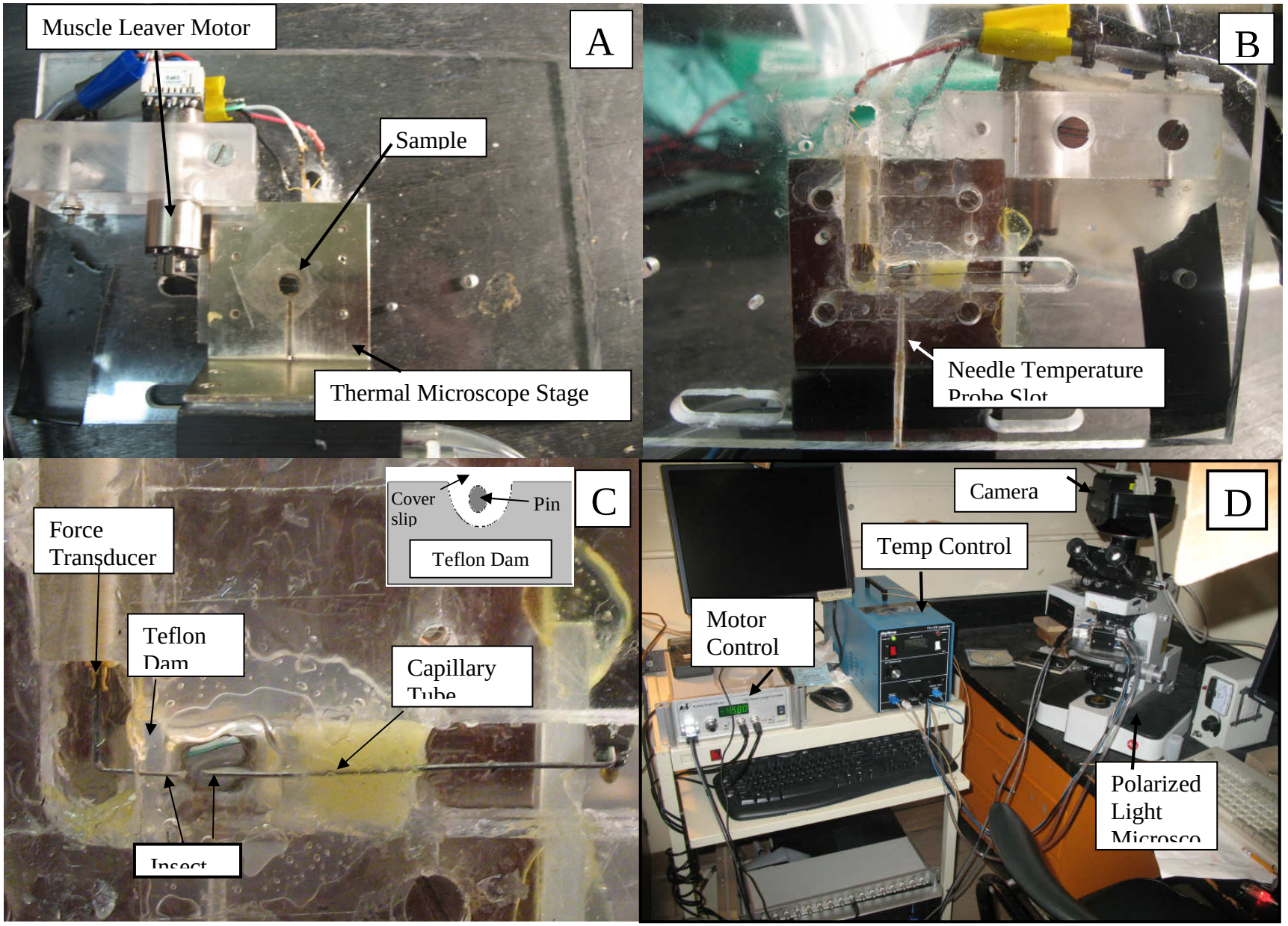

Figure 2.4: A- Top view of test mechanism. B- Bottom view of mechanism. C- Close up of bottom view. Insert schematic of nylon dam D- Lab set up.

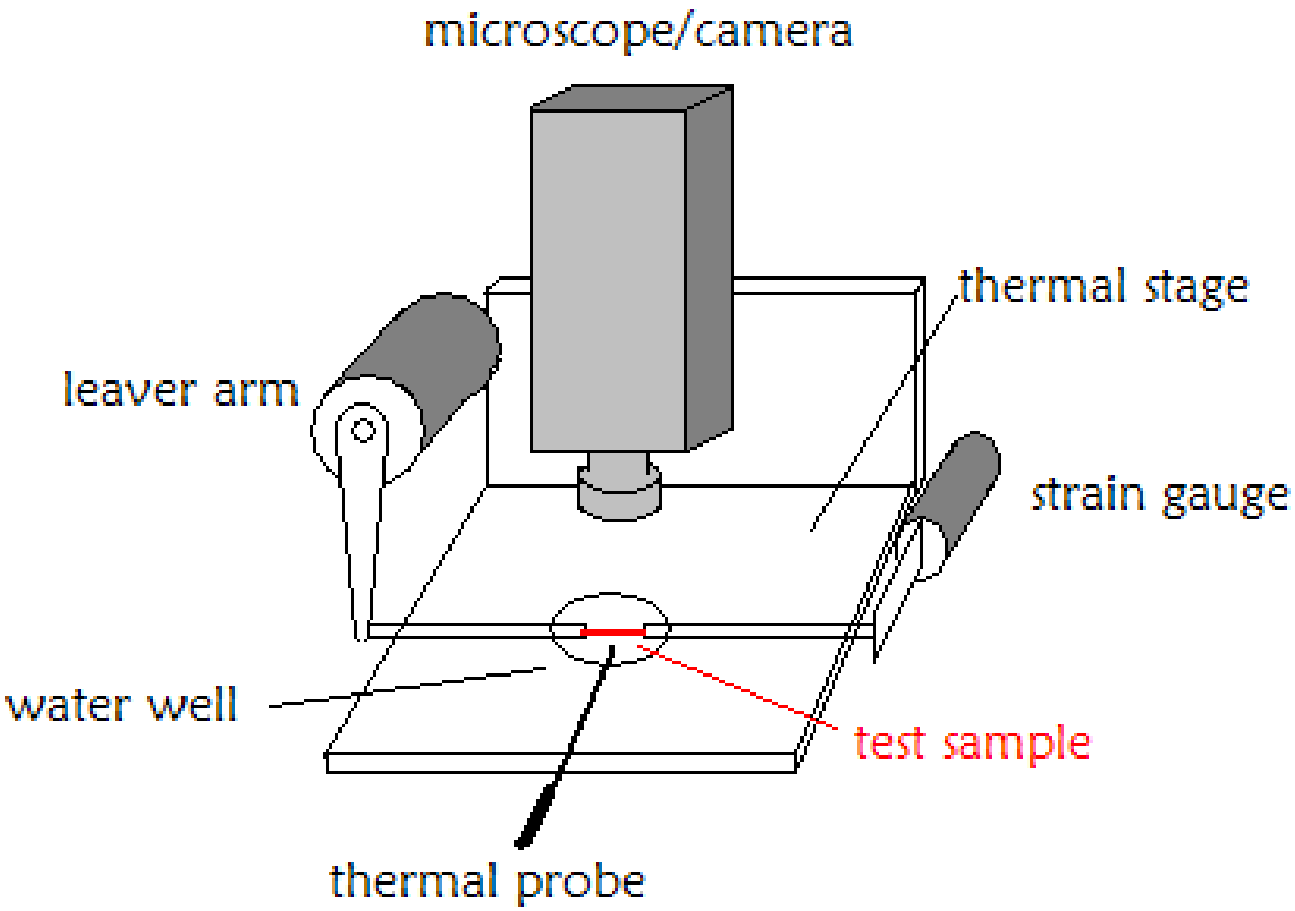

Figure 2.5 A schematic of the test apparatus.

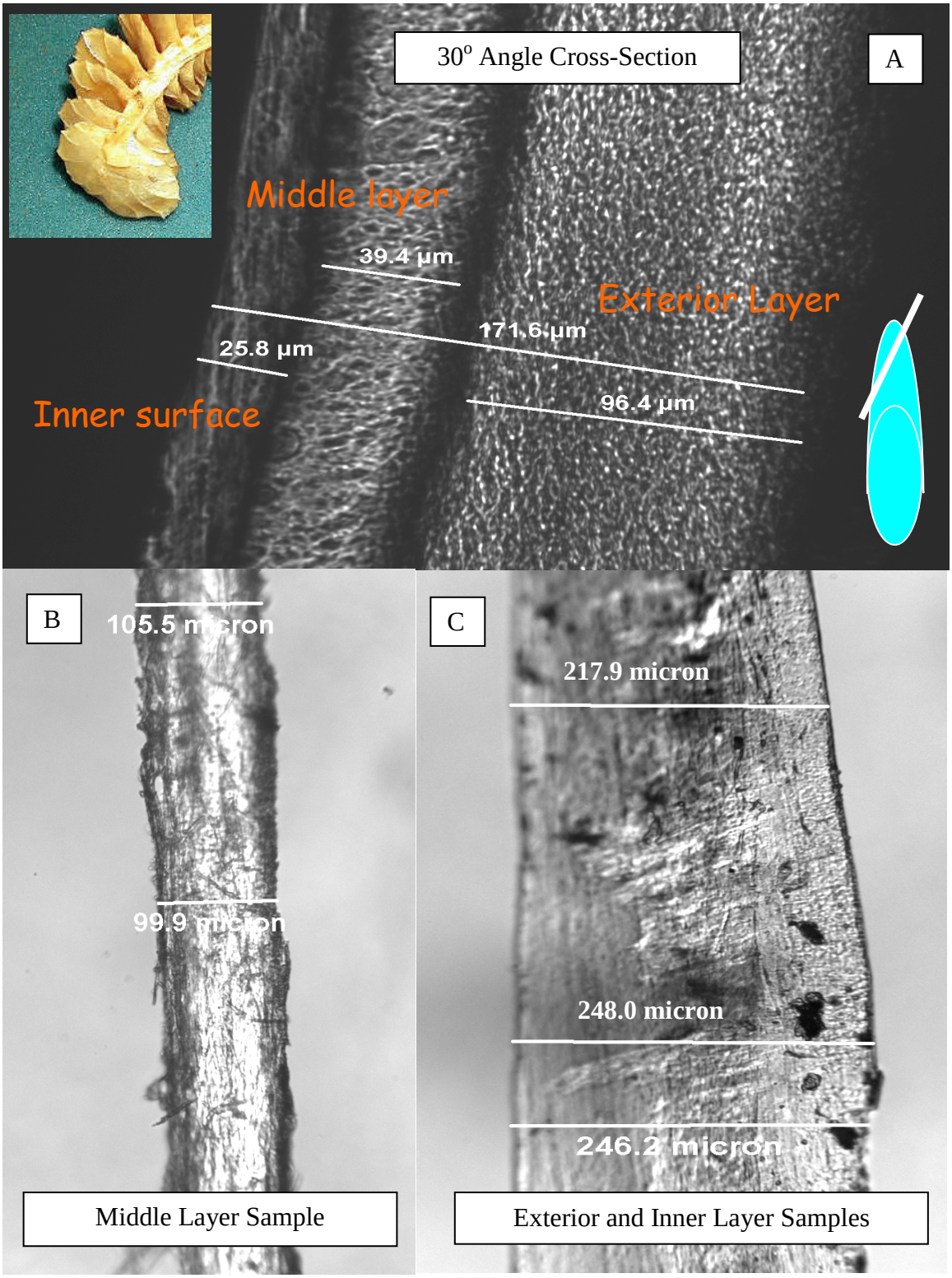

Figure 3.1: A series of photos showing the make up of the egg capsules studied. A: The three distinct layers of the capsule are identified. B & C: Top views of mounted WECP samples, showing the difference in appearance and uniformity of shape (gray scale photo viewed under polarized light with cross polarizers set at 10 deg to illuminate the back ground). Each layer itself is made up of 10 µm laminations of WECP.

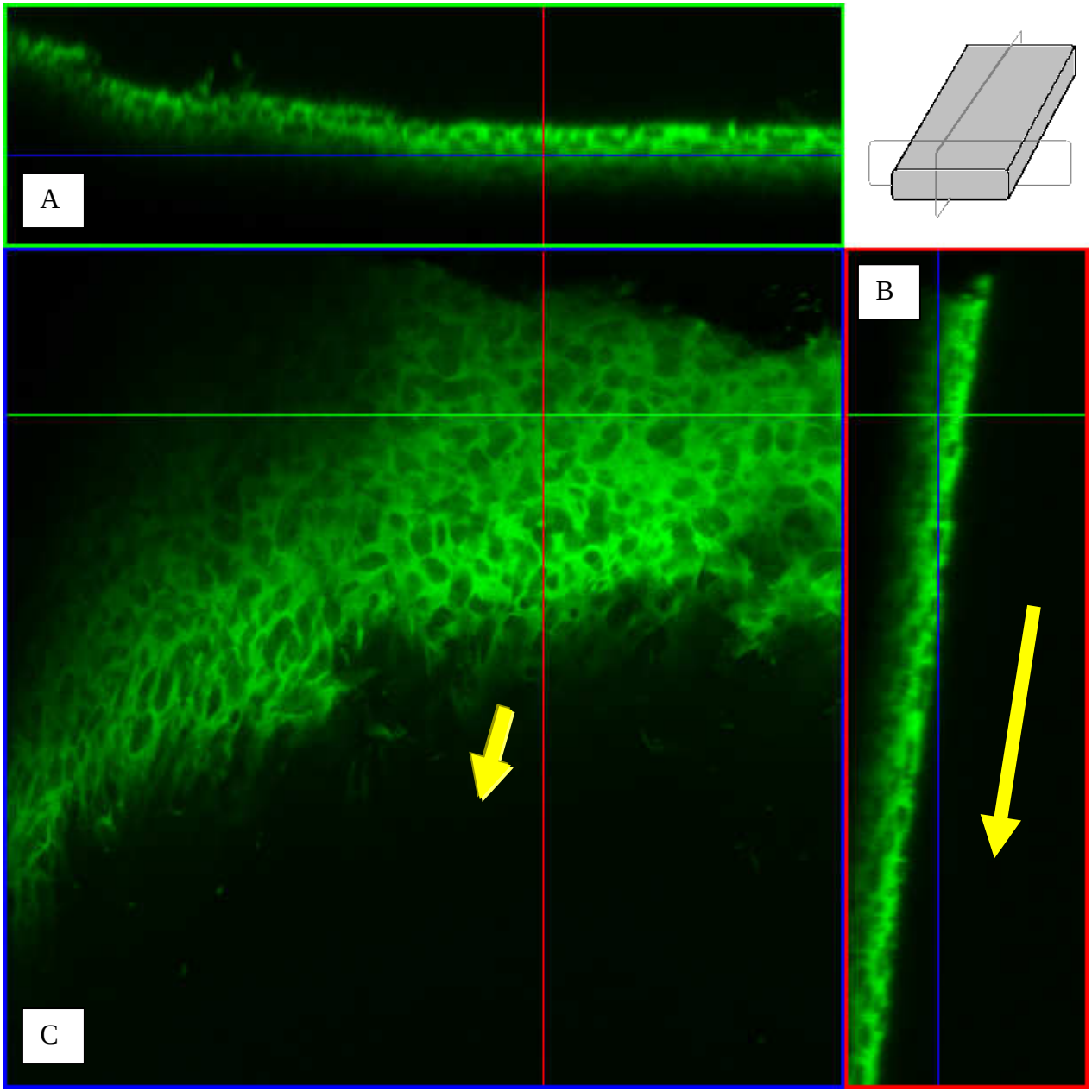

Figure 3.2: C false colour 3D image generated from a stack of second harmonic scans of a strip of the fibrous network from the middle section of a egg capsule. Image obtained by using Zeiss 510 Meta (Laser Scanning Confocal Microscope). The image is generated by capturing the second harmonic light signal generated by the natural fluoresce of WECP. A: Cross-section B: longitudinal section. C: 3D composite view, axis of alignment coming out of the page. Arrows indicate axis of alignment (alignment in A is strait out of the page).

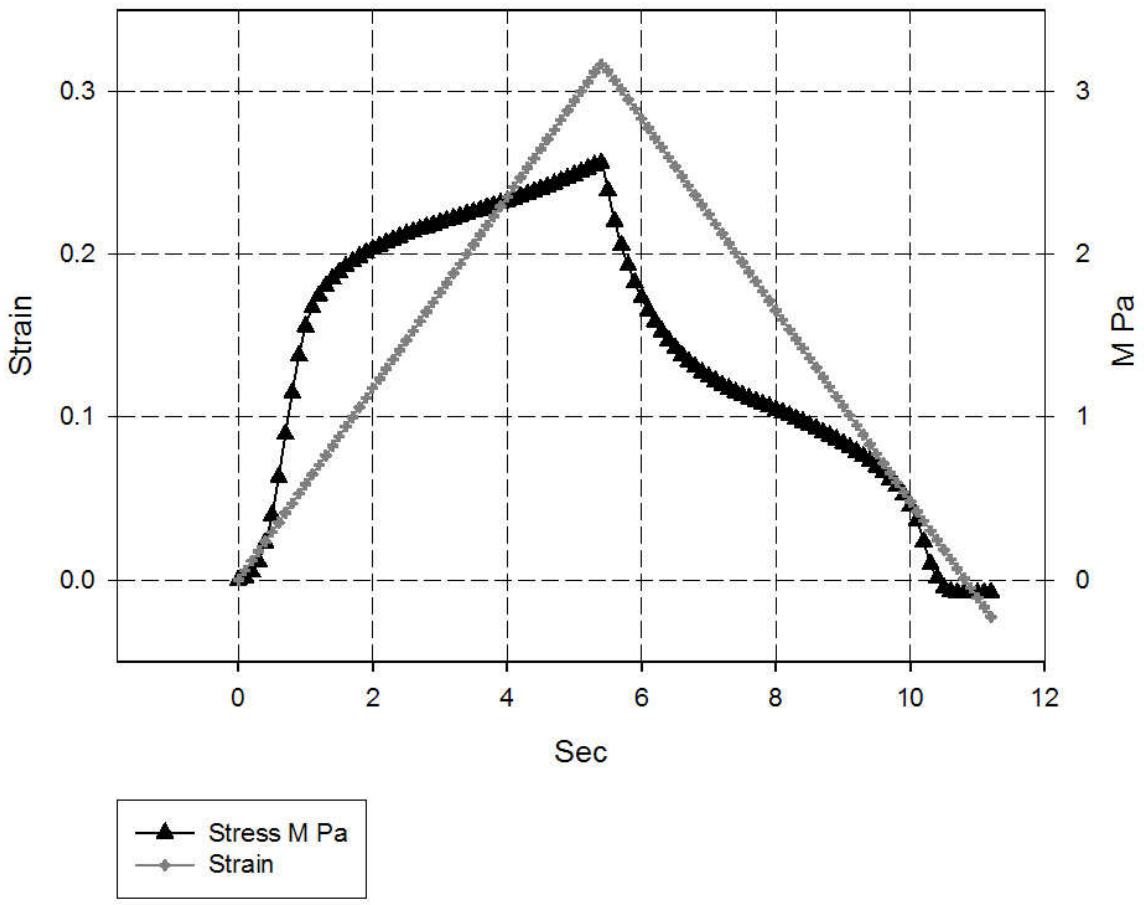

Figure 3.3: Typical stress and strain data for mechanical testing. This data is included in the Stress/Strain plot below. The rate of strain is constant, but there are well-defined changes in the slope of the force curve.

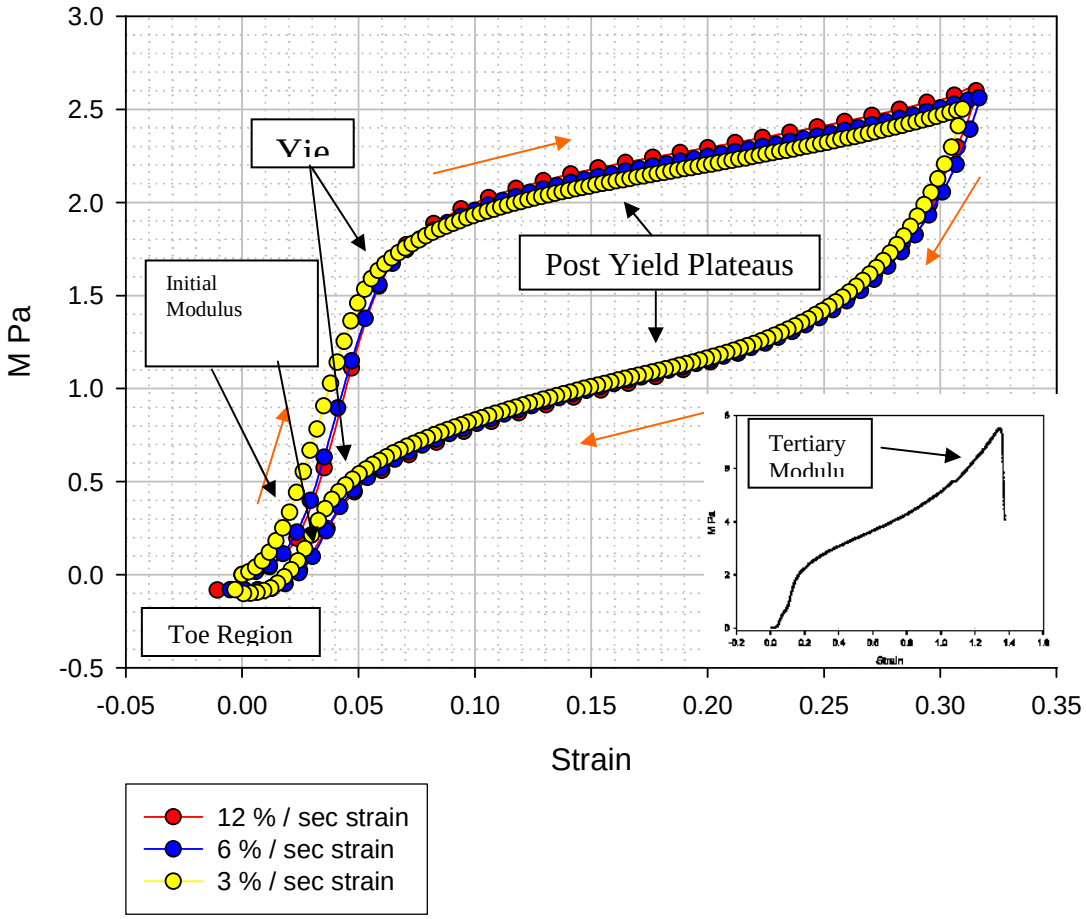

Figure 3.4: A stress / strain plot of a whelk egg capsule fiber bundle (20C). The fiber was stretched once at a rate of 12% per second and then at 12%, 6% and 3%. The initial conditioning stretch is not shown here. There is an initial toe region where forces are small especially in thin samples. This is followed by a stiff region referred to as the Hookean region in pervious papers. The material then goes through a yield point and levels of in to a post yield plateau. The insert shows a failure test. Failure occurred at a strain of 1.35 and a stress of 7.5 M Pa. Prior to failure the graph shows an increasing slope referred to as the Tertiary Modulus.

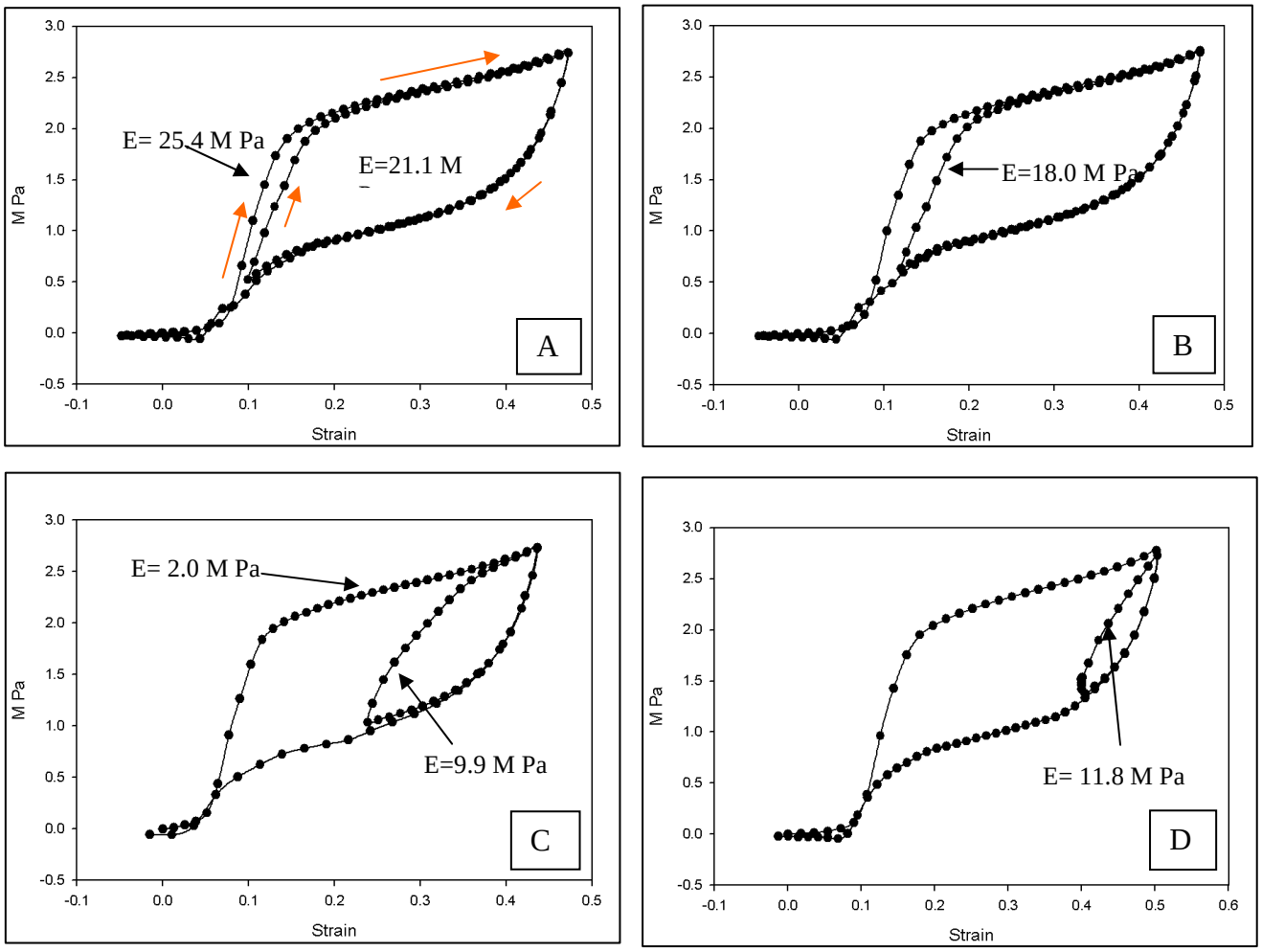

Figure 3.5: The graphs show how the affects of restraining the fibers before complete relaxation has taken place. A and B show that the stiff Hookian properties regenerate if the material is allowed to recoil below the yield strain. C and D show an increased stiffness that is intermediate of the yield and Hookian region moduluses when the recoil stops in the yield region.

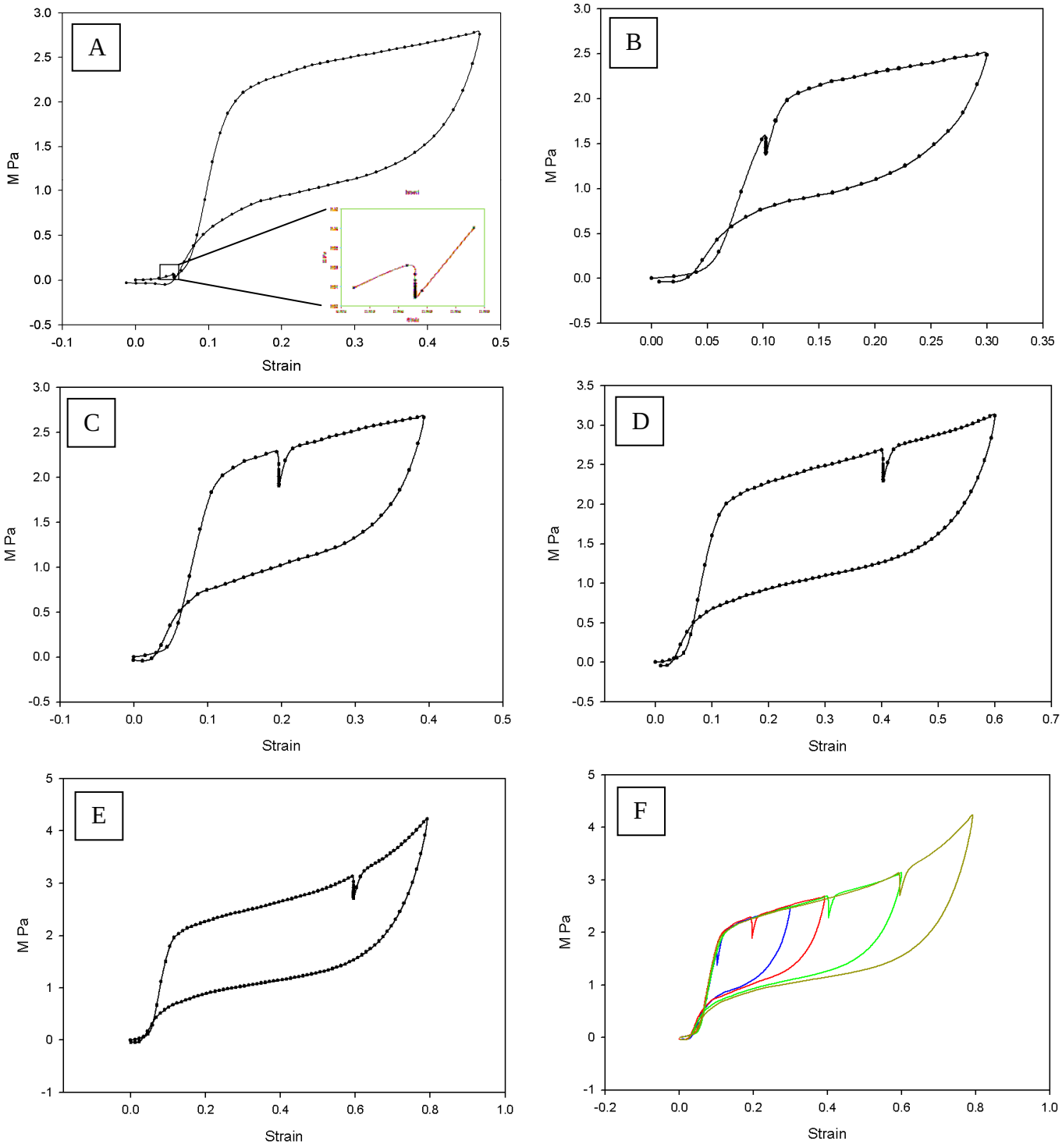

Figure 3.6: The effects of pausing during extension. In all cases there is a measurable drop in the force when the sample is held at a fixed strain. A-E shows the progressive movement of the holds from the pre-yield into the post-yield region. F shows a summary plot that combines the curves in B-E.

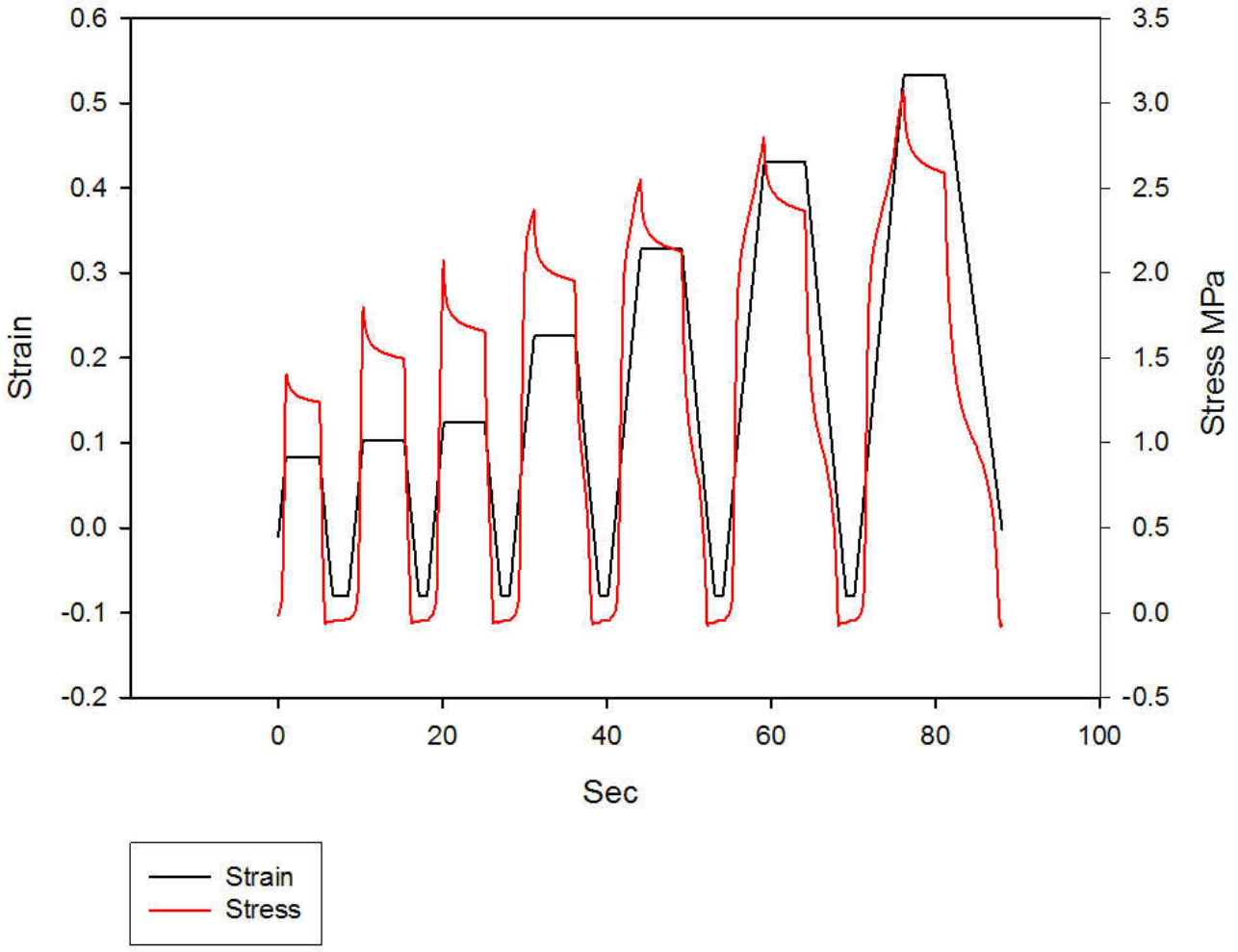

Figure 3.7: Stress relaxation experiment readouts. There is a rapid initial drop in force then a slower but continuous decline in force.

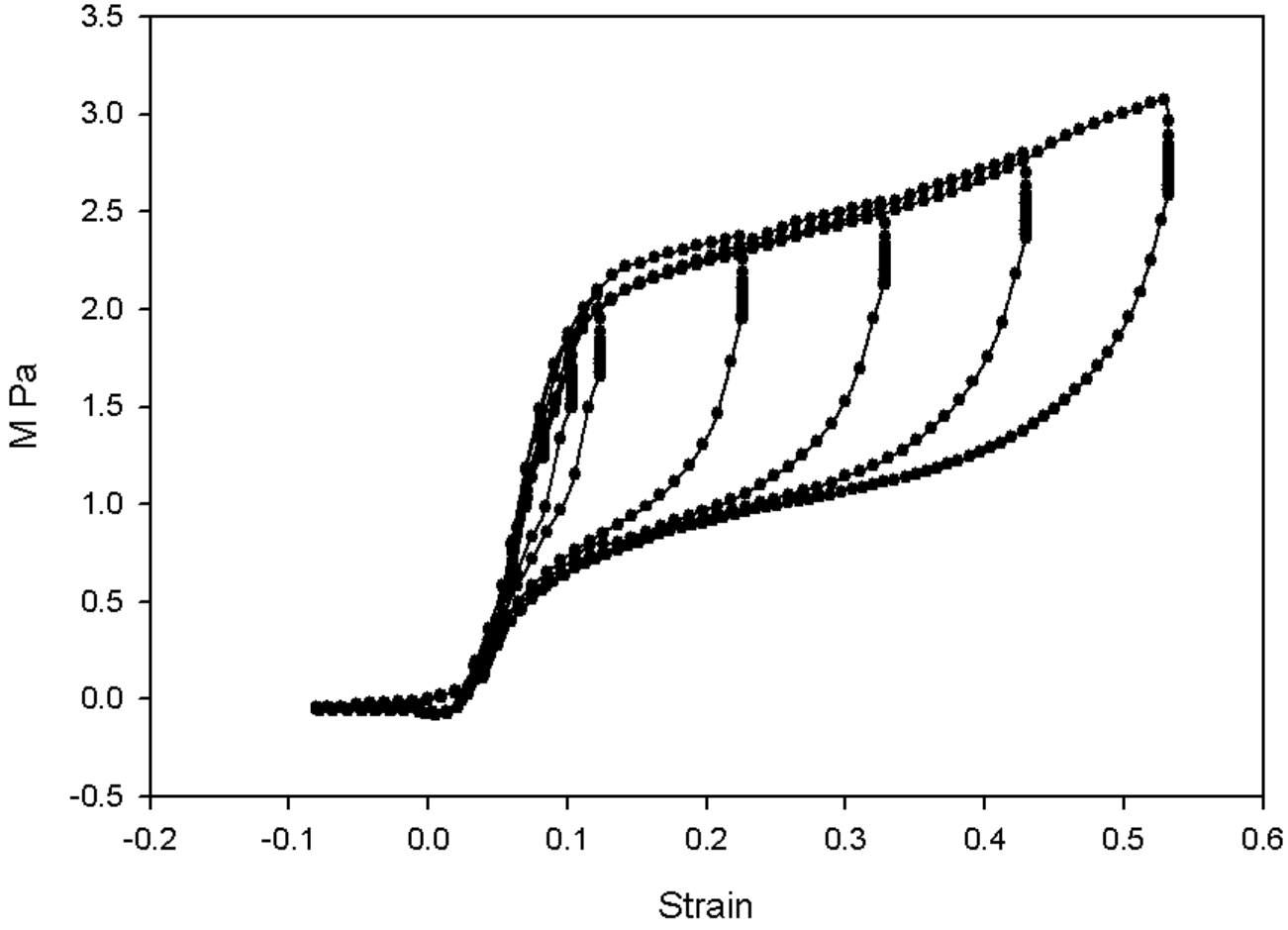

Figure 3.8: Stress / Strain plot of data from figure 3.7. There is a rapid initial drop in force then a slower but continuous decline in force

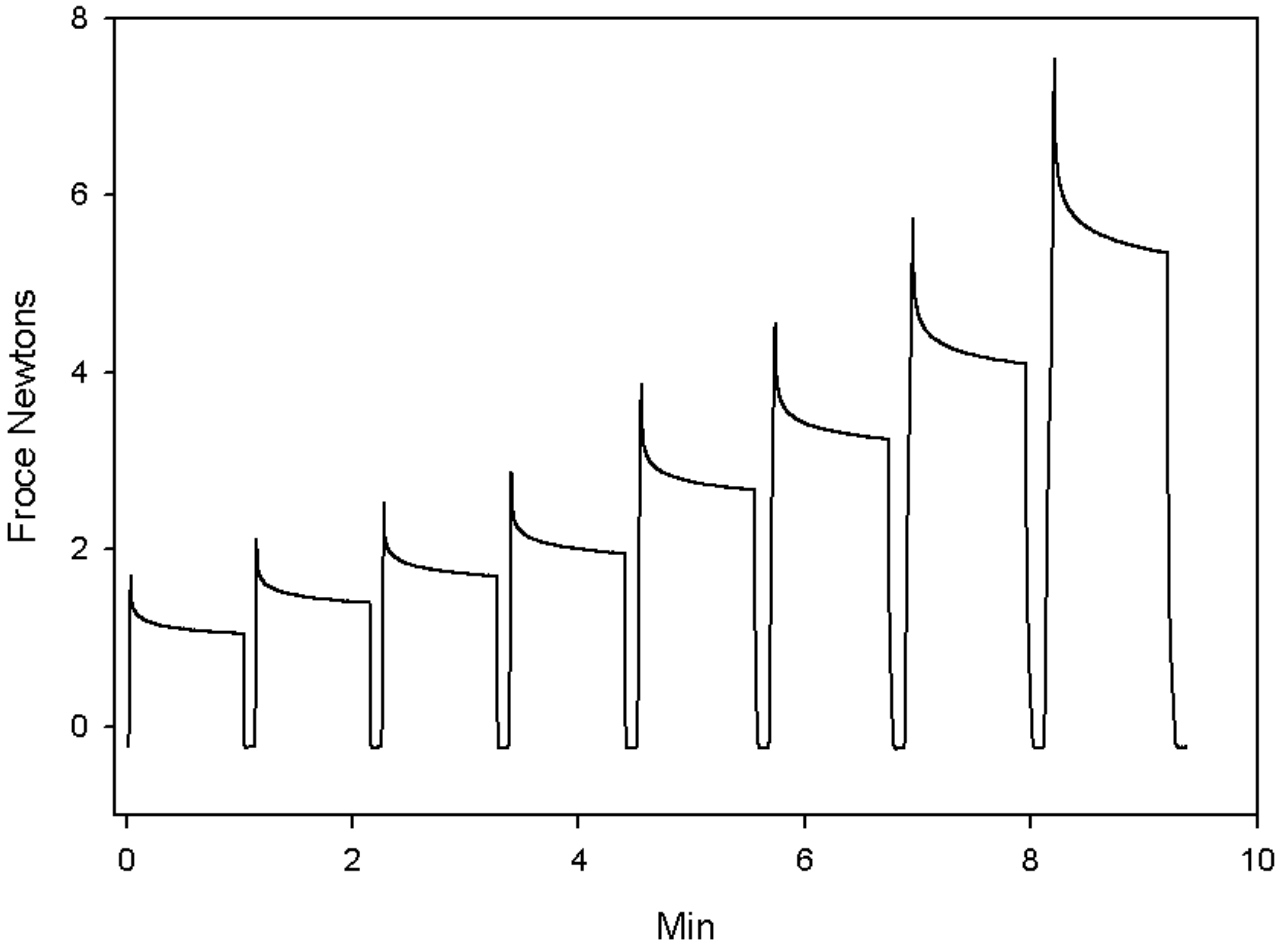

Figure 3.9: Raw force data for a series of one minute holds at increasing strains. The pattern is the same as for the 10 sec hold, a rapid decline followed by a slower continuous decline.

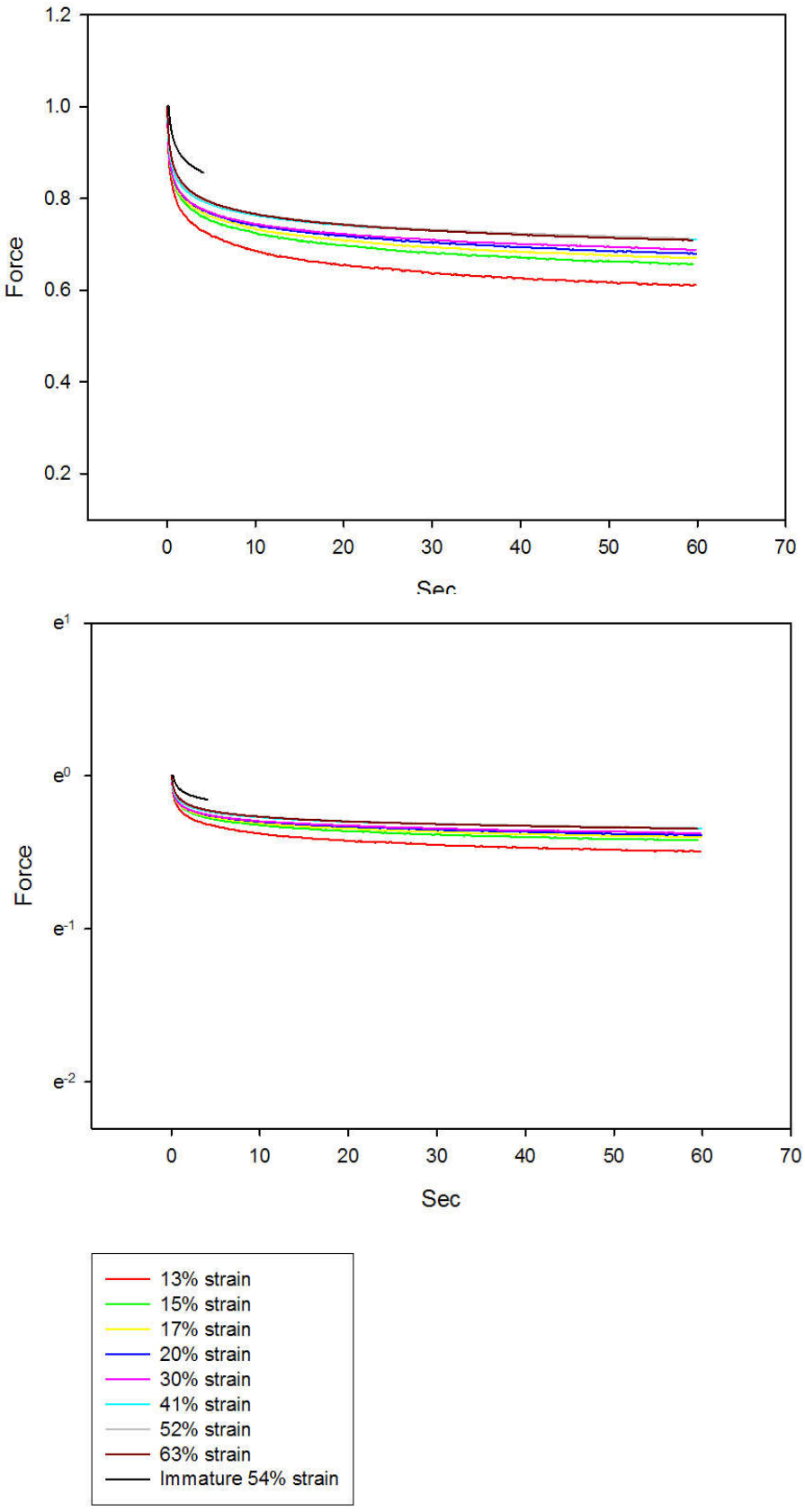

Figure 3.10: Normalized plots of the force relaxations in figure 3.9. The first plot shows a normalized plot that arbitrarily sets the starting force as 1. The second plot changes the scale of force to a log scale, demonstrating that the first plot is not a simple exponential decay. A force decay from an immature sample has also been plotted to show that the viscoelastic properties are already present and that the sample have similar relaxation curves.

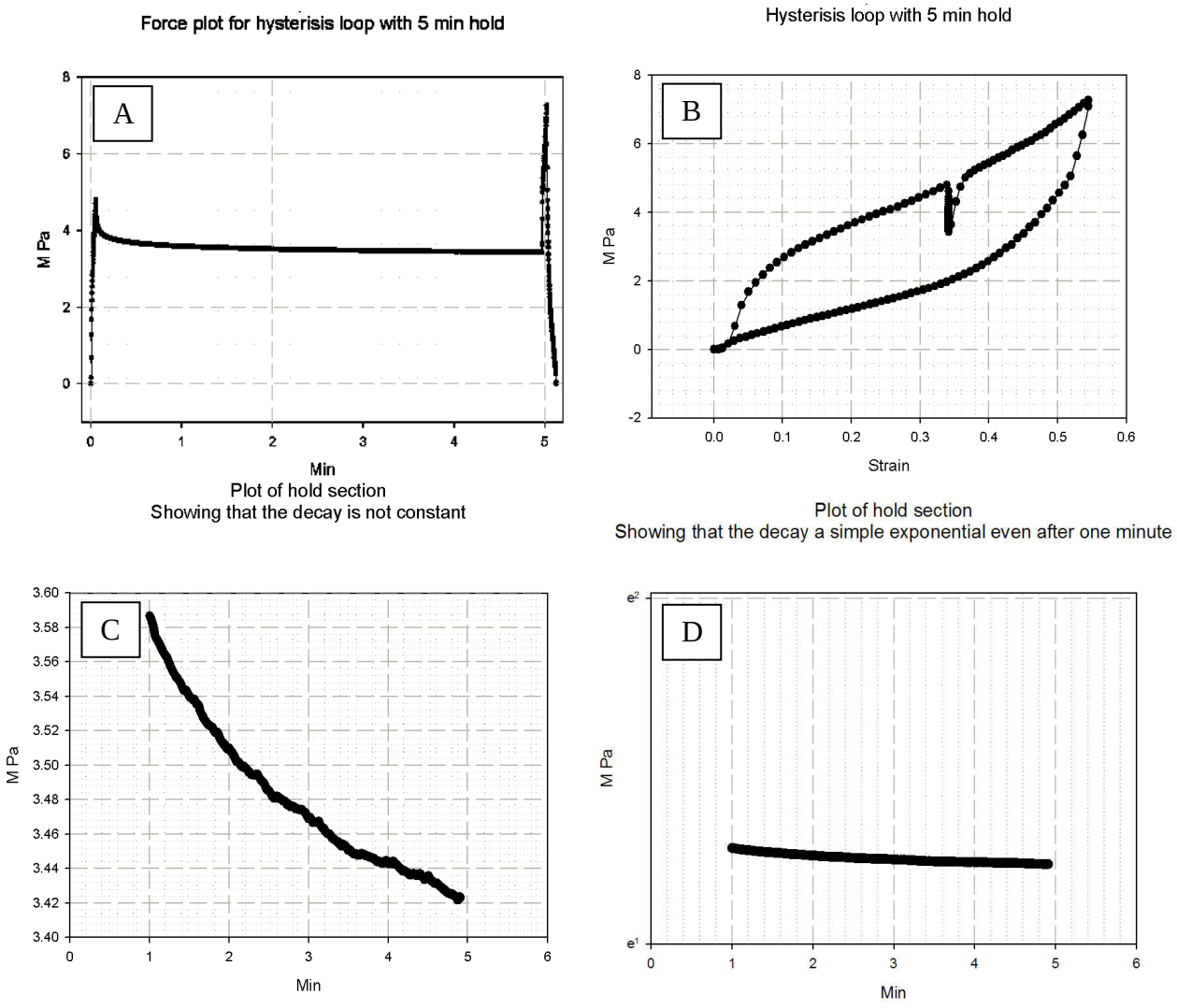

Figure 3.11: Data for a five-minute hold. The first plot show Stress dropping off during the hold and appearing to level out to a steady decay. The second plot is a close-up of the 1-5min section of the hold plot demonstrates that the force decay is not constant (only the Stress scale is changed). The final plot shows that the effect of holding the sample for five min vs 10 sec result in a lower minimum force decay but that the general shape of the loop is the same.

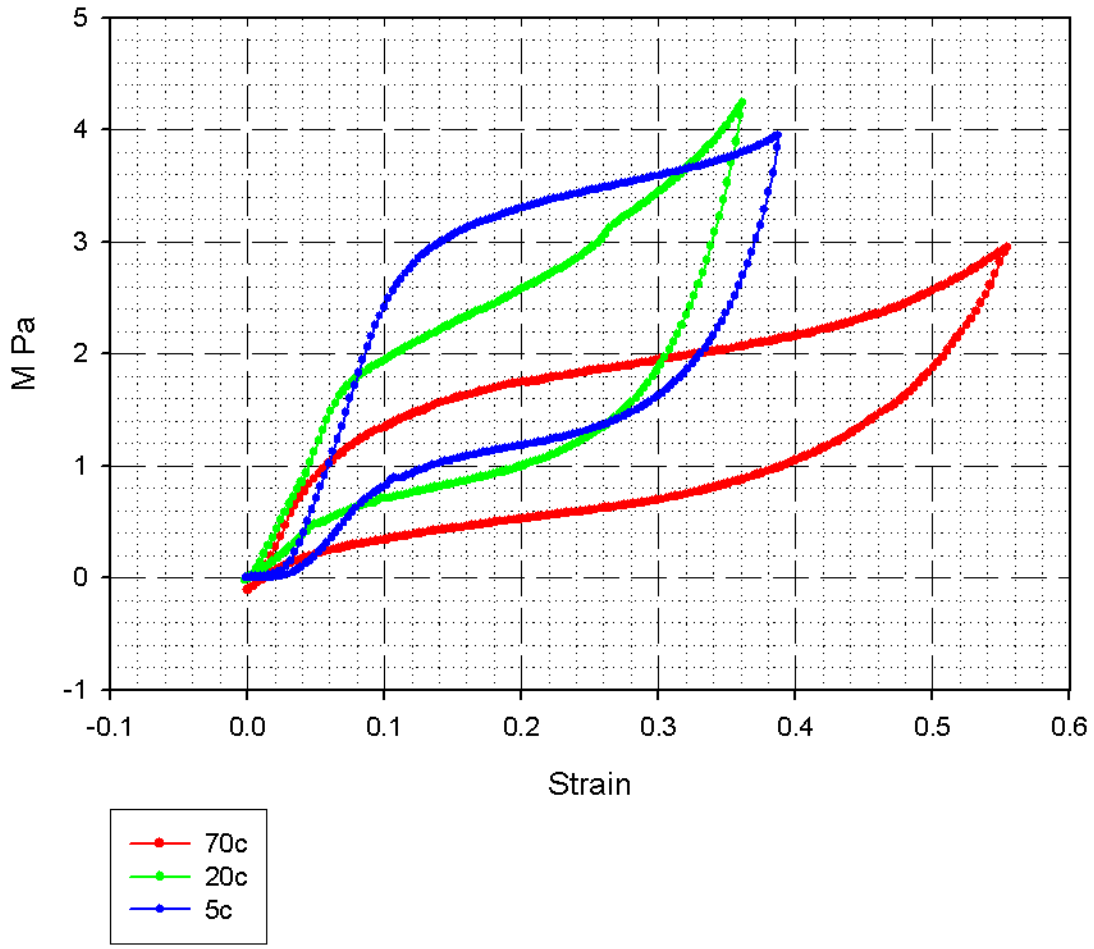

Figure 3.12: Data for varying temperatures, strain rate of 3%/sec. The size of the Hookian region and the hysteresis are declining with increasing temperature.

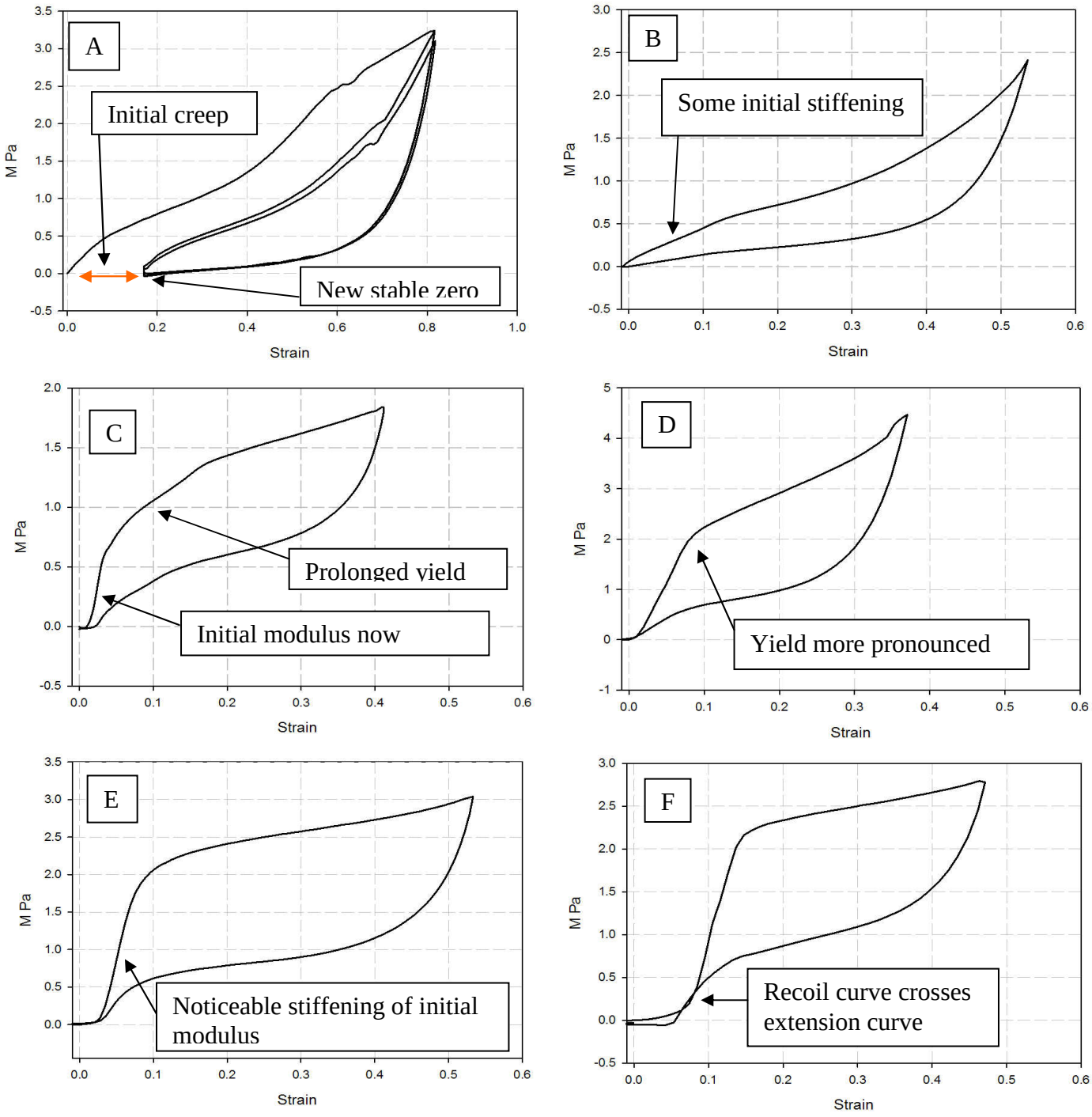

Figure 3.13: A examples of the different shaped hysteresis loops produced by the same protocol on different samples. A & B samples have no initial modulus (Hookian region) and the A sample did not fully recover from the first extension. The B loop was very pliable on extension and fully recovered on every loop. The C & D samples have a definite Hookian regions in the loading curve but not on the unload curve. Sample E has Hookian regions for loading and unloading. Sample F has well defined initial modulus and now the unload curve crosses over the loading curve. There is a progressive sharpening of the yield region from its first appearance in sample B through to sample F.

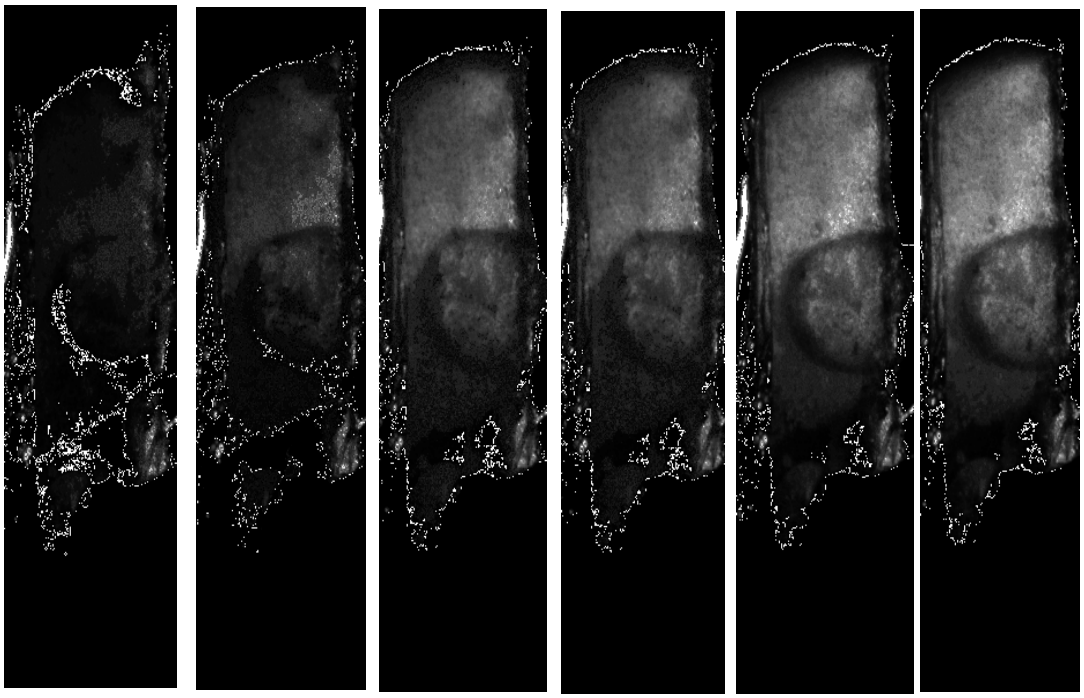

Figure 3.14: Photographic series showing the effect produces by straining latex rubber. In the first photo the rubber is in a relaxed state, i.e. a random network that has no birefringence. The sample appears dark. As the series progresses the sample is subjected to increasing strains. The system is experiencing a strain induced increase in order and the sample becomes birefringent. Increasing amounts of light are retarded by the sample and the sample appears to glow.

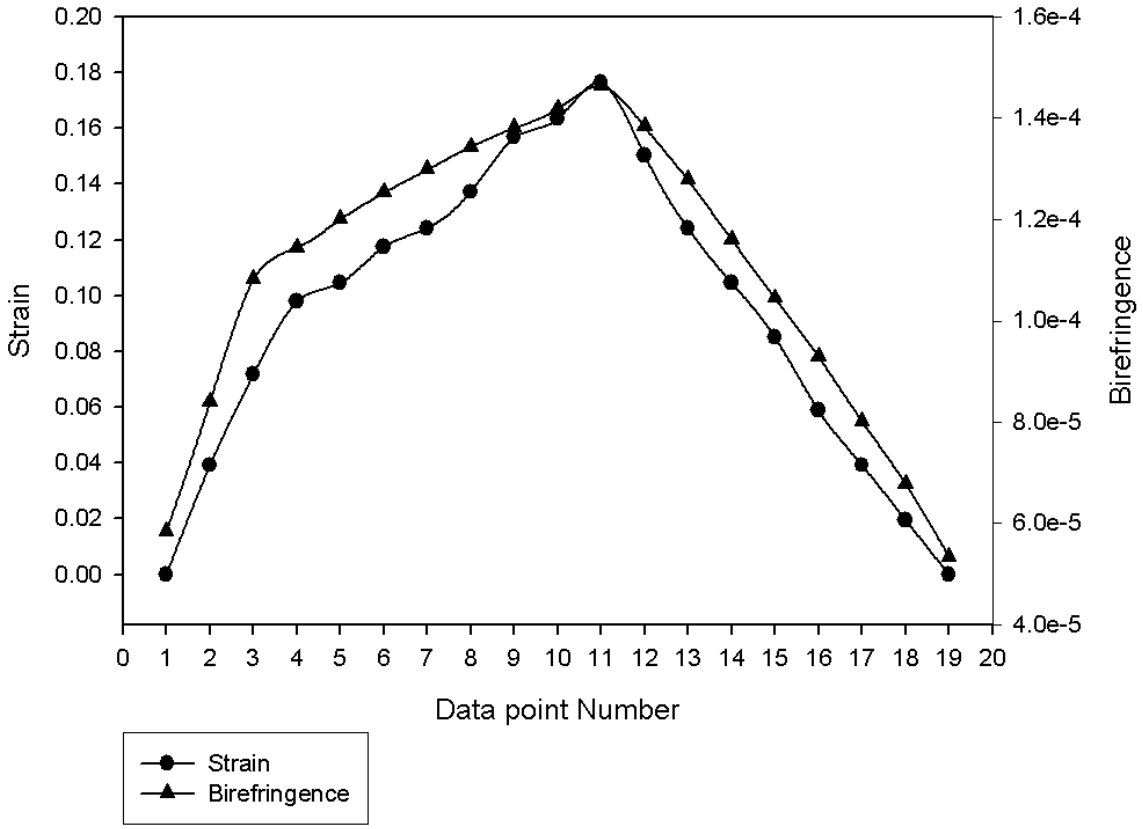

Figure 3.15: A graph showing retardation measurements and strain. Note that retardation rises and falls in direct relation to the strain.

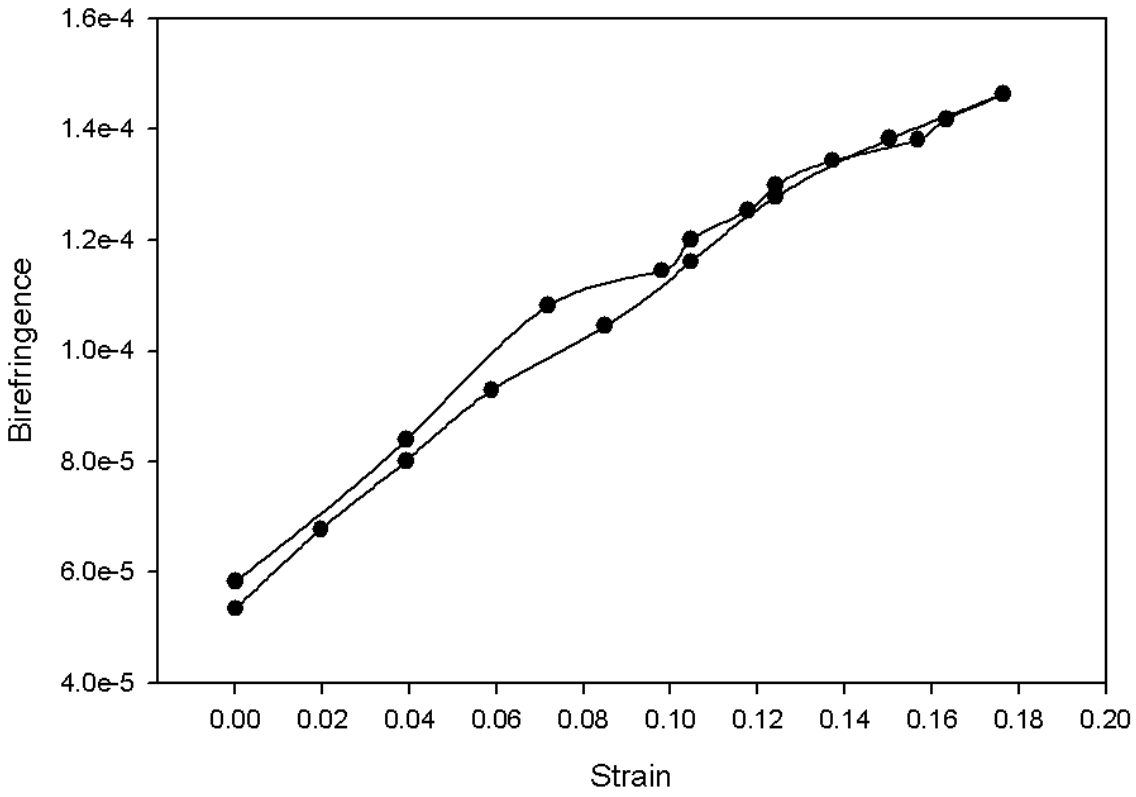

Figure 3.16: Retardation plotted against strain for latex rubber. The graph shows a direct relationship between strain and birefringence as predicted by the random coil model of elasticity.

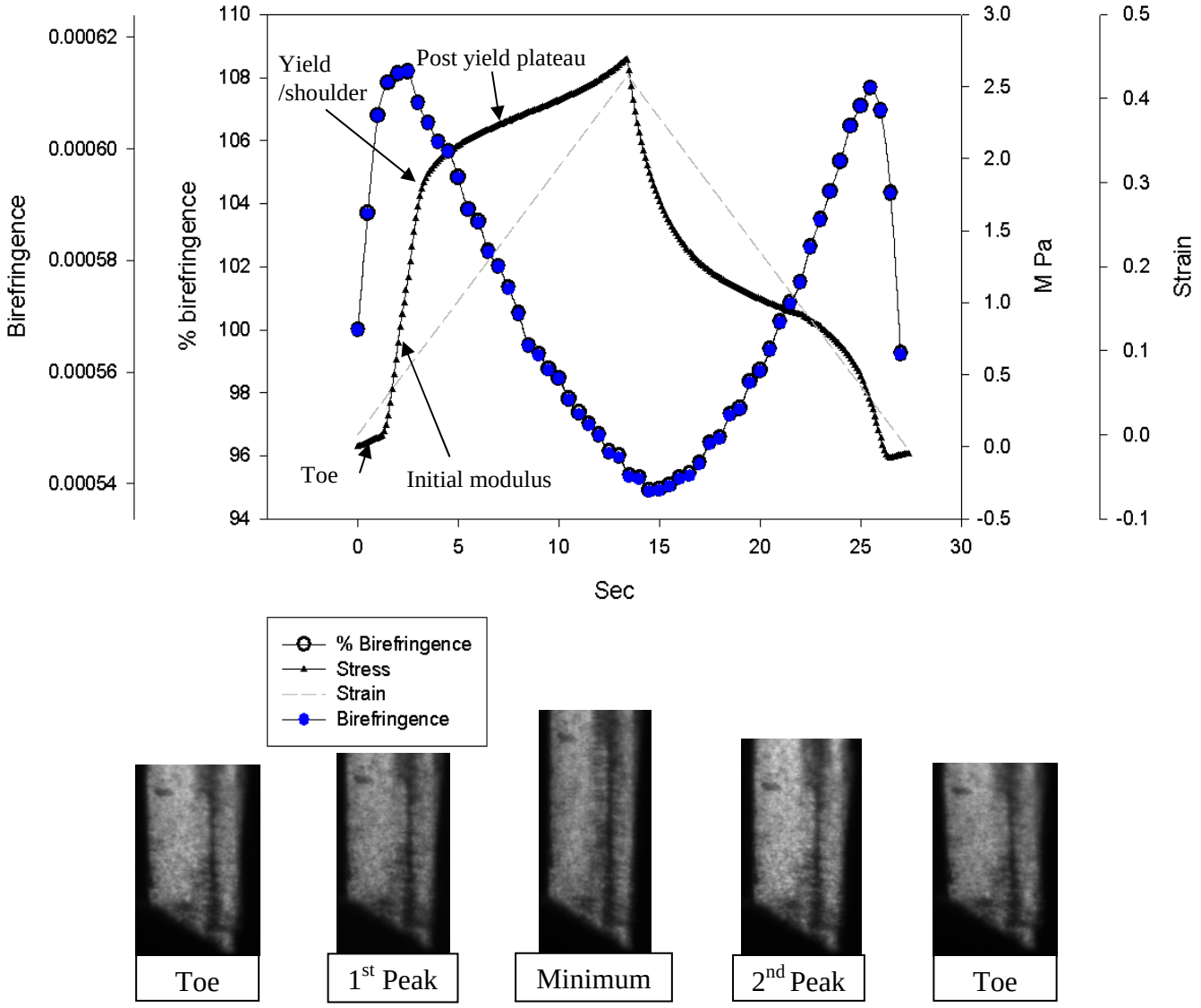

Figure 3.17: This multi plot shows how stress and birefringence change in response to strain (20C). The strain plot shows that the ramp extension and retraction of the leaver arm attached to the sample was a smooth constant rate. The force trace has very defined shoulder regions in loading and unloading phases. The birefringence is reported in two ways in this graph. It is reported as a normalized % of birefringence and as the birefringent value for this extension. This is done to show that the normalization does not affect the observable trend and to allow the reader to gauge the actual change in birefringence. The equivalent regions of the stress/strain curves seen in the biomechanical section of this thesis have been added to orient the reader. Photos corresponding to the minimums/maximums of the birefringence graph are shown below. The photos clearly show the extension of the sample, but the change in light intensity is subtler. It can be observed by noting how shadowy regions of the images darken/lighten.

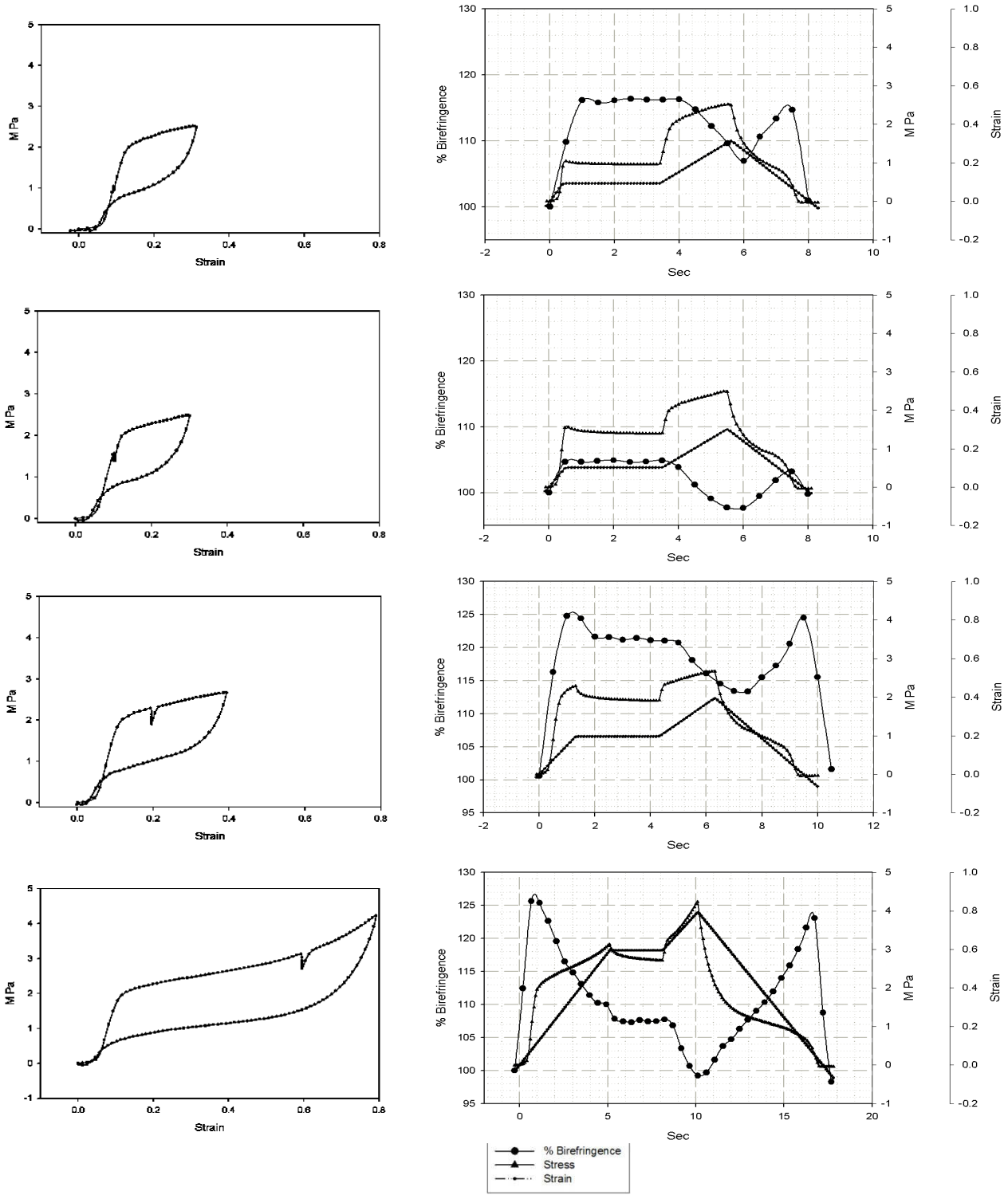

Figure 3.18: A progressive series showing how pausing while extending the sample affects birefringence. The graphs on the left are stress/strain plots that show how stress relaxation during a pause. The graphs on the right plot Stress, Strain and birefringence vs. time. They show that the birefringence clearly tracks with the strain. The time axis is adjusted to accommodate tests to larger strains.

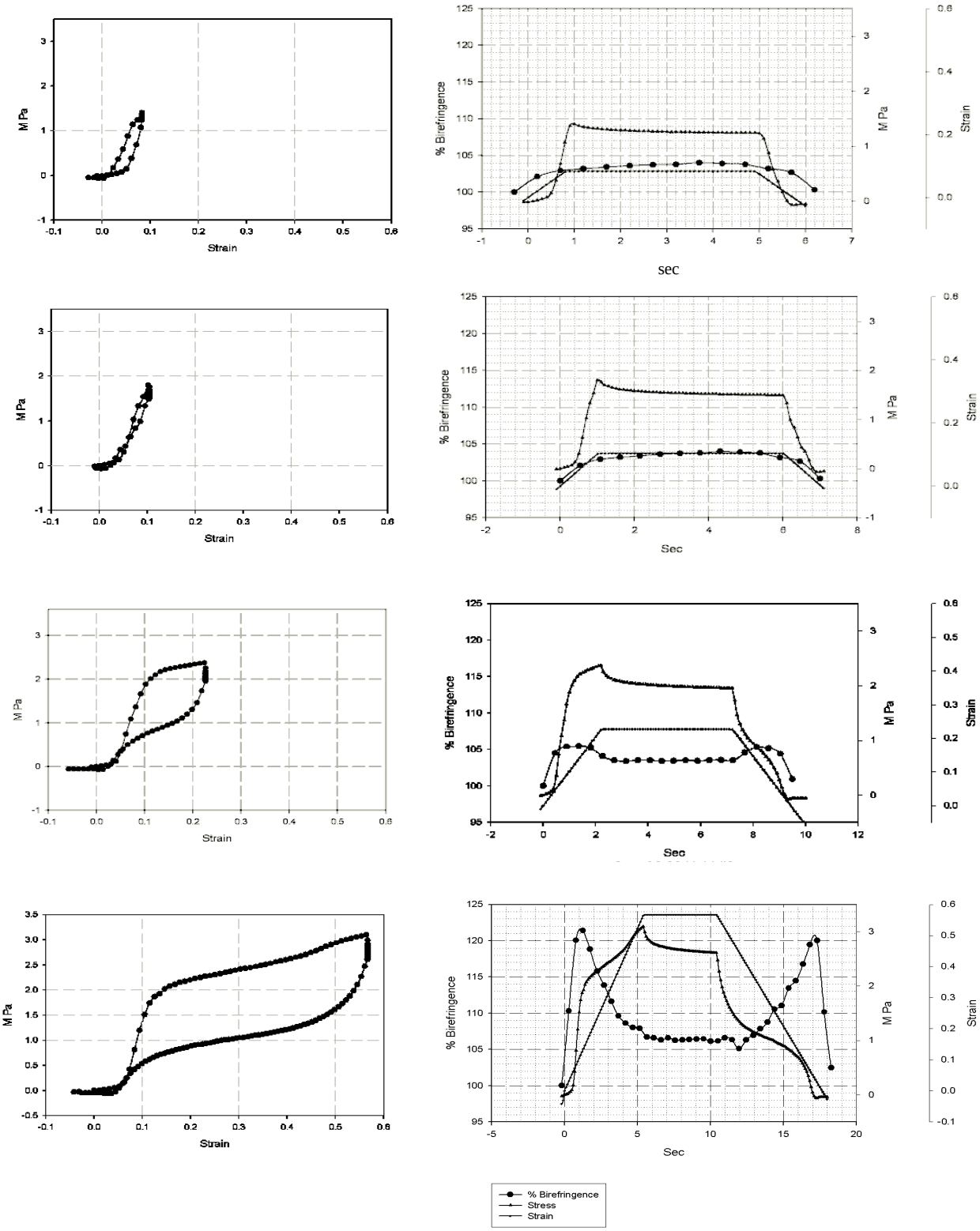

Figure 3.19: A series of force relaxation plots. Graphs on the left show stress/strain curves for force relaxations at the end of 12% per second ramp extensions. The graphs on the left plot force, strain and birefringence data for the graph on the left. Once again the birefringence clearly tracks with the strain and it changes directions at the shoulders.

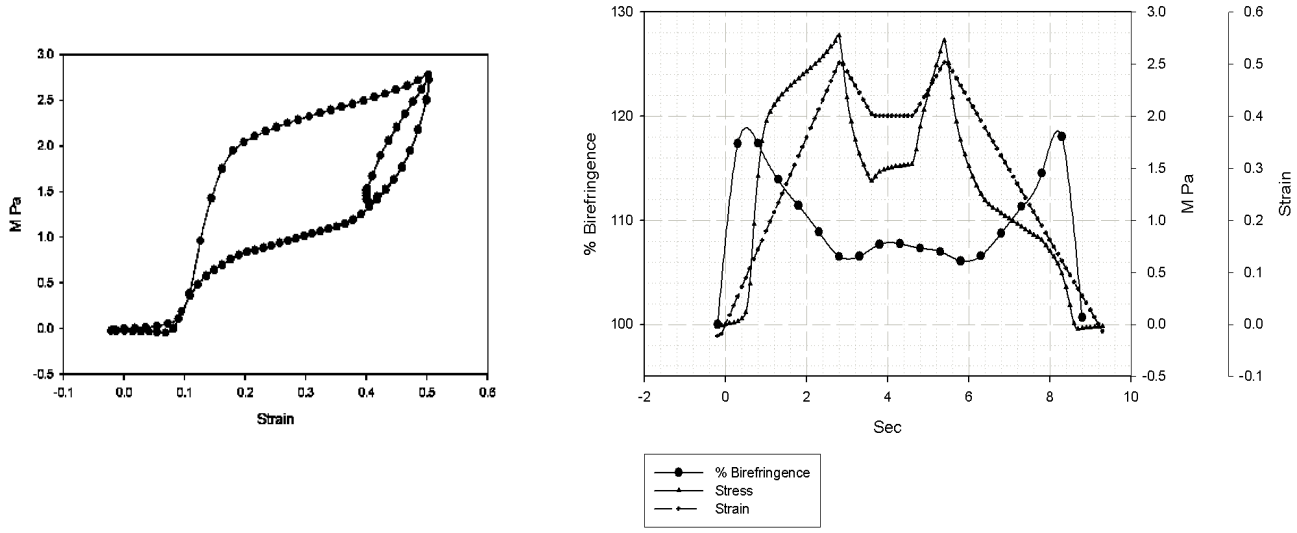

Figure 3.20: Plots showing the effect of pausing during recoil and re-extension. Force clearly rises during the pause. The birefringence trace shows a corresponding increase during the pause.

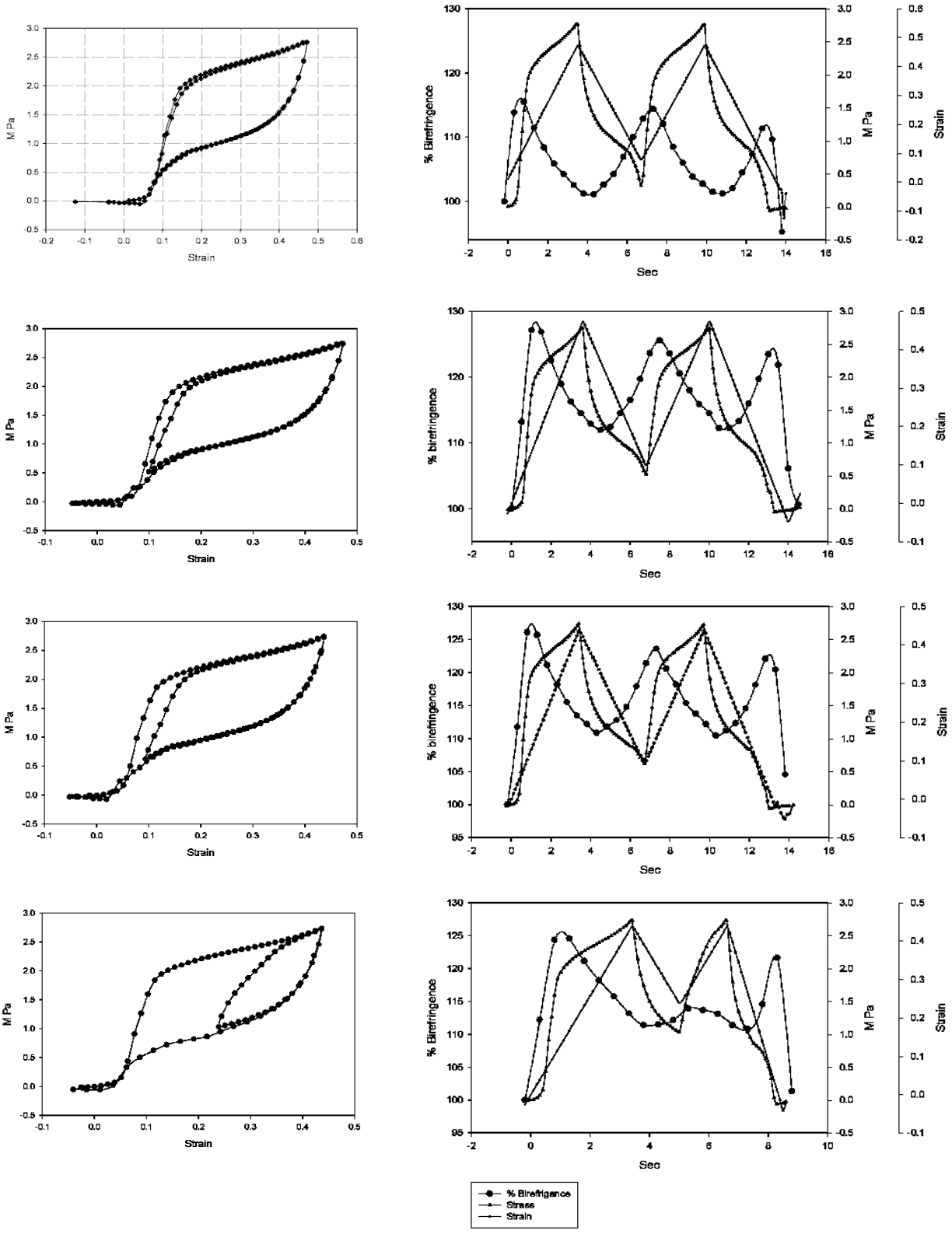

Figure 3.21: Series of graphs showing the effects of incomplete recoil on birefringence:

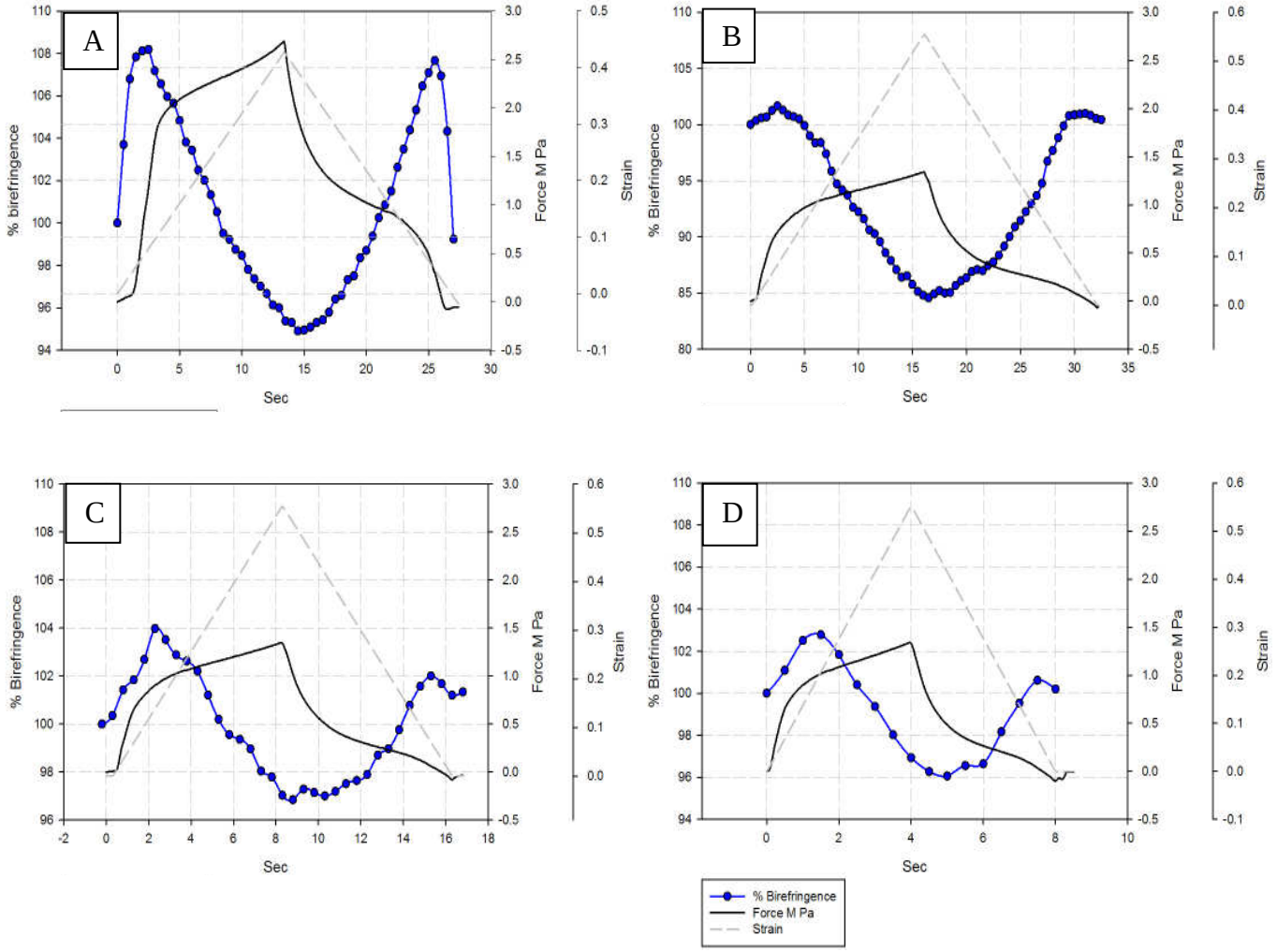

Figure 3.22: A shows a birefringence plot for a typical ramp extension at 20c and 3%/sec strain (12%/sec – 3%/sec produce the same curves at 20c). B, C and D show the same sample at 66c undergoing the same ramp extension at12%/sec, 6%/sec and 3%/sec. The initial rise in birefringence that is attributed to the toe region is diminished in all of them. In the 3%/sec plot it is almost absent. I do not have a sufficient number of samples to say if this is a statistically significant but given the consistent clean results seen in other test runs I suspect that there is some real drop in the birefringence peaks.

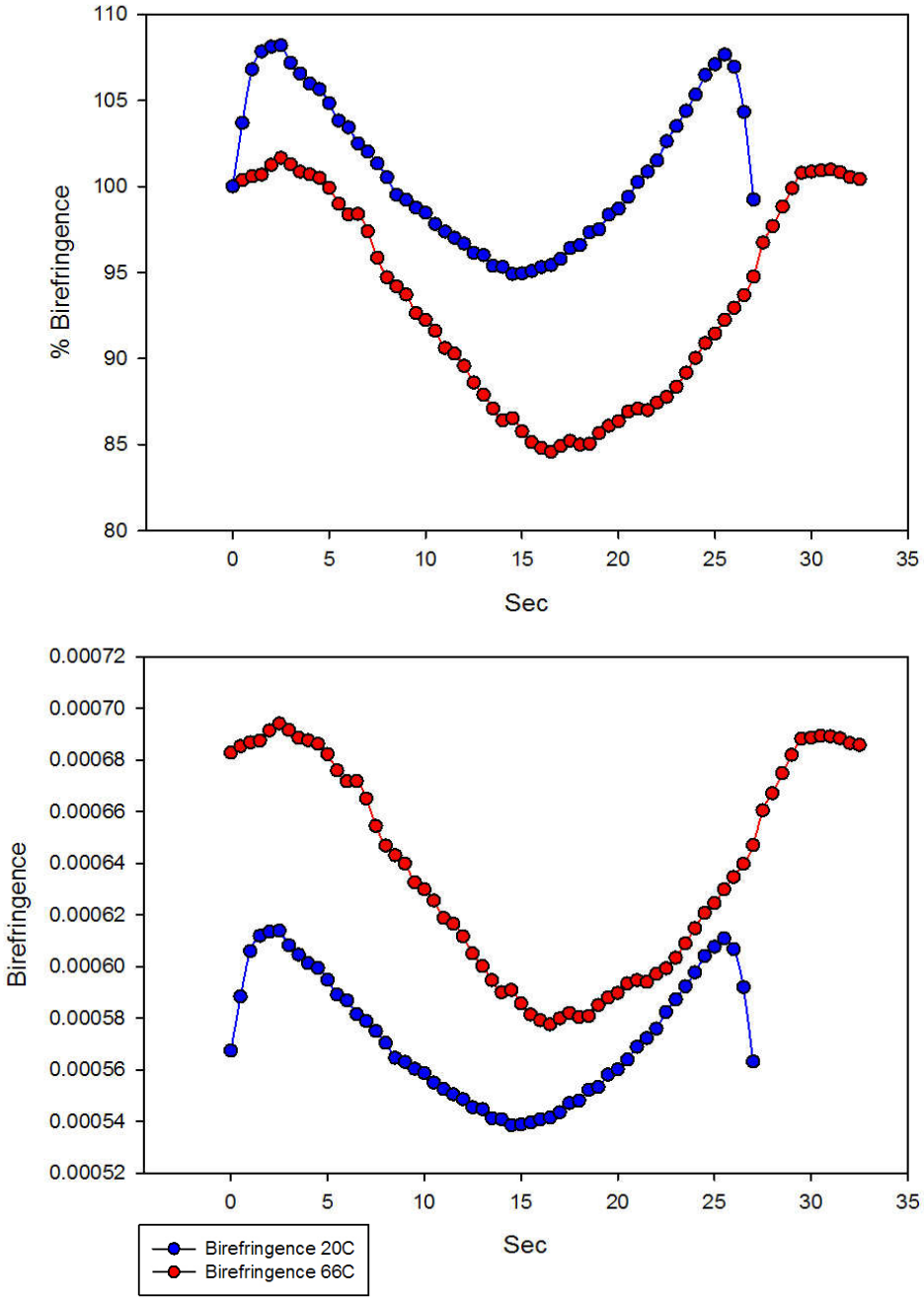

Figure 3.23: Comparing normalized birefringnce (top) and absolute birefringence (bottom). Note normalization did not change the shape of the data and it makes it easy to see trends. Plotting the actual birefringence value showed that actual birefringence increased with temperature. Both plots give useful information from different prespectives.

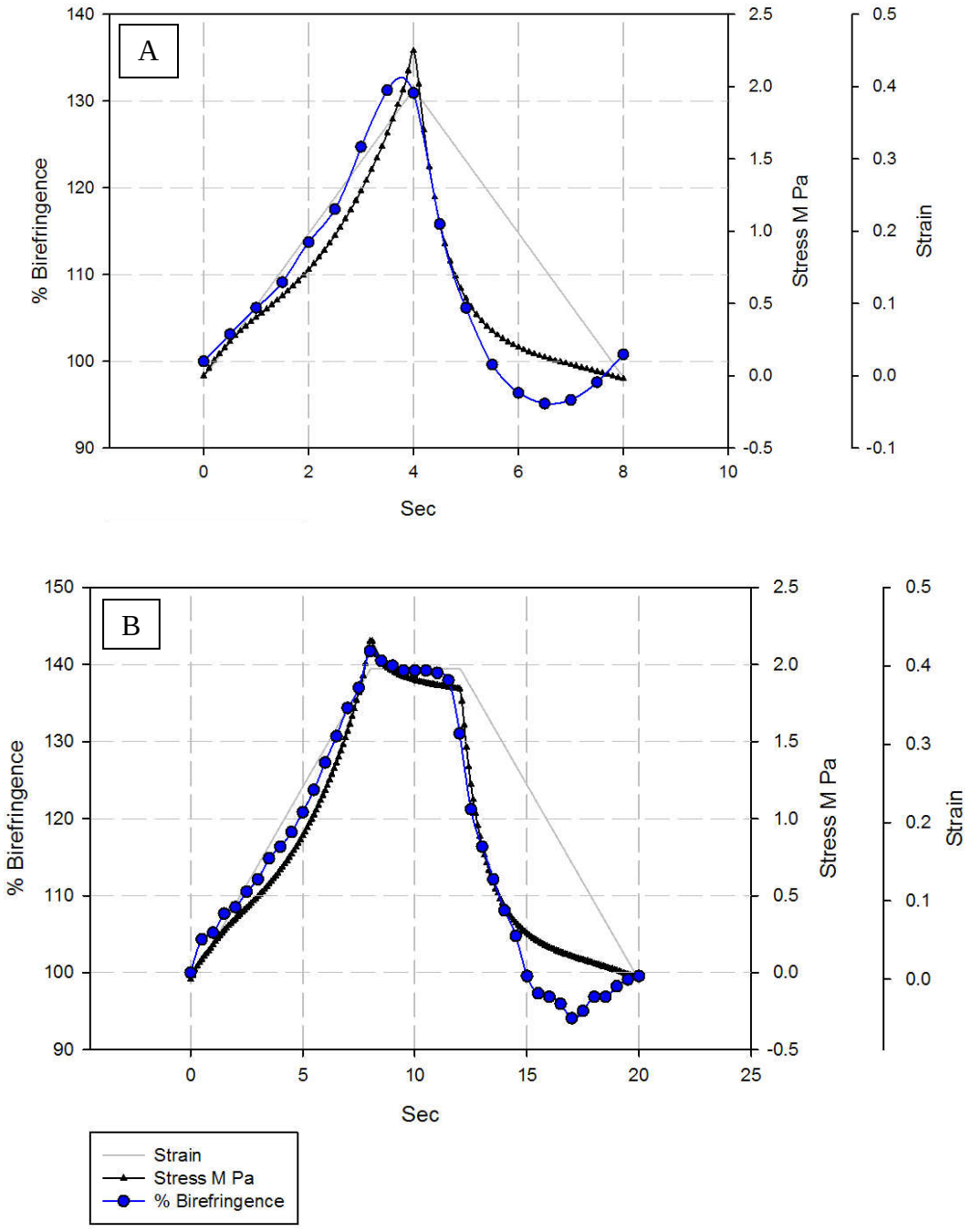

Figure 3.24: Birefringent plots for A, a ramp extension and B, a force relaxation of immature fiber samples. In both A and B birefringence shows a positive correlation with strain. This is in complete contrast to the mature sample, which had a negative correlation between strain and birefringence at strains above 5-10% (yield point) indicating that the stress/strain response in immature samples is mechanistically different than mature samples. Birefringence in both sample dips below the initial value during recoil and there is a drop in birefringence associated with the force relaxation; both of these results are seen only in the immature sample.

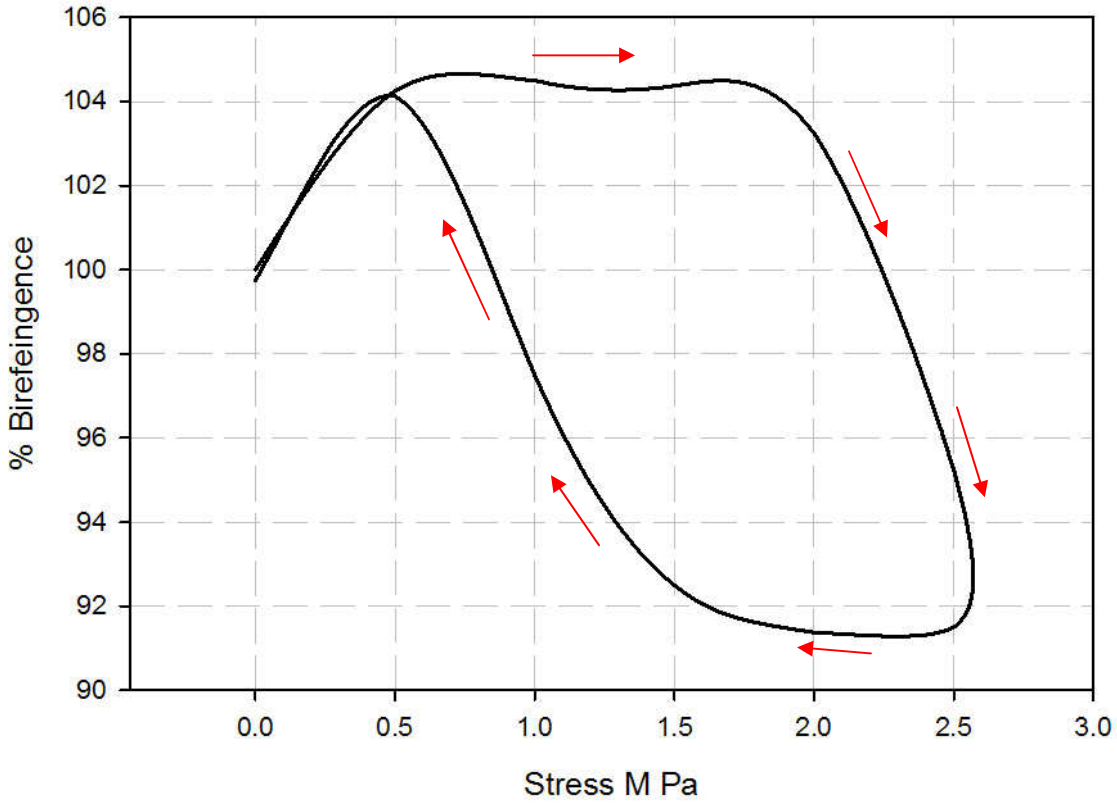

Figure 3.25: Comparing birefringence with stress. Birefringence initially rises with stress, plateaus then falls. As stress is falls the birefringence rises again to a peak just below initial peak and then falls back to its starting value. The graph shows a hysteresis in the birefringence indicating that the restoration of order in the post yield plateau region lagged behind the falling stress.

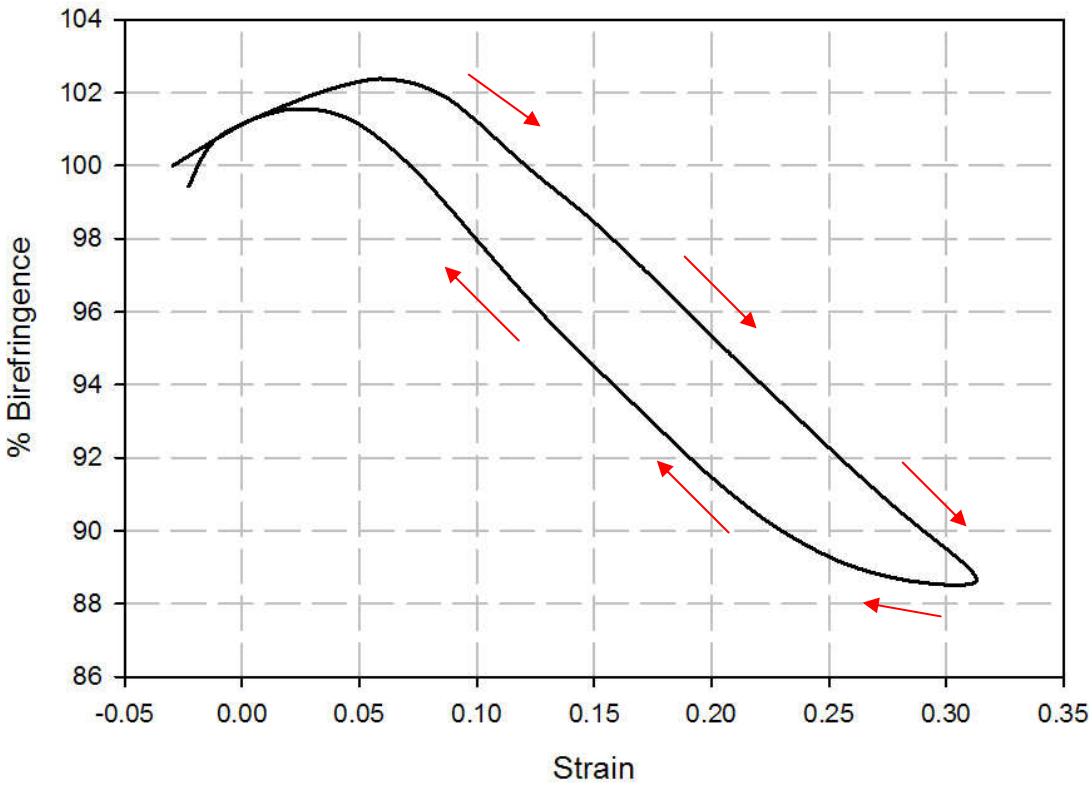

Figure 3.26: A comparison of birefringence with strain. Initially birefringence rises with strain and then falls steadily after the yield point. As strain falls birefringence rises again to a peak slightly less than the initial peak. The graph shows a hysteresis in the birefringence indicating that the restoration of order in the post yield plateau region lagged behind the falling strain.

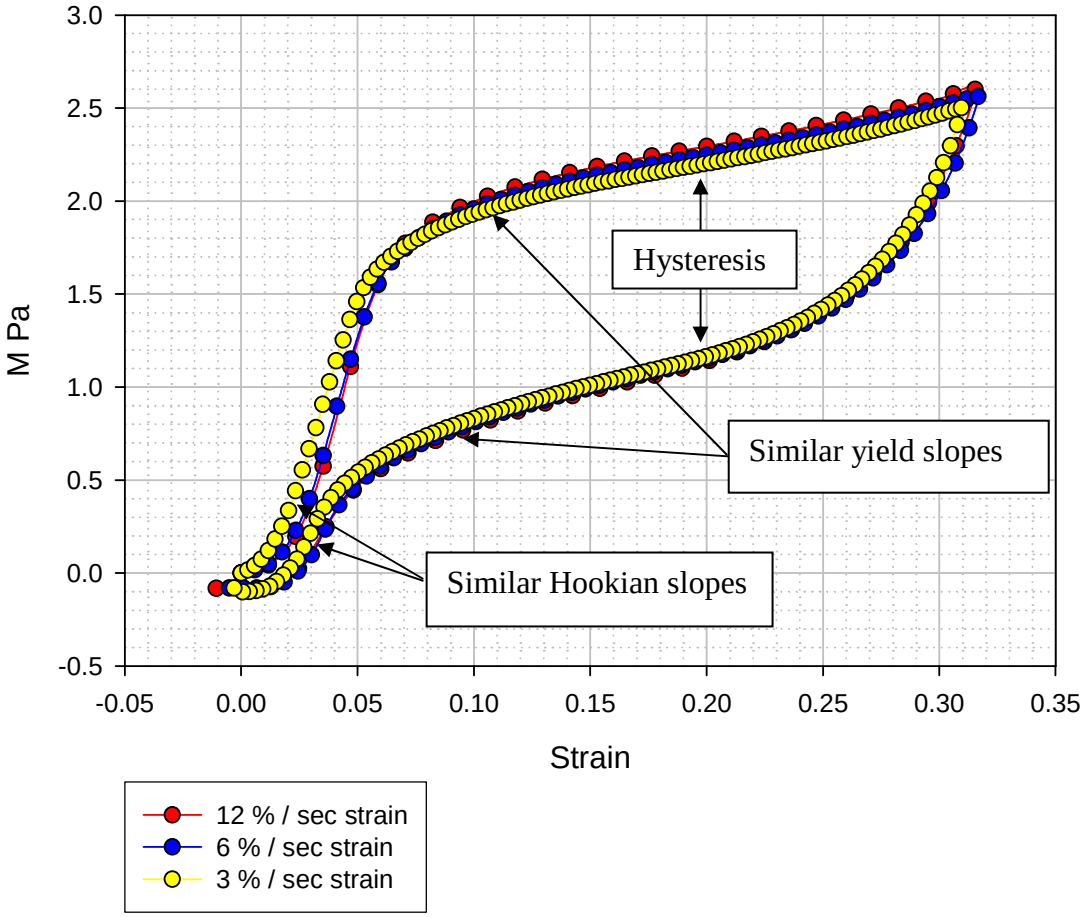

Figure 4.1: A typical stress/strain curve for WECP showing the similarities in slopes during extension and recoil. The large hysteresis loop is also highlighted out.

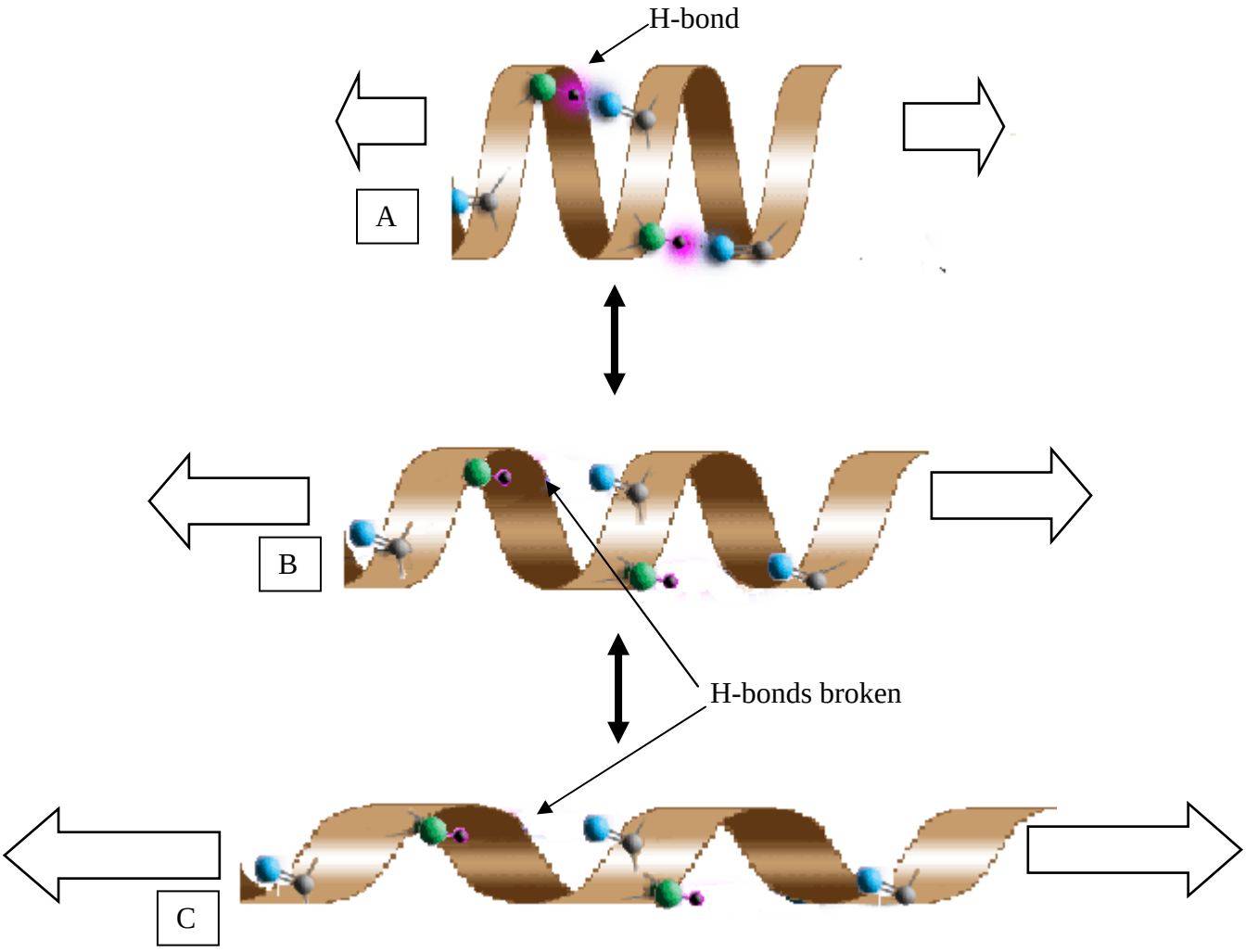

Figure 4.2: Cartoon close-up of an a-helix, depicting the proposed model of how the intermediate filaments elongate. A. The toe region and initial modulus: The helixes are intact and bearing the strain. H-bond length in a helix is 2.67 A. B. Yield region: The H-bonds are overstrained and pulled apart. C. Post yield Plateau: The helix is stretched until all the H-Bonds have been pulled apart, the slack is gone and the backbone of the helix is under strain.

The original of image used in 4.2 A was obtained from Google images. <http://www.brooklyn.cuny.edu/bc/ahp/LAD/C4b/graphics/C4b_alphaHelix.GIF>

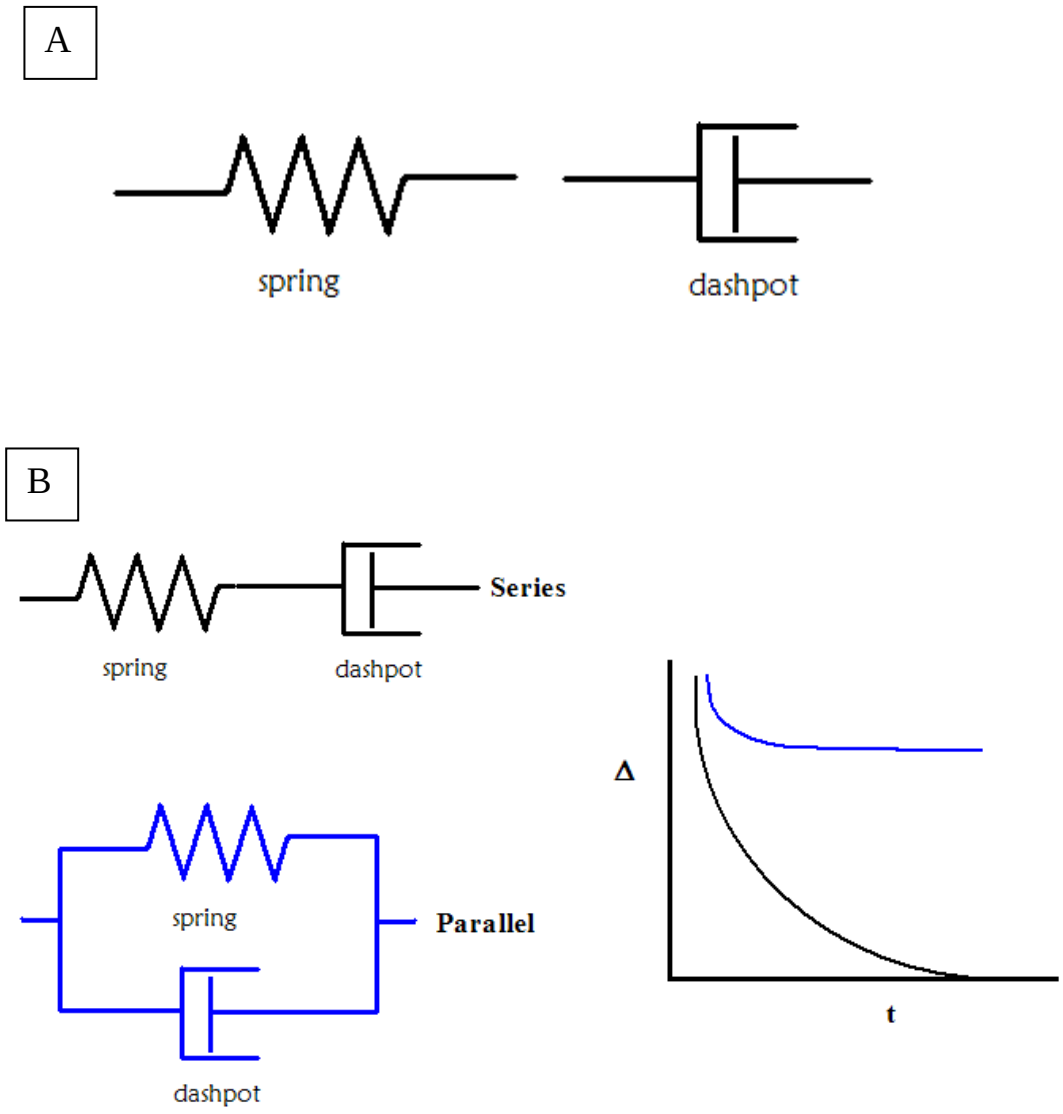

Figure 4.3: A: Example of model elements use to model the behavior elastic (spring) and, viscous (dashpot) behaviors. Viscoelastic materials exhibit both elastic and viscous properties. In some case the behavior of a simple viscoelastic material can be modeled by simple combinations of springs and dashpots. WECP however exhibits a complicated relaxation curve that makes modeling it in this way non-trivial and no attempt is made in this thesis. B: Cartoon example of simple dashpot and spring models that explain exponential decays. Corresponding decay lines are shown in the cartoon force/time graph on the right. The models can quickly become complicated as more and more springs and dashpots are incorporated into the model to produce a force relaxation curve that matches the real material force relaxation curve.

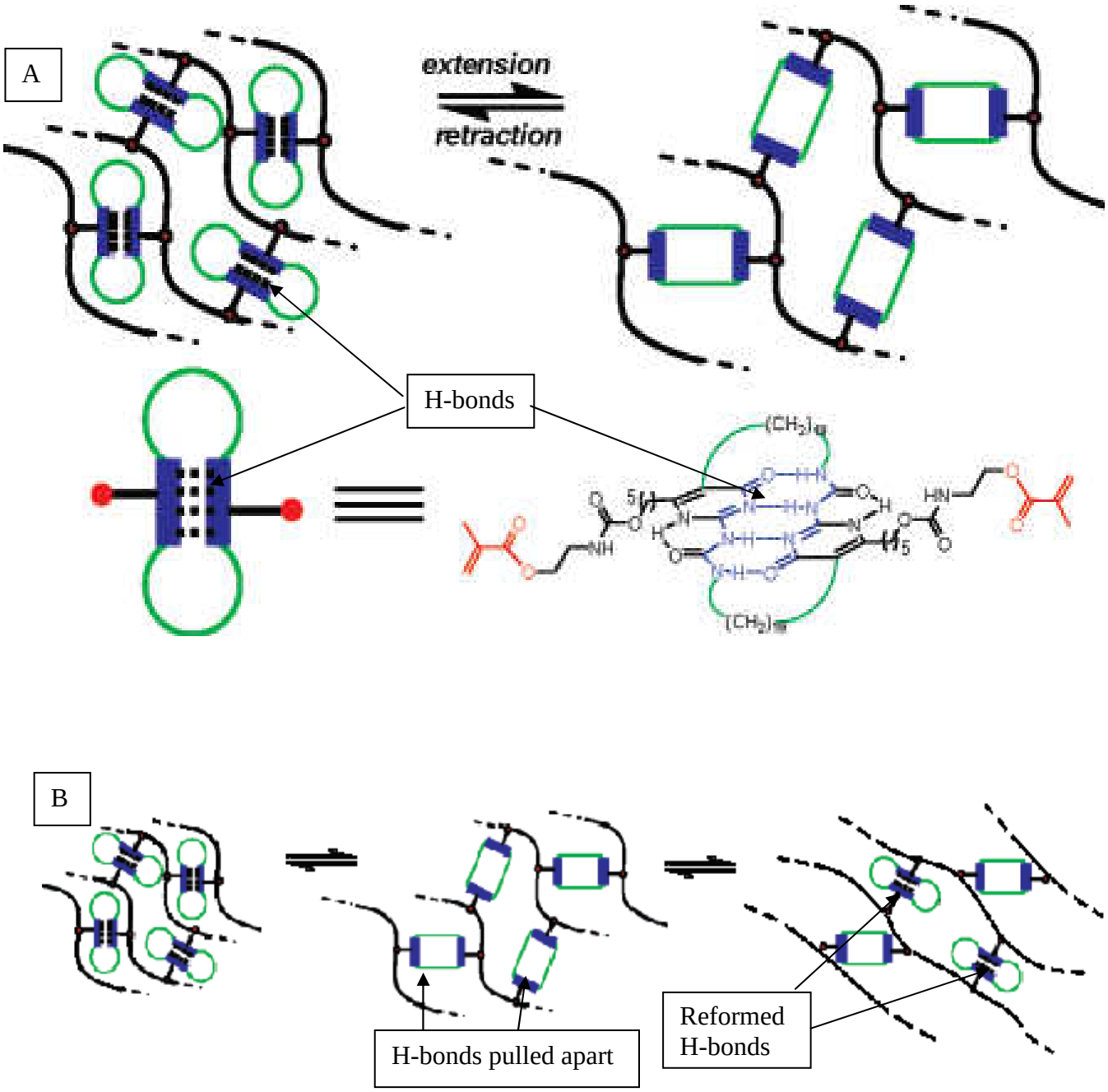

Figure 4.4: A: Concept of biomimetic design of biomimetic modular crosslinker for enhancing network mechanical properties. H-bonds stabilize the structure and covalent bonds preserve the overall molecular structure during extension. Reproduced and modified with permission from Journal of American Chemical Society Kushner et al (2007) B: a representation of how a partial recovery H-bonds could occur. The initial strain opened all four H-bond domains but viscoelastic flow of slack generated by the opening of the H-bond domains allows some H-domains to re-bond.

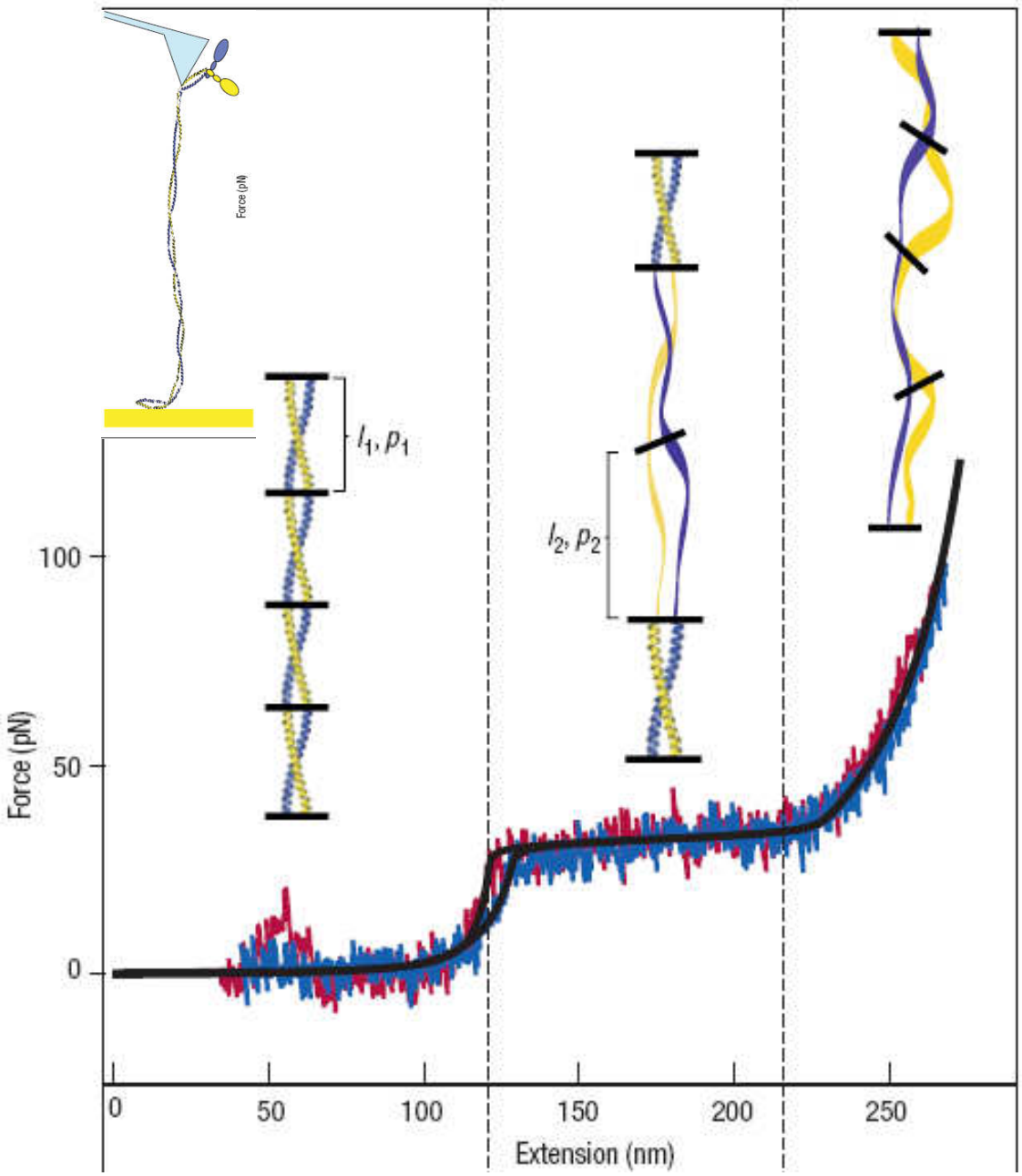

Figure 4.5 Stress/strain data and model for a single myosin coiled-coil. The stress/strain plot has very similar shape compared to the WECP data. The most noticeable difference is the small hysteresis loop. WECP must be undergoing a more complex interaction that uses up more energy. This may be due to uncoiled α-helixes tangling with adjacent molecules and/or β-sheets trying to form. Reproduced with permission from Nature Materials, Schwaiger et al (2002).

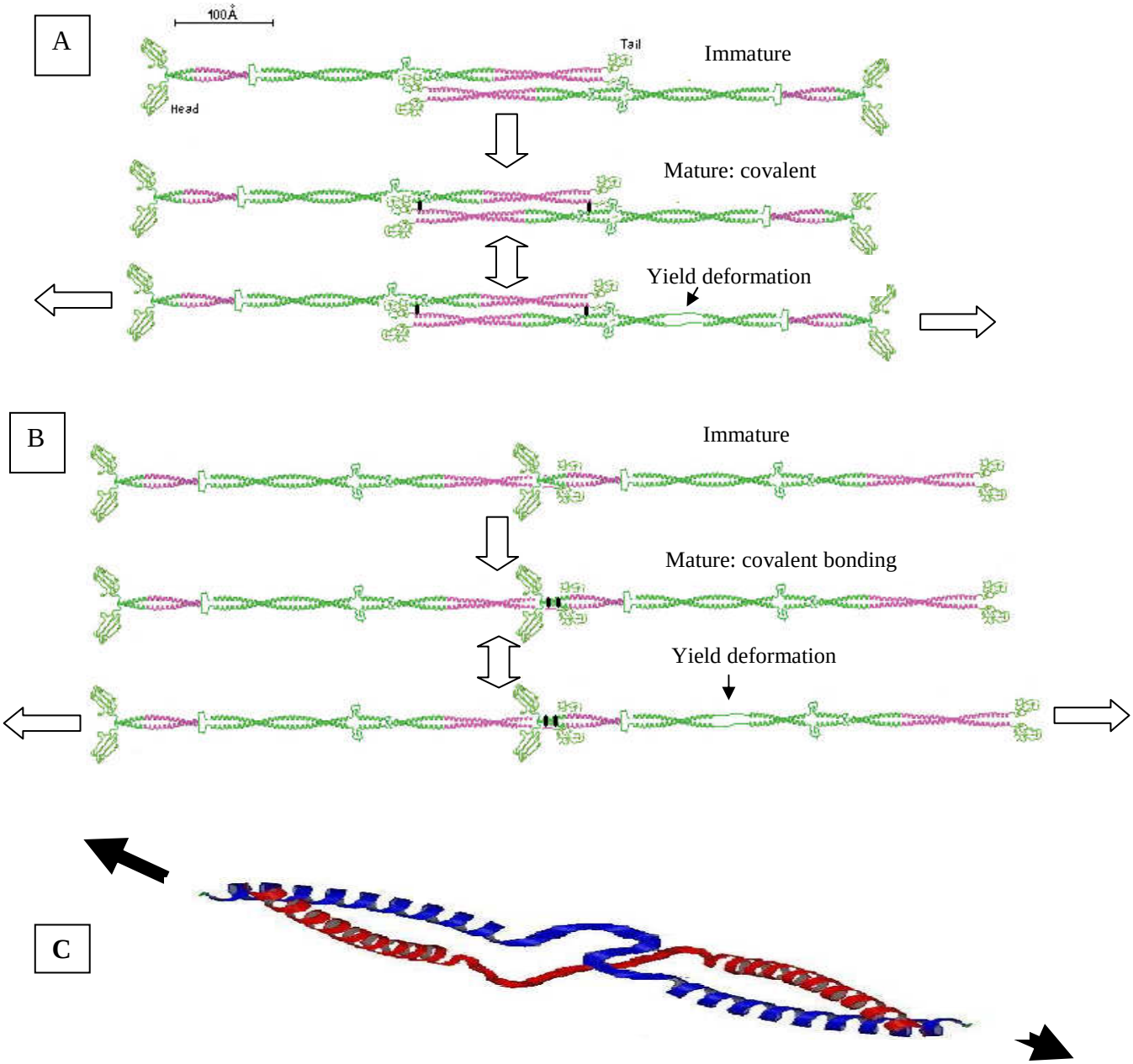

Figure 4.6: Models illustrating how α-helical elements could be linked. In this diagram the coiled coils are represented as being analogous to intermediate filament coiled coils. In the immature state they are joined by soft globular components that yield easily. In the mature state the coiled coils are depicted as having been bonded together covalently, thus bridging the load to the strong helixes and by passing the soft globular components. A & B represent different ways that this joining could occur. Both models assume that the immature state self-assembles if the molecules are brought into alignment. The maturation process is assumed to be aided by an enzyme or other chemical agent. Original image reproduced and modifiedwith permission from BioEssays, Strelkov, Herrmann,[2] and Aebi (2007) C: a close-up of a yield deformation. Popped open α-helixes introduce random sections of disorder, which can be stretched into parallel sections of the macromolecule. If these sections where held in the right configuration β-sheets could form.

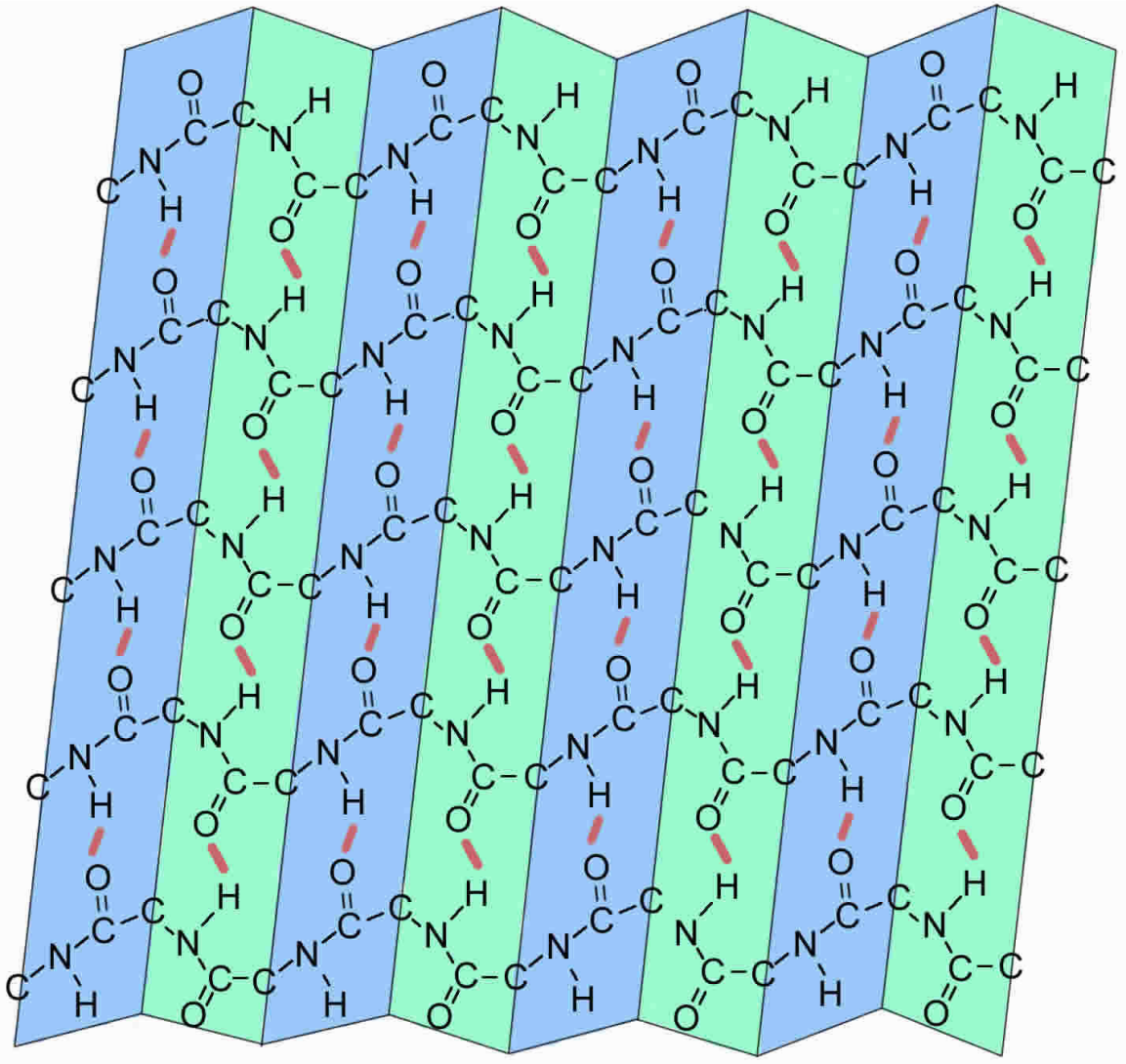

Figure 4.7: B-pleated sheet. A depiction of how the same primary structure that forms α-helixes can also form a β-pleated sheet if strained α-helixes forming molecules are lined up with one another. Lateral (R) groups not shown. H-bonds (red lines) between adjacent molecules stabilize the β-sheet.

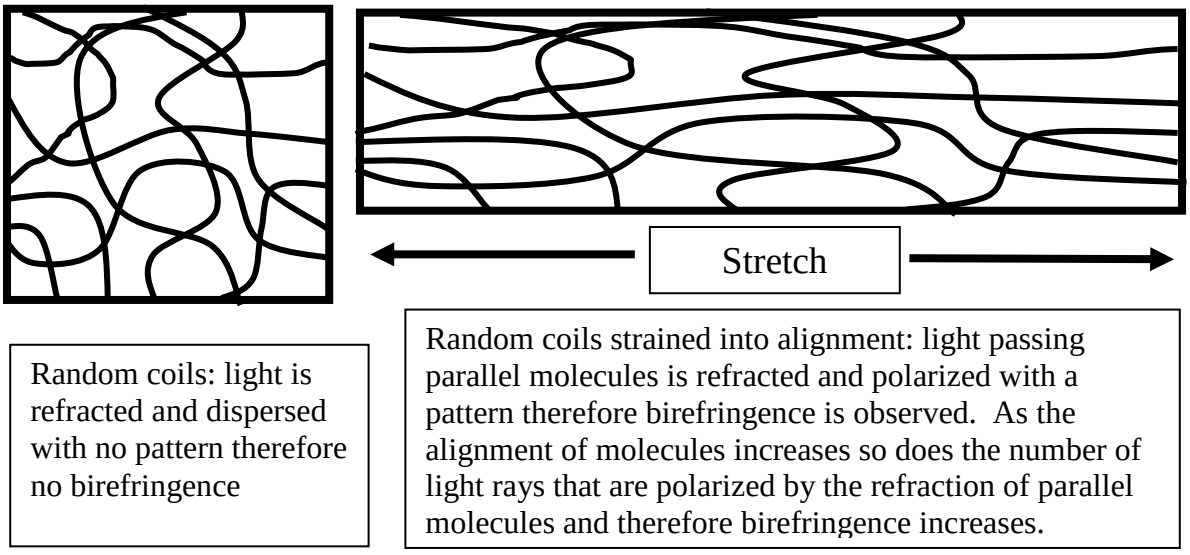

Figure 4.8: Explanation of Intrinsic birefringence cause by straining random coil network.

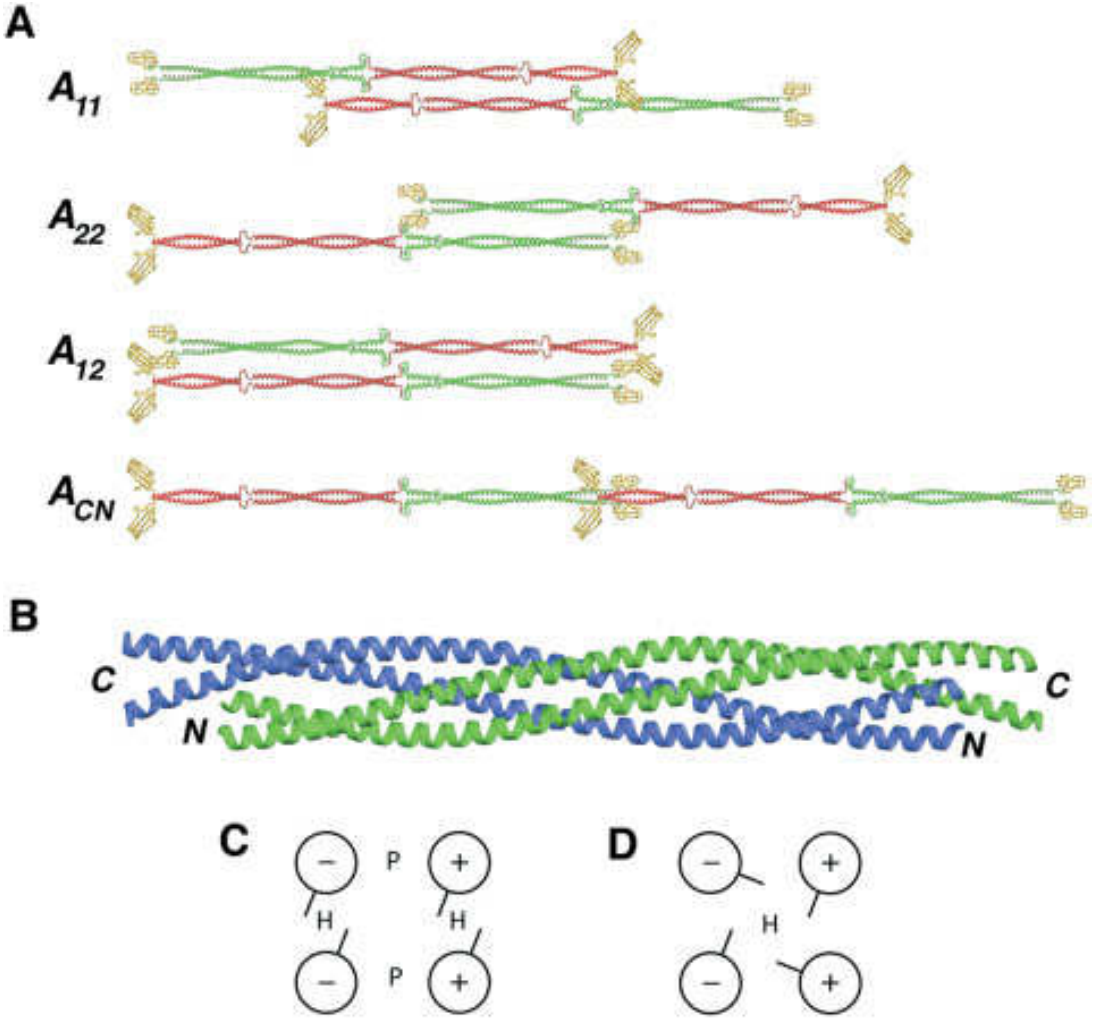

Figure 4.9: Reproduced with permission from BioEssays, Strelkov, Herrmann,[2] and Aebi (2007) a summary of possible models Dimer–dimer association. A: Four association modes A11, A22, A12 and ACN. Coil 1 and coil 2 are coloured red and green, respectively. B: Model for the overlap region of the A22 tetramer based on the known atomic structure of segment 2B.(21) The two antiparallel coiled-coil dimers are in blue and green, respectively. C: Cross-section of the tetramer model shown above. The two coiled coils are joined together by a predominantly polar interface (P). 'Up' and 'down' orientations of the ahelices are designated by plus and minus signs, respectively. D: An alternative model: a fourstranded, antiparallel-coiled coil with a common hydrophobic core (H).

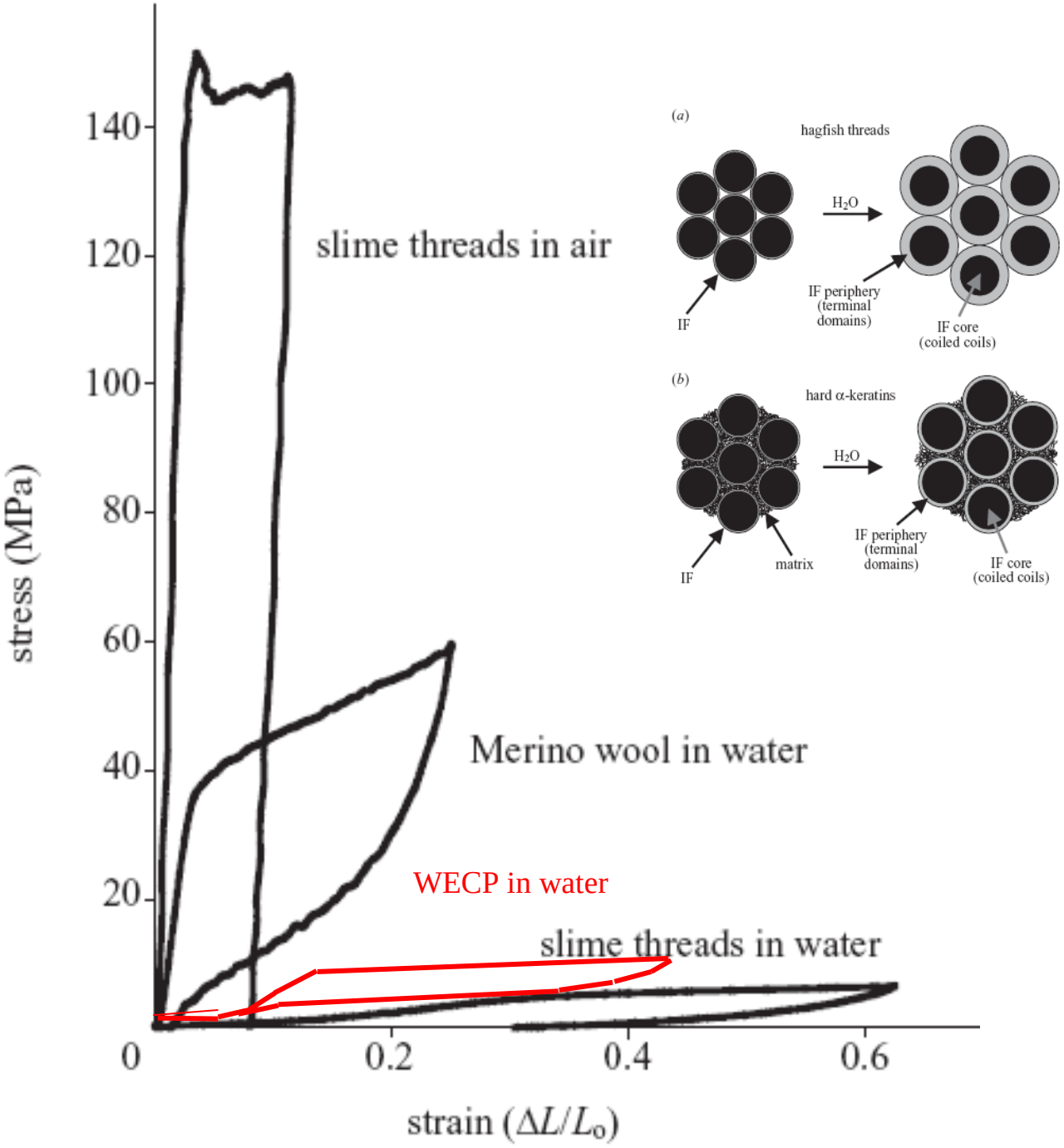

Figure 4.10: Reproduced and modified with permission from Proceedings of the Royal Socociety, Fudge and Gosline (2004). A stress strain curve comparing wet wool to wet and dry hagfish threads. The general shape of the wool curve resembles that of whelk egg capsule proteins. The proposed mechanism that accounts for the difference between hagfish intermediate filaments is the matrix that surrounds the intermediate filaments in the hard keratin wool (highlighted in inserts a & b). The whelk data has been superimposed in red for comparison. The whelk data has been adjusted by a factor of three for this comparison to compensate for voids in its porous structure. WECP appears to be an intermediate between merino wool and hagfish slime threads.

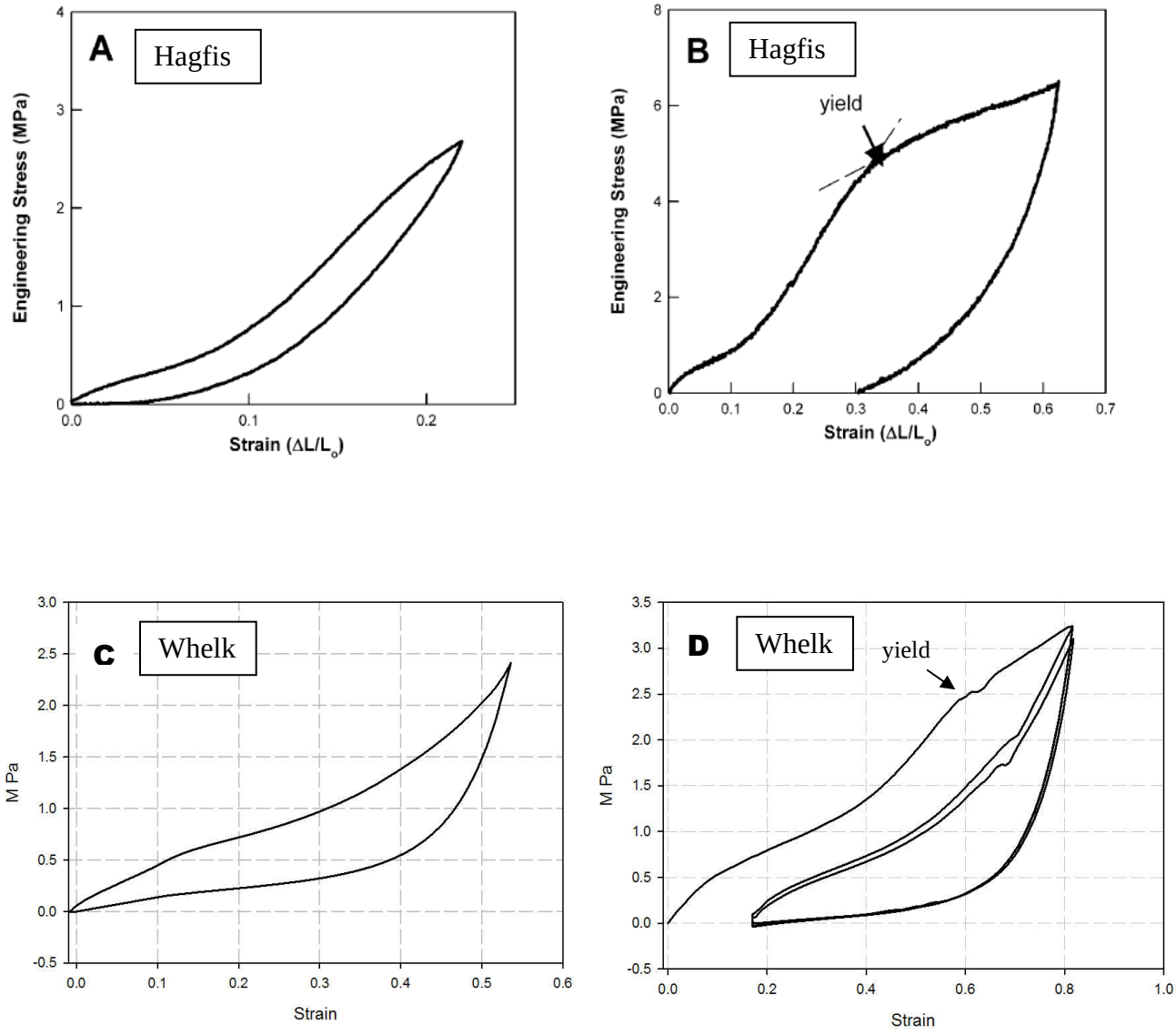

Figure 4.11: Graphs showing similar traits between hagfish slime fibers, which are known to be made up of intermediate filaments (Fudge and Gosline, 2003) and immature whelk protein samples. Figure D show a deformation on the first extension similar to curve B for the hagfish slime. Subsequent extensions in D look like curve A for the hagfish slime and C resembles A with a slight modification of the initial modulus.

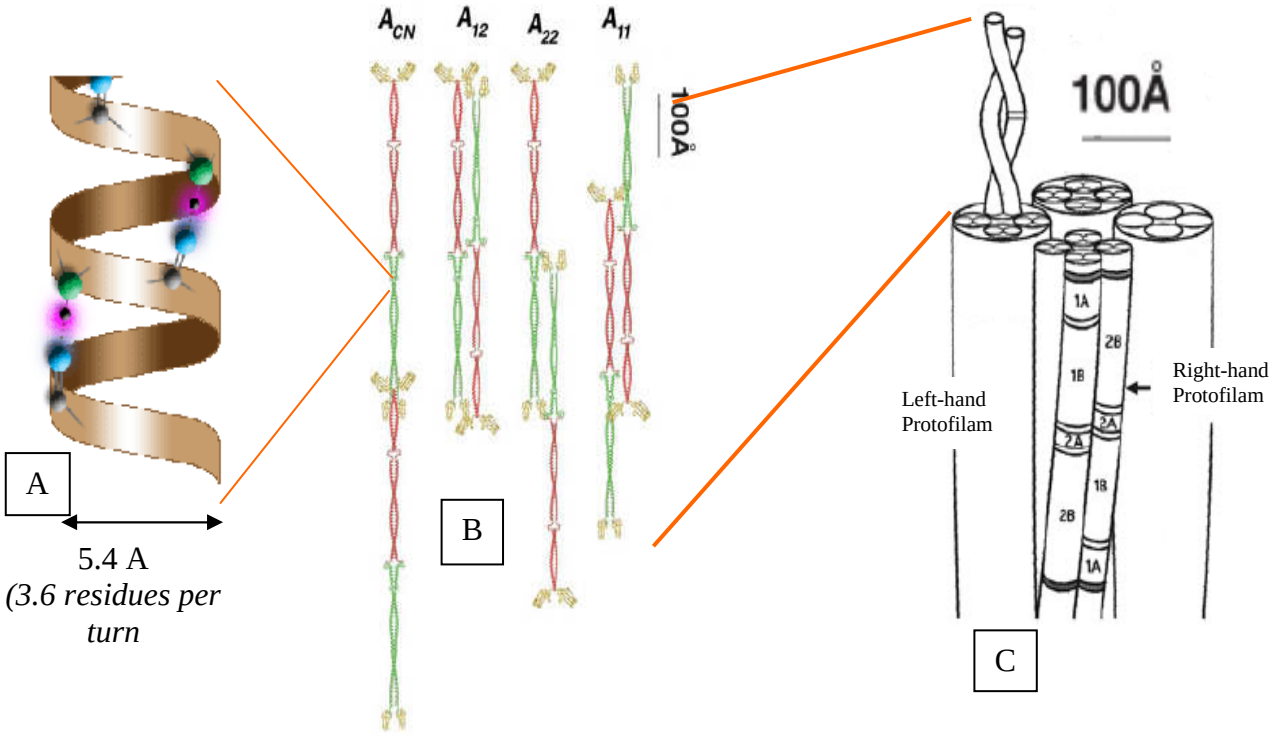

Figure 4.12: A: α-Helix; Known to be a component of WECP. B: Models of how coiled coil components of IF could join. Our model assumes that WECP is made up of similar components, linked by covalent bonds. C: A model of Intermediate filaments; WECP exhibit similar properties. D: TEM of Whelk Capsule Protein. E: False colour 3D second harmonic scan of WECP from the middle layer. F: Light microscopy; 30 deg cross section of Whelk egg Capsule

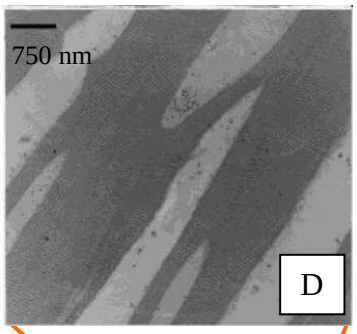

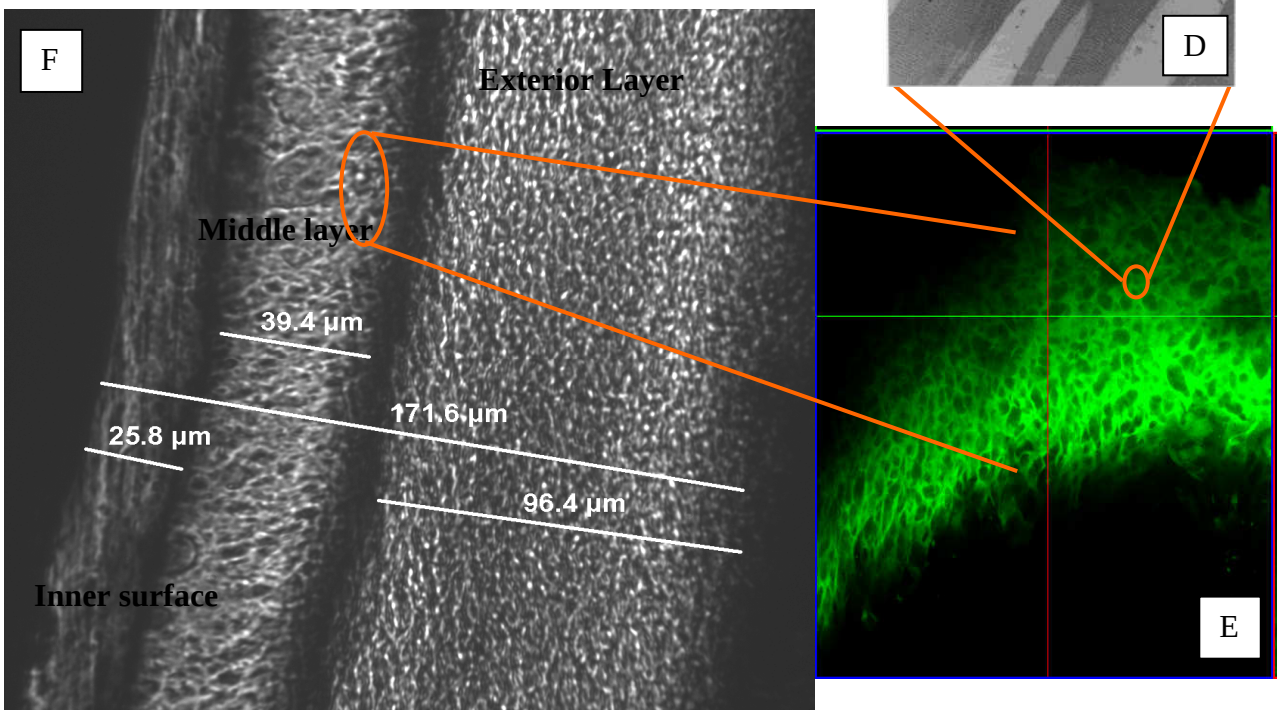

References:

Aaron B. B. and Gosline J. (1980), Optical Properties of Single Elastin Fibers Indicate Random Protien Confermation, Nature **87** 865-867

Bennett-Clark H. (2007), The First Description Of Resilin, Journal of Experimental Biology Classics, 3879-3881

Delly J G, (2004)**, '**Sénarmont Compensation: How to Accurately Measure Small Relative Retardations (0-1λ)"**,** College of Microscopy, Westmont, IL Oct 7, 2007 <www.modernmicroscopy.com/main.asp?article=14&page=2>

Ferry J.D., (1980), Viscoelastic Properties of Polymers 3rd Edition, John Wiley and Sons, Toronto Ont.

Fester W. and Davidson M.(2009), The de Sénarmont Compensator, Olympus Microscopes Online Tutorial, Olympus inc., Gainesville, FL <www.olympusmicro.com/primer/techniques/polarized/desenarmontcompensator.html>

Fraser B., Parry D. (2005), TheTree-dimensional Structure of Trichocyte (hard □-) Keratin Intermediate Filaments: Features of the Molecular Packing Deduced fro the Site of Induced Crosslinks, Journal of Structural Biology 151 171-181

Fraser B., Parry D. (2008), Molecular packing in the feather keratin filament, Journal of Structural Biology **162** 1–13

Fudge D. (2002), The Biomechanics of Intermediate Filamnt-Based Materials: Insights From Hagfish Slime Threads, Ph.D. Thesis University of BC.

Fudge D. Gardner K.,Forsyth V., Riekel C., and Gosline J. (2003),The Mechanical Properties of Hydrated Intermediate Filaments: Insights from Hagfish Slime Threads Biophysical Journal, 85, 2015–2027

Fudge D. S. and Gosline J. M. (2004), Molecular design of the α-keratin composite: insights from a matrix-free model, hagfish slime threads, *Proc. R. Soc. Lond.* B **271**, 291–299

Gosline J. (1971), Connective Tissue Mechanics of Metridium Senile, Journal of Experimental Biology, **55**, 763-774

Gosline J, Lillie M., Carrington E., Guerette P., Ortlepp C. and Savage K. (2002), Elastic Protiens: Biological Roles and mechanical Properties, The Royal Sosiety **357**, 121-132

Harrington M. and Waite J. (2007), holdfast Herics: Comparing the molecular Properties of Mytilus califonianus Byssa Threads, Journal of Experimental Biology **210**, 4307-4318

Haskell R. C., Carlson F. D., and Blank P. S. (1989), Form birefringence of , Biophys. J. Biophysical Society **56**, 401-413

Jarosch R. (2005) The alpha-helix, an overlooked molecular motor, Protoplasma 227: 37–46

Kato A. and Takagi T. (1988), Formation of intermolecular .beta.-sheet structure during heat denaturation of ovalbumin, ***J. Agric. Food Chem.***, **1988**, **36** (6), pp 1156–1159

Kerplak L., Doucet J. and Briki F. (2004), New Aspects of the α-Helix to b-Sheet Transition in Stretched Hard a-keratin Fibers, Biophysical Journal, **87**, 640-647

Kliger, D.S., J.W. Lewis, and C.E. Randall. (1990). Polarized light in optics and spectroscopy. Academic Press Inc., London, Ont.

Kushner A. M., Gabuchian V., Johnson E. G., and Guan Z. (2007), Biomimetic Design of Reversibly Unfolding Modular Cross-linker to Enhance Mechanical Properties of 3D Network Polymers, Journal of American Chemical Society, **129** 14110-14111

Lau J. H, Erasmus S., and Zou Y. (2003) Thermal Stress and Deflection Analysis of a Glass Window (Circular Plate) Elastically Restrained Along its Edge in a Photonic , Journal of Electronic Packaging, **125** 603-608

Maestre M. F. and Kilkson R. (1965), Intrinsic Birefringence of Multiple-Coiled DNA, Theory and Applications, Biophysical Journal **5** 275-287

Miserez et al. (2009), Non-entropic Elasticity in an Encapsulating Biolastomer, Unpublished work from the University of California, Santa Barbera

Moreaux L. Sandre O, Charpak S, Blanchard-Desce M, and Mertz J. (2001), Coherent Scattering in Multi-Harmonic Light Microscopy
Biophysical Journal **80** 1568–1574

Norman R. Watts, Jones L., Cheng N., Wall J., Parry D. and Steven A. (2002), Cryo-Electron Microscopy of Trichocyte (Hard α-Keratin) Intermediate Filaments Reveals a Low-Density Core, Journal of Structural Biology **137,** 109–118

Rapoport H. S. and Shadwick R. E. (2002)**,** Mechanical Characterization of an Unusual Elastic Biomaterial from the Egg Capsules of Marine S nails (Busycon spp.) Biomacromolecules **3**, 42-50

Rapoport H. S. and Shadwick R. E. (2007), Reversibly labile, sclerotization-induced elastic properties in a keratin analog from marine snails: whelk egg capsule biopolymer (WECB), Journal of Experimental Biology 210, 12-26

Strelkov S. V., Herrmann H., and Aeb U. (2003)**,** Molecular architecture of intermediate filaments BioEssays 25:243–251, Wiley Periodicals, Inc.

Schwaiger I., Sattler C., Hostetter D. and Rief M. (2002), The myosin coiled-coil is a truly elastic protein structure, Nature Materials 1, 232 - 235

TaylorE. and Cramer W., (1963), Birefringence of Protien Solutions and Biological Systems, Biophysical Journal **3** 127-141

Vaccora E. and Waite J. (2001), Yield and Post Yield Behavior of Mussel Byssis Trhead: A Self-Healing Biomolecular Material, Biomaromolecules, **2**, 906-911

Watts R., Jones L., Cheng N.; Wall J.; Parry D.; Steven A. (2002), Cryo-elctron Microscopy of Trichoccyte (hard -keratin) Intermediate iliments Reviels a Low-density Core, Journal Of Structural Biology **137** 109-118

Wood, E.A. (1964). Crystals and light. An introduction to optical crystallography. The Commission on College Physics. D. Van Nostrand Co. Inc.: Princeton, NJ.

Zhuang W. and Prohofsky E.W. (1990), Dependancd of defect-mediated hydrogen-bon melting in the DNA double helix on the side of an induced defect, Physical Review A 41:10 5677-5683